Doctoral Dissertation (Shinshu University)

Study on development of three-dimensional woven composites and their mechanical behavior

三次元織物複合材料の開発とその力学挙動に関する研究

March 2022

LIU YAJUN

Graduate School of Medicine, Science and Technology

Department of Science and Technology

Contents

Abstract

Three-dimensional (3D) woven textiles with three groups of yarns arranged in three perpendicular directions have drawn much attention from researchers as reinforcement materials in fiber-reinforced composites. 3D woven textile-reinforced composites exhibit excellent out-of-plane mechanical performance compared to traditional laminated composites owing to the reinforcement in through-thickness direction. Developing 3D woven composites with various reinforcement woven structures is of interest to the composite research area for specific engineering applications.

In this study, a new weaving technology with a modified heddle position system based on a self-built 3D weaving loom is designed, and four typical 3D woven-structure textile groups are manufactured: layer-to-layer orthogonal woven, through-thickness orthogonal woven, layer-to-layer angle-interlock woven, and through-thickness angle-interlock woven. The new weaving technology has great potential for manufacturing various 3D woven structures effectively and efficiently. The developed glass/aramid fiber hybrid 3D woven textile-reinforced epoxy-resin composites underwent three-point bending tests and low-velocity drop-weight impact tests to study the influence of the woven structure on the quasi-static and dynamic flexural performance as well as failure modes of these composites. On the other hand, carbon fiber 3D woven textile-reinforced epoxy-resin composites with four types of 3D/2.5D reinforcement structures (named as 3D-a, 3D-b, 3D-c and 2.5D) are developed based on a traditional weaving technology and their quasi-static and dynamic flexural performance are also studied. The four types of 3D/2.5D woven composites with special structural design in which binder yarn lies in weft direction, have same yarn densities along textile warp and weft directions in textile preforms during weaving process as well as same composite fiber volume fraction.

For the glass/aramid fiber hybrid 3D woven composites, the beam specimens which are along the textile warp and weft directions are tested under three-point bending tests. The composites along the weft direction have a larger flexural modulus but smaller failure strain compared with the warp direction for all woven-structure types. Among the designed 3D woven composites, the angle-interlock woven structures have a larger flexural strength (50%), modulus (40%), and failure resistance than have the orthogonal-woven structures. Overall, the through-thickness angle-interlock woven structure

has the best quasi-static flexural-failure resistance among all textile structures, and is the optimal structural design based on this modified weaving technology. Woven structure has an obvious influence on the composite failure modes after three-point bending test. Low-velocity drop-weight impact tests on the 3D woven composites were conducted under impact energy levels of 10, 20, and 30 J. Load-bearing capacity, deflection characteristics, and energy characteristics of the composites were studied to clarify their impact resistance. Among the developed 3D woven composites based on this new weaving technology, it is found that the through-thickness angle-interlock woven structure is the optimal structure with a quasi-penetration energy of 30 J, whereas the other structures have a quasi-penetration energy of 20 J. The results also confirmed that the woven structure has an obvious influence on the composite failure modes: angle-interlock woven structures exhibit more limited delamination failure and keep a structural completeness after impact, whereas orthogonal woven structures exhibit more fiber fracture failure. Angle-interlock woven structures are more suitable for manufacturing based on the new weaving technology to develop impact-resistance composite materials.

For the carbon fiber 3D woven composites, the textile warp- and weft-direction beam specimens are also tested under three-point bending tests. Woven structures with different weft-to-binder yarn ratio and yarn waviness degree, have an obvious influence on the quasi-static flexural mechanical performance. Among the four designed 3D woven composites, 3D-a exhibits the best quasi-static flexural mechanical performance, followed with 2.5D, 3D-b, and 3D-c. Binder yarn with small waviness has both interlayer binding/interlacing ability and in-plane load-carrying ability. Compared with 2.5D structure in which weft yarn interlaces with warp yarn, 3D-a structure in which there is no interlacement between weft and warp yarns could achieve a better quasi-static flexural mechanical performance. Low-velocity drop-weight impact tests on the carbon fiber 3D woven composites were conducted under impact energy levels of 3, 6, and 9 J. There is an opposite mechanical behavior between quasi-static three-point bending tests and dynamic low-velocity drop-weight impact tests for these designed carbon fiber textile composites. 3D-c exhibits the best dynamic flexural mechanical performance, followed with 3D-b, 3D-a, and 2.5D. In-plane yarn waviness and through-thickness binder-yarn path may contribute to better impact performance. woven structure has an obvious influence on the failure mode in impacted composites, the binder

yarn lies more in through-thickness direction will survive more from through-thickness crack failures, exhibit more limited delamination or debonding failures, leaving better impact-resistance ability for the developed 3D woven composites.

With the new weaving technology based on the proposed modified heddle position system and special structure design based on the traditional weaving technology, various 3D woven structures could be designed and manufactured to develop advanced fiber-reinforced composite materials. These weaving technologies have great potential to develop complex net-shaped woven composites such as composite engine fan blade with additional modifications. The through-thickness angle-interlock woven composite developed based on the new weaving technology has superior out-of-plane mechanical performance and may meet requirements of specific engineering applications. With successful development of these 3D woven composites and comprehensive studies of their quasi-static and dynamic flexural performance, some textile design parameters could be drawn out for future development of advanced 3D woven composites. Proper structural design of 3D woven composite based on specific fiber selection and weaving technology is key issue to develop advanced composites with better flexural performance.

Abbreviations

2D	Two-dimensional
3D	Three-dimensional
2.5D	2.5-dimensional
FRP	Fiber-reinforced plastic/polymer
CFRP	Carbon fiber-reinforced plastic/polymer
PAN	Polyacrylonitrile
BPO	Polybenzoxazole
UHMWPE	Ultra-high-molecular-weight polyethylene
PE	Polyethylene
PP	Polypropylene
PA	Polyamide
RTM	Resin transfer molding
VARTM	Vacuum-assisted resin transfer molding
LLOW	Layer-to-layer orthogonal woven
LLAIW	Layer-to-layer angle-interlock woven
TTOW	Through-thickness orthogonal woven
TTAIW	Through-thickness angle-interlock woven
DRR	Deflection recovery ratio
IRI	Impact resistance index

Chapter 1 General introduction

Fiber-reinforced plastic/polymer (FRP) is a composite material made of polymer matrix and fiber reinforcement. FRP with two different substances, i.e., polymer and fiber, each with its own characteristics, is superior to original substance in specific applications. FRPs are commonly used in aerospace, automotive, marine, civile, sports, and other fields since the FRPs have many advantages: high mechanical performance, low weight, easy manufacturing, and so on.

1.1 Fiber-reinforced plastic composites

1.1.1 High-performance fibers

Fiber which is the reinforcement material in FRP composite mainly carries load when the composite under loading and plays a vital role. High-performance fibers usually have high levels of properties such as tensile strength and modulus, limiting oxygen index, chemical resistance. As the reinforcement materials, fibers with high mechanical performance have drawn much attention from researchers. Some high-performance fibers which are commonly used to manufacture composite materials are listed as flowing:

Glass fiber

Glass fiber refers to a material consisting of numerous extremely fine filaments of glass which is around several to a dozen micrometers in diameter. Glass fiber is formed by extruding mainly silica-based glass into many continuous filaments with small diameters which is suitable for textile manufacturing. Glass fiber is a kind of inorganic material with outstanding properties such as electrical and thermal insulation, excellent mechanical performance. The most common types of glass fiber used is E-glass, which is used as reinforcement in fiber-reinforced composites. Glass fiber has many advantages: low cost, easy manufacturing, and so on.

Carbon fiber

Carbon fiber refers to a fiber containing at least 90% carbon and is created by carbonizing polyacrylonitrile (PAN) fiber, pitch resin or rayon at high temperatures. Carbon fiber is also an inorganic material with excellent properties such as high stiffness, high tensile strength, low weight, high chemical resistance, high temperature tolerance and

low thermal expansion. Due to the relative low modulus and poor thermal resistance of glass fiber which is not suitable for aerospace industries, carbon fiber with high modulus and strength, low density was developed. Carbon fiber is usually used as the reinforcement material in fiber-reinforced composites. Carbon fiber is respected firstly developed by Thomas Edison in 1879 for light bulbs carbonizing natural cellulosic fibers such as cotton, linen, or bamboo. In the late 1950s, producing carbon fiber by carbonizing synthetic rayon fiber was renewed. In the late 1960s, introduction of the PAN process by Japan took in lead in manufacturing PAN-based carbon fiber with superior physical properties compared to rayon-based carbon fiber. PAN fiber is recognized as the most important and promising fiber for manufacturing high strength carbon fiber nowadays[1].

Aramid fiber

Aramid fiber (aromatic polyamides) is a synthetic organic fiber synthesized by aromatic diamines and diacids or diacid chlorides with high strength and modulus, low density, outstanding resistance to impact and heat. Common brand names of aramid fiber include Kevlar, Nomex, and Twaron. In the early 1960s, aramid fibers were introduced in commercial application by DuPont, with a meta-aramid fiber under the trade name Nomex, and a para-aramid fiber under the trade name Kevlar in 1972. Kevlar is the best-known para-aramid fiber nowadays. Compared with meta-aramid, para-aramid fiber exhibits higher strength and modulus, and has many high-tech applications such as aerospace and bullet-proof body armor.

Other high-performance fibers

Other mainly applied organic high-performance fibers include polybenzoxazole (BPO) fiber, ultra-high-molecular-weight polyethylene (UHMWPE) fiber, and so on. BPO fiber was developed by Toyobo in 1998 under the brand name Zylon which has higher strength and modulus, thermal and flame resistance than aramid fiber and other organic fibers. BPO fiber has applications such as firefighter garment, sports goods, industrial materials, and is respected as the most competing organic fiber. UHMWPE fiber is made from UHMWPE, which is a thermoplastic polyethylene (PE) with extremely long chains, high level of orientation and crystallinity. Dyneema is one of the commercial brands of UHMWPE fiber and is developed by DSM and Toyobo companies.

UHMWPE fiber has applications such as composite plate armor, cut-resistance gloves, sports goods. Other inorganic high-performance fibers used in composites mainly include ceramic fiber, basalt fiber, and so on. Basalt fiber with advantages such as super mechanical properties especially at high temperatures, low cost, sustainable manufacturing, is expected as an alternative to glass fiber.

Natural fibers

In recent years, natural fibers have drawn much attention from researchers as reinforcement materials to develop green composites, mainly due to their ecofriendly nature and sustainability[2, 3]. Researchers have studied the natural fiber-reinforced composites such as banana fiber composite[4], hemp fiber composite[5], bamboo fiber composite[6], and found that some of them have comparable properties with glass fiber-reinforced composites.

1.1.2 Polymer matrix system

Polymer matrix system in FRP composites could be divided into two main groups: thermosetting resin and thermoplastic resin. Polymers such as epoxy, vinyl ester, polyester are usually used as matrix materials.

Thermosetting resin

Thermosetting resins (also called thermosets) which are used as matrix materials in FRP composites, mainly include epoxy resin, polyester resin, phenolic resin, vinyl ester resin, and so on. Polymer chains in thermosetting resin are cross linked to form a rigid, non-reversible three-dimensional (3D) network structure. The starting materials for manufacturing thermosetting resin are usually a liquid prepolymer and a curing agent (catalyst or hardener). The chemical reaction between prepolymer and curing agent transfer the thermosetting resin to a solid one and the hardened thermoset cannot be melted or reshaped. Thermosetting resin is generally stronger than thermoplastic resin due to its 3D network structure in molecular scale.

Thermoplastic resin

Thermoplastic resin (also called thermoplastic) is a polymer material that melt when heated and harden when cooled. The polymer chains associate by intermolecular forces weaken radially with increased temperature, yielding a viscous liquid. Thermoplastics

could be reshaped or remolded under this stage and keep the remolded shape when cooled down, thus thermoplastic could be recycled. Thermoplastics mainly include polypropylene (PP), polyethylene (PE), Polyamide (PA), and so on.

1.1.3 FRP manufacturing technology

There are numerous techniques for fabricating fiber-reinforced composite materials. Selection of a technique for a specific composite material will depend on the factors such as resin property, preform (reinforcement) property and geometry, composite shape, end-use or application, and so on. Basically, thermosetting composite can be manufactured based on the techniques such as hand lay-up, resin transfer molding (RTM), autoclave molding, compression molding, resin infusion, and so on, whereas thermoplastic composite can be manufactured based on compression molding, injection molding, and so on. Some of commonly used techniques are listed as following:

Hand lay-up

Hand lay-up is the simplest technique and costs the least for composite manufacturing. The reinforcement preform is placed inside a mold, and then, resin-hardener mixture is applied on the surface of the preform evenly by a brush, this procedure is repeated and other layers of preform are laminated. After laying up, the preform is under curing process, finally the cured composite is removed from the mold. Hand lay-up technique always leaves a relatively poor quality.

Resin transfer molding

RTM technique has a mold consisting of male and female parts. The preform is placed inside the female mold part, and the mode is closed with the male part on the female one. The resin-hardener mixture is then infused into the mold cavity until the mold is filled, and then leave the preform under curing. After curing, the closed mode is opened, and the composite is removed. An advanced technique of RTM is vacuum-assisted resin transfer molding (VARTM), which a vacuum circumstance is applied in the closed mold or a closed plastic bag to remove air bubbles in the infusion process. VARTM is also a commonly used technique and leaves a relatively high quality of composites.

Autoclave molding

Autoclave is a machine which supplies high temperature and pressure as well as vacuum circumstance during composite manufacturing. A preform with thermosetting resin-hardener mixture is placed into a vacuum bag, and the vacuum bag is placed into the autoclave machine, high temperature, high pressure, high vacuum condition could be applied at the same time during curing process. This technique yields a high quality of composites.

Compression molding

Compression molding is a method of composite fabrication which the heat and pressure are applied by a specific machine[7]. Both thermoset and thermoplastic composites could be manufactured based on this technique. A preform with thermosetting resin-hardener mixture or stacked thermoplastic resin sheet is placed into a mold or plastic bag, and the heat and pressure are maintained during curing. A vacuum circumstance could also be applied with aid of a vacuum pump.

Filament winding

Filament winding is a technique to manufacturing cylindrical composite structures such as pipes, pressure vessels, storage tanks, aircraft body [8]. In this process, pre-impregnated filaments, which are filaments passed through a resin bath, are wound onto a rotating mold (mandrel), and the pre-impregnated filament preform is cured in an oven or under radiant heaters (laser) or ultraviolet light depending on the types and properties of resin used. This technique offers a high speed and precise method for placing many composite layers and could yield a high fiber volume fraction.

Injection molding

Injection molding is one of the common techniques for manufacturing short fiber-reinforced composites and is suitable for both thermosetting and thermoplastic resin. Heated thermoplastic resin which is in a viscous liquid state, or thermosetting resin mixed with short fibers is injected into a mold with specific curing temperature. Complex-shaped composite could be manufacturing with this technique.

3D printing

3D printing or additive manufacturing is a technology to create physical objects from a 3D model data by successive addition of materials[9, 10]. In recent years, 3D printing has attracted much attention to fabricate composite materials, especially fiber-reinforced composites. 3D printing technology offers many advantages in the fabrication of composite materials, including high precision, cost effective and customized geometry[11]. There are several challenges for manufacturing fiber-reinforced composites based on the 3D printing technology, including the low fiber volume fraction for developed composites, difficulty of the addition continuous fibers, and so on.

1.1.4 Applications of fiber-reinforced composites

Fiber- or textile-reinforced composites have a wide application in aerospace[12-14], automotive[15-17], civil engineering[18-20], sports and leisure[21, 22], etc., due to their many advantages such as high mechanical properties, low weight, and other excellent properties. Particularly, 3D textile-reinforced composite with a complex net-shape and high through-thickness strength and delamination resistance has drawn much attention since decades ago. Some applications are listed as following:

Aerospace applications

Aerospace industry consumes largest advanced composites owing to the high mechanical properties and low weight of such materials. Weight reduction of up to 40% for fiber- or textile-reinforced composites could save much energy for aerospace compared with metal alloys. Composite materials accounts for up to 50% weight of the whole weight for modern aircrafts. Carbon fiber is mostly used in aerospace industry due to its high strength and stiffness aa well as low weight. Epoxy resin is the most preferred matrix material due to its high mechanical properties and durability.

Automotive applications

Fiber- or textile-reinforced composites are used in automotive industries in recent years, mainly due to their high specific strength and stiffness as well as low weight. Weight reduction of composite materials reduces the fuel consumption as well as CO_2 emission of vehicles.

Civil engineering applications

Fiber- or textile-reinforced polymer composites have become the most attractive candidate material for civil engineering applications and have been increasingly used in the rehabilitation and replacement of the old degrading traditional structures or building new structures. One example of the civil engineering applications of such materials is that large-scale structure constructions such as traffic bridges and pedestrian bridges[23].

Sports, leisure, and healthcare applications

Composite materials with designed mechanical properties and low weigh have a wide application in sports equipment and prosthetic devices. Carbon fiber composites are used to manufacture bicycle frames, tennis racket frames, and so on. Particularly, the developed carbon fiber composite prostheses improves amputee sport performance greatly in the past decades[24].

1.2 Three-dimensional woven textile

Textiles can be produced by weaving, knitting, braiding, stitching, felting, and other technologies. Woven textiles have been used as the reinforcements in textile-reinforced composites for decades, due to their special textile structure and yarn arrangement. Traditional 2D woven textiles are flexible sheet in which there are two groups of yarns: warp and weft yarns in perpendicular directions and interlaced with each other with various pattens. Textile structural composites usually have stacked 2D woven textiles as reinforcement in a laminated composite. Such laminated composites have good in-plane mechanical performance but poor out-of-plane mechanical performance due to that there is no reinforcement in through-thickness direction. To overcome the shortcomings of thus laminated composites, many technologies have been applied such as stitching, tufting, and so on. On the other hand, 3D textile structures which there is one set of yarns in through-thickness direction, have attracted much attention since decades ago as the reinforcement in composite materials to improve their out-of-plane mechanical performance. The 3D textile preforms can be processed by many ways as shown in **Fig. 1-1**. 3D woven textile has been defined as the textile with whole three-dimensional shape or with inner three-dimensional yarn interlacement[25]. In a typical 3D woven textile with inner 3D yarn interlacement, there are three groups of yarns: warp, weft,

and binder yarns which are in three liner perpendicular directions. 3D woven textiles are mainly used as reinforcement in fiber-reinforced composites, due to the benefits such as high interlayer strength, delamination resistance and impact resistance.

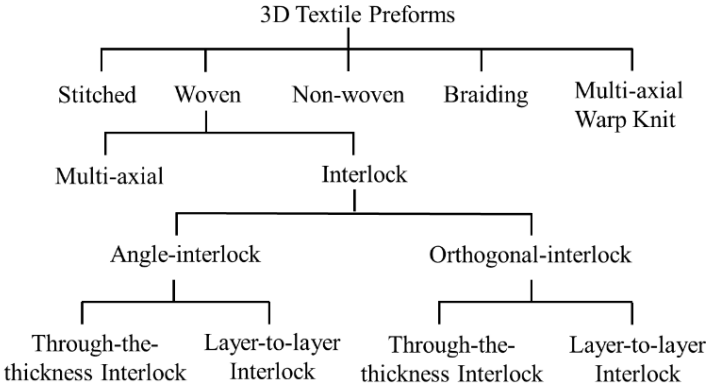

Fig. 1-1. Classification of 3D textile preforms[26].

1.2.1 Classification of 3D woven textile

There are several classification systems for 3D woven textile based on textile whole geometries, textile inner yarn interlacement, weaving process[27, 28], and so on, according to different researchers. The classification of 3D woven textile is complex owing to the complexity of textile structure and weaving technology. Based on the whole shape of textile, 3D textile could be classified into solid, hollow, shell, nodal, sandwich, spacer, etc. Chen[25] classified 3D woven textiles into four categories based on the textile geometries, regardless of weaving technology, as listed in **Table 1-1**.

Table 1-1. Classification of 3D woven textiles[25].

Structure	Architecture	Shape
Solid	Multilayer Orthogonal Angle interlock	Compound structure, with regular or tapered geometry
Hollow	Multilayer	Uneven surfaces, even surfaces, and tunnels on different level in multi-directions
Shell	Single layer Multilayer	Spherical shells and open box shells
Nodal	Multilayer Orthogonal Angle interlock	Tubular nodes and solid nodes

Based on the binder-yarn path and binding conditions, 3D woven textiles can be classified into orthogonal, angle-interlock, through-thickness, layer-to-layer, and multilayer structure groups, etc. Some of the woven structures, such as multilayer, layer-to-layer angle-interlock, are defined as 2.5-dimensional (2.5D) woven structure. Gokarneshan, N and coworkers[29] gave a fundamental definitions of 2D, 2.5D and 3D woven textiles:

1. 2D textile: it is one in which the component yarns (warp and weft) are placed in a single plane.

2. 2.5D textile: it is one in which the component yarns are placed in two mutually perpendicular planes in relation to one another.

3. 3D textile: it is one in which the component yarns are placed in three mutually perpendicular planes in relation to one other.

In Gokarneshan, N' definition system, multilayer structures are classified into 2.5D textile category, because that there are two groups of yarns, i.e., warp and weft to form a multilayer textile, in which parts of the warp or weft yarns interlacing with each other between layers in thus structures. It should be noted that some woven structures with three orthogonal sets of yarn (similar X-, Y- and Z- dimensions) have been defined as "true" 3D woven textiles.

Moreover, multiaxial 3D woven textiles[30, 31] also attracted much attention in the past decades. Multiaxial woven textile consists in-plane yarns of warp (0°), weft (90°), and bias yarns ($\pm\theta$°) as well as binder yarn in through-thickness direction. The stacking sequence and layer numbers of the in-plane yarns could be designed to meet the end-use requirements. The bias yarn increases the in-plane strength in bias directions (e.g., ±45°) of the textile preform and its textile-reinforced composite.

3D textiles with various structures and geometries meeting the end-use requirements of composite materials such as rails and joints[32, 33], engine fan blade[34] in advanced applications, have been designed and studied.

1.2.2 Weaving technology of 3D woven textiles

Weaving is an ancient technology to produce textiles using a loom, and its theory and practice are firmly established. In a conventional weaving process, there are three

primary motions: shedding, weft insertion and beating. Secondary motions include warp beam winding (or warp creel set-up), warp let-off, warp tensioning, and take-up of the finished fabric. On the loom, there are two sets of yarns: warp yarn which runs longitudinally in loom direction and weft yarn which runs from one side to the other side of the loom, interlacing with each other to form a fabric.

So far, various 3D woven structures have been manufactured based on a large variety of weaving looms and machines: conventional 2D weaving loom, Jacquard loom, 3D weaving loom, as well as specially modified or designed weaving looms or machines. There are limitations for 3D woven textiles manufacturing based on each weaving loom or machine due to weaving technologies, fiber properties and textile structures, etc.[28, 35]. Through-thickness orthogonal weaving structures have been basically fabricated based on 3D weaving loom. On the other hand, angle-interlock woven structures and multilayer structures have been mostly fabricated based on conventional or modified weaving loom due to their relative structural complexity. Manufacturing complex woven structures such as angle-interlock woven structures on 3D weaving loom is rarely reported due to the weaving technology limitations. Some 3D woven textile manufacturing technologies are listed as following:

Based on conventional 2D weaving loom

There are basically two groups of yarns, i.e., warp and weft yarns, to form textiles on a conventional 2D weaving loom, and part of the warp or weft yarns serve as binder yarn to form 3D woven textile structures. In some research, 3D woven textiles were manufactured on a conventional weaving loom, and these 3D woven textiles have some limitations in yarn selection, yarn density, as well as whole textile thickness and structural design. Behera B and coworkers[36, 37] prepared 2D plain woven textile and several 3D woven textiles: 3D orthogonal woven, 3D warp-interlock woven and 3D angle-interlock woven, as shown in **Fig. 1-2**, on a conventional 2D sample weaving loom with some modifications. A separate negative let-off arrangement was made behind the loom to hold binder yarn beam in manufacturing process of 3D woven textile due to that the let-off speed of binder yarn and warp yarn is different. Zahid B and coworkers[38] designed and manufactured a 3D through-thickness angle-interlock woven textile based on a conventional shuttle loom successfully.

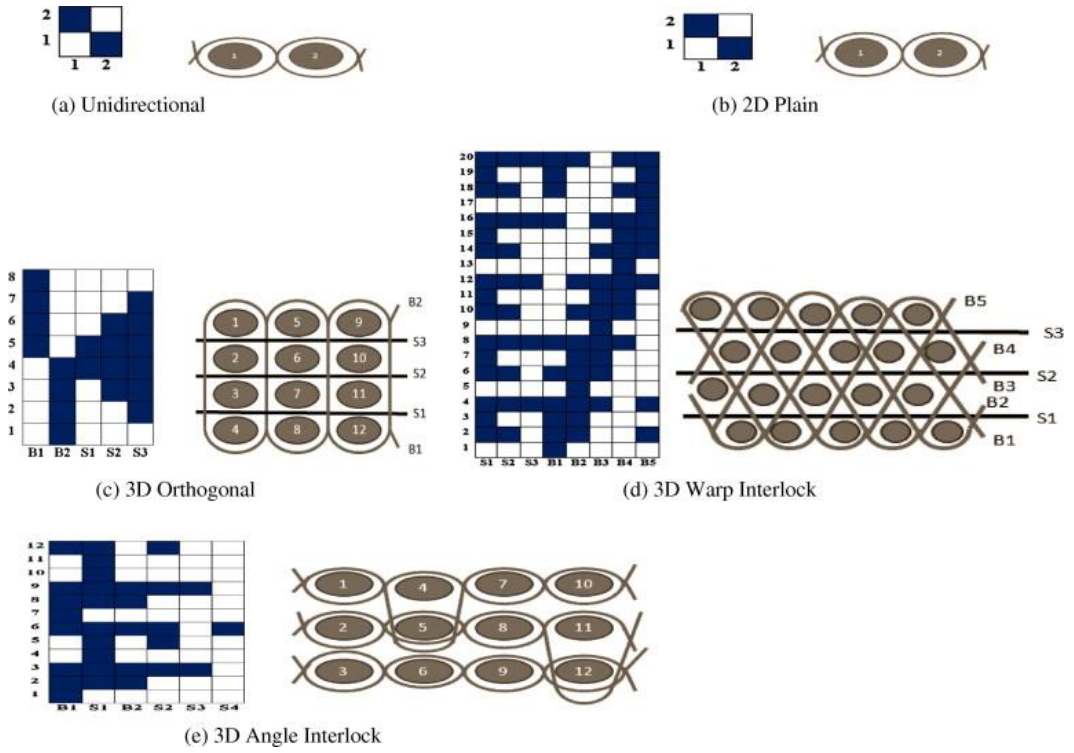

Fig. 1-2. Pegplan, and yarn architecture in cross section of unidirectional, 2D plain, orthogonal, warp interlock and angle interlock structure manufactured on 2D weaving system[37].

There are several drawbacks of manufacturing these 3D woven structures on conventional 2D weaving loom[39]:

1. Low productivity due to that building up layers one pick at a time.
2. Difficulty in maintaining proper stacking of the filling yarns in the different layers.
3. Fiber damage caused by abrasion. This is due to that all the warp yarns pass through heddle eyes and move up and down with heddles during every weaving cycle to form sheds, even if the structural design does not require them to move. And this increases the yarn abrasion between warp yarn and the heddle, as well as between the warp yarns in different layers.

Based on Jacquard loom

Jacquard loom is also used to fabric 3D woven textiles, especially for 3D woven textiles with complex net-shape structures, owing to its special shedding mechanism. One of applications of such complex 3D woven composites is composite engine fan blade [34].

The 3D textile used for the reinforcement in a composite engine fan blade has a complex near-net shape and geometry in which different woven structures exhibit in different sections, thus, the Jacquard loom with its unique shedding system and ability of weaving unlimited varieties of complex woven patten is suitable for manufacturing such 3D textiles. Rudov-Clark S and coworkers[40] manufactured a 3D orthogonal woven textile based on a Jacquard loom, as shown in **Fig. 1-3**. YU, B and coworkers [41] manufactured two types of woven structures: 3D angle-interlock and modified layer-to-layer fabric based on a conventional rapier weaving loom equipped with electronic Jacquard shedding system.

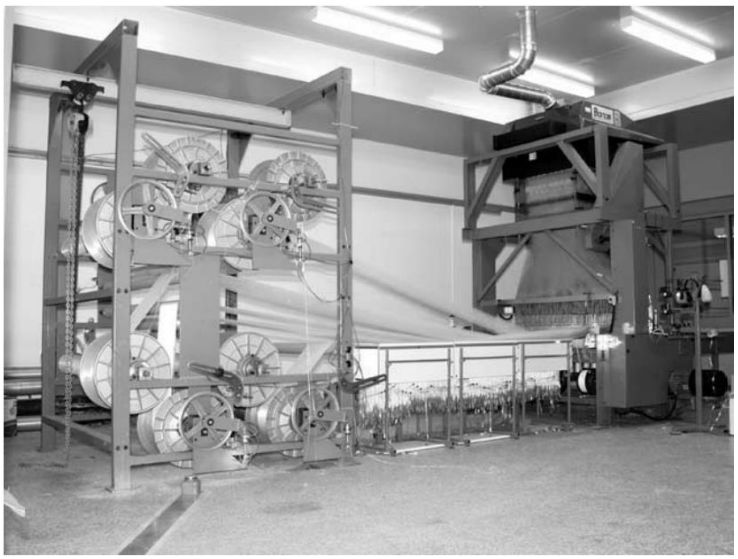

Fig. 1-3. Jacquard loom used to weave 3D woven fabric[40].

Based on 3D weaving loom

Basically, orthogonal woven structures are manufactured on 3D weaving loom. There are similarities between 2D and 3D weaving technologies, and a schematic of the two weaving technologies is depicted in **Fig. 1-4**. There are two groups of yarns: warp and weft, on a conventional 2D weaving loom. Warp yarns run in loom direction, pass through heddle eyes, and move upwards and downwards with heddles to form shed, weft yarns run from one side of the loom to the other side and pass through shed to interlace with warp yarns to form a 2D woven fabric. On a 3D weaving loom, there are three groups of yarns: warp, weft, and binder yarns to form 3D woven textiles. In a typical 3D weaving process, the warp yarns do not pass through heddle eyes and keep stable whereas binder yarns pass through heddle eyes and form sheds to allow weft

yarns pass through to form a 3D orthogonal woven structure. In these 3D orthogonal woven structures, there is no interlacement between warp and weft yarns, and thus no crimp or waviness for the warp and weft yarn theoretically. However, it is difficult for these yarns keeping straight in composite, and the term "non-crimp 3D orthogonal woven" is always used to indicate the 3D woven composite with nearly straight in-plane yarn arrangement. Limited woven structures could be manufactured with the 3D weaving technology.

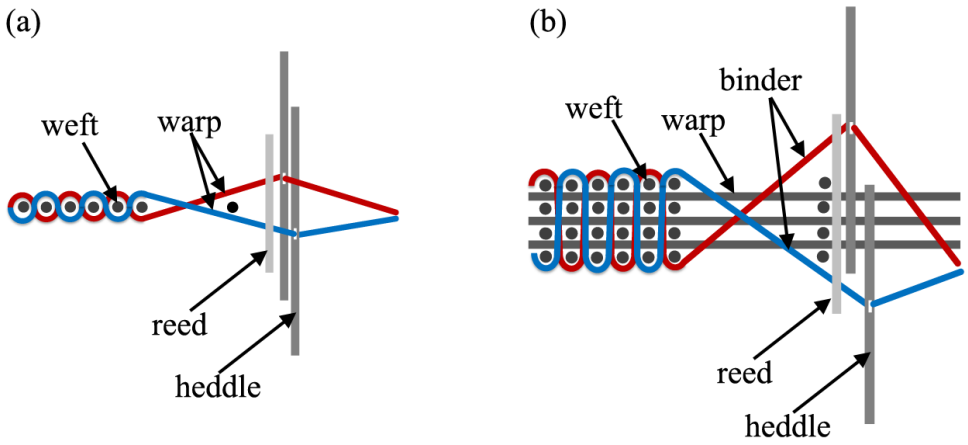

Fig. 1-4. Schematic of (a) 2D weaving and (b) 3D weaving.

Based on modified looms and machines

For some specific 3D woven structures, specially modified or designed weaving looms or machines are needed to manufacture them. For example, in Labanieh AR and cobwekers' research[42], multiaxial 3D woven structures could be manufactured based on a specific designed multiaxial 3D weaving loom, as shown in **Fig. 1-5**. A guide blocks technique which positioning the bias yarns in weaving zone is used to produce the multiaxial 3D woven structures, the warp yarn, bias yarn as well as binder yarn run in the direction of the weaving loom, whereas weft yarn (filler yarn) runs transversely from one side to the other side of the loom.

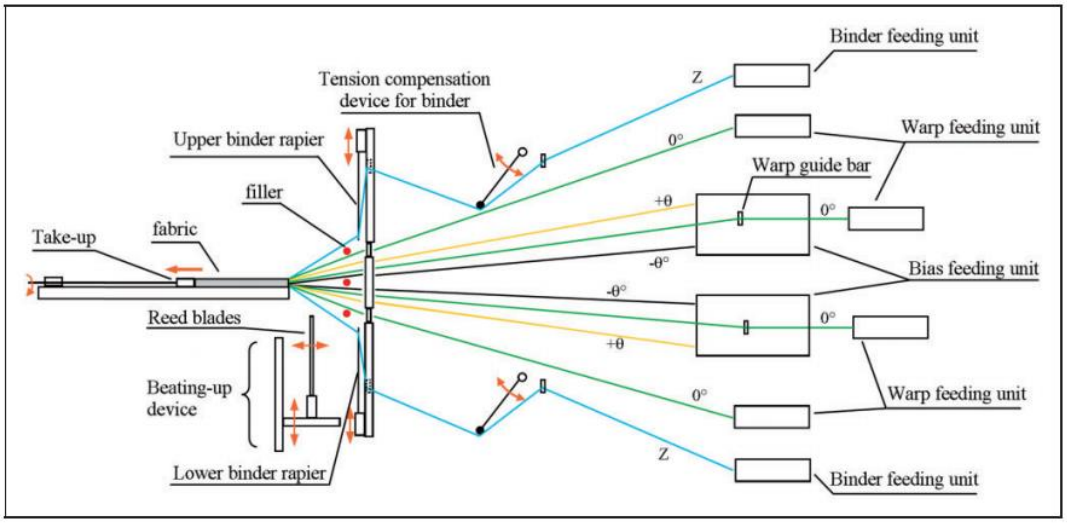

Fig. 1-5. Schematic view of multiaxial 3D weaving loom prototype illustrating the different weaving systems[42].

1.2.3 Woven structure and its mechanical performance

Woven structures have an obvious influence on the mechanical performance of the textile-reinforced composites, due to those yarns which carry most load in a composite, have different arrangement, waviness degree in different woven structures. For 3D woven reinforced composites, the existence of binder yarn in composite through-thickness direction increases the inter-layer strength significantly compared with laminated composites, and thus improves the out-of-plane mechanical performance, even though the resin pockets are easily appeared at the binder yarn and decrease the in-plane mechanical performance due to the stress concentration. There are many types of 3D woven composites which differ in fiber architecture, fiber type, fiber volume fraction, resin type, as well as manufacturing of textile reinforcement and fabrication of composites. It is difficult to draw conclusions that which structures super than others because of the complexity of woven structure. However, it is important to clarify the effect of 3D woven structure parameters on their mechanical performance. The weave parameters include yarn waviness, yarn density, binder yarn characters, and so on.

In-plane yarn waviness

Warp- and weft-yarn waviness in 3D woven composite could reduce in-plane properties, especially in compression. Yarn waviness could be caused by a range of factors including textile structural design, manufacturing-induced distortions, and so on. Many

researchers have studied the effect of yarn waviness of 3D woven composite on its mechanical properties. Mahadik, Y and coworkers[43] studied the effect of yarn waviness on compressive performance, and found that compression strength and failure mechanisms are very dependent on the highly crimped sections present in the direction of the load bearing yarns. Green, S.D. and coworkers[44] studied the effect of yarn waviness in 3D orthogonal woven composites on the tensile mechanical performance using a finite element analysis method. The results shows that yarn waviness level has a significant influence on the mechanical properties.

In-plane yarn density

In-plane yarn density influences the textile structural compaction and yarn waviness in 3D woven textiles. Higher yarn density increases the composite fiber volume content and decreases the resin rich regions. Dahale, M and coworkers[45] studied the effect of yarn density on the mechanical properties of 3D woven glass fiber-reinforced composites. 3D layer-to-layer woven structure composites with different weft-yarn densities were manufactured and tested. The results show that the mechanical properties were improved with increasing weft-yarn density by the decrease in waviness degree and misalignment of the load-carrying fibers. Higher weft-yarn density increases tensile and compressive properties in both warp and weft directions. Neale, G. and coworkers[46] studied the effect of yarn density on the crush energy absorption in 3D woven composites. 3D woven layer-to-layer interlock carbon fiber epoxy-resin composites with different weft-yarn densities were manufactured and tested. The results show that weft-yarn density increases the energy absorption, compression, and flexural properties.

Binder yarn characters

Binder yarn characters including yarn type, content, architecture, path, and so on, influence both out-of-plane and in-plane properties of 3D woven composites. This is due to that the binder yarn binds in-plane yarn layers into an integration and lies both in through-thickness direction and in-plane direction. The effect of binder yarns is complex due to the complexity of 3D woven structures. The binder yarn increases the out-of-plane mechanical performance of the 3D woven composites but decreases in-plane performance according to many researchers. Rudov-Clark, S. and coworkers[47] studied the effect of binder yarn volume content on the tensile fatigue properties of a 3D

orthogonal woven composite. The results show that the existence of binder yarns in 3D woven structures lower the fatigue properties (fatigue life and residual fatigue strength) compared to the 2D woven counterpart, and the fatigue properties of the 3D woven composites decrease with increasing of binder yarn content.

1.3 Research aims and objectives

The research aims and objectives of this dissertation mainly focus on developing advanced 3D woven textile-reinforced composite materials and clarifying the relationship between the woven structure and composite out-of-plane mechanical performance. A new weaving technology is introduced to manufacture glass /aramid fiber hybrid 3D woven textiles more efficiently and effectively based on a self-built 3D weaving loom. The optimal woven structure based on this new weaving technology is acquired to achieve good out-of-plane mechanical performance which may be suitable for specific engineering applications. Carbon fiber 3D/2.5D woven composites with special structural design in which binder yarn lies in weft direction, four structures having same yarn densities and different structural design were manufactured based on a traditional weaving technology. Some weave parameters could be drawn out for the future structural design to develop advanced 3D woven composites with better mechanical performance.

1.4 Outline of the dissertation

This dissertation is structured to provide a summary of “Study on development of 3D woven composites and their mechanical behavior”. There are six chapters in this dissertation.

In Chapter 1, an overview of fiber-reinforced composites, 3D woven textiles, relationship between woven structure and composite mechanical performance is presented.

In Chapter 2, a new weaving technology was designed and proposed to manufacture glass/aramid fiber hybrid 3D woven textiles based on a self-built 3D weaving loom with a modified heddle position system. Four typical 3D woven structures are manufactured with this new weaving system: layer-to-layer orthogonal woven (LLOW), through-thickness orthogonal woven (TTOW), layer-to-layer angle-interlock woven (LLAIW) and through-thickness angle-interlock woven (TTAIW). VARTM

technology was applied to fabricate 3D woven textile-reinforced composites and internal geometry of the developed composites was analyzed.

In Chapter 3, the quasi-static flexural performance of the glass/aramid fiber hybrid 3D woven composites developed in Chapter 2 was studied. Textile warp- and weft-direction beam specimens of each woven structure were tested under three-point bending to investigate their quasi-static flexural performance. Failure mode of the beam specimens was analyzed.

In Chapter 4, the dynamic flexural performance of the glass/aramid fiber hybrid 3D woven composites developed in Chapter 2 was studied. Composite plate specimens of each woven structure were tested under 10, 20 and 30 J low-velocity drop-weight impacts to investigate their impact resistance. Failure mode of the plate specimens was analyzed.

In Chapter 5, four types of carbon fiber 3D/2.5D woven composites with special structure design in which having same yarn densities in textile warp and weft directions and same composite fiber volume fraction, but different woven structures were developed based on a traditional weaving technology and VARTM technology; the quasi-static and dynamic flexural performance of these 3D/2.5D woven composites were studied. Failure mode of the composites was analyzed.

In Chapter 6, summary and conclusions of this dissertation are presented.

References

[1] Chand S. Review carbon fibers for composites. Journal of materials science. 2000;35:1303-13.

[2] Mohammed L, Ansari MN, Pua G, Jawaid M, Islam MS. A review on natural fiber reinforced polymer composite and its applications. International Journal of Polymer Science. 2015;2015.

[3] Joshi SV, Drzal L, Mohanty A, Arora S. Are natural fiber composites environmentally superior to glass fiber reinforced composites? Composites Part A: Applied Science and Manufacturing. 2004;35:371-6.

[4] Venkateshwaran N, Elayaperumal A. Banana fiber reinforced polymer composites-a review. Journal of Reinforced Plastics and Composites. 2010;29:2387-96.

[5] Shahzad A. Hemp fiber and its composites–a review. Journal of composite materials. 2012;46:973-86.
[6] Khalil HA, Bhat I, Jawaid M, Zaidon A, Hermawan D, Hadi Y. Bamboo fibre reinforced biocomposites: A review. Materials & design. 2012;42:353-68.
[7] Park C, Lee W. Compression molding in polymer matrix composites. Manufacturing techniques for polymer matrix composites (PMCs): Elsevier; 2012. p. 47-94.
[8] Peters ST. Composite filament winding: ASM International, 2011.
[9] Shahrubudin N, Lee TC, Ramlan R. An overview on 3D printing technology: Technological, materials, and applications. Procedia Manufacturing. 2019;35:1286-96.
[10] Ngo TD, Kashani A, Imbalzano G, Nguyen KT, Hui D. Additive manufacturing (3D printing): A review of materials, methods, applications and challenges. Composites part B: Engineering. 2018;143:172-96.
[11] Wang X, Jiang M, Zhou Z, Gou J, Hui D. 3D printing of polymer matrix composites: A review and prospective. Composites part B: Engineering. 2017;110:442-58.
[12] Mangalgiri P. Composite materials for aerospace applications. Bulletin of Materials Science. 1999;22:657-64.
[13] McIlhagger A, Archer E, McIlhagger R. Manufacturing processes for composite materials and components for aerospace applications. Polymer composites in the aerospace industry: Elsevier; 2015. p. 53-75.
[14] Mrazova M. Advanced composite materials of the future in aerospace industry. Incas bulletin. 2013;5:139.
[15] Elmarakbi A. Novel composite materials for automotive applications: concepts and challenges for energy-efficient and safe vehicles. 2015.
[16] Friedrich K, Almajid AA. Manufacturing aspects of advanced polymer composites for automotive applications. Applied Composite Materials. 2013;20:107-28.
[17] Mallick P. Advanced materials for automotive applications: An overview. Advanced materials in automotive engineering. 2012:5-27.
[18] Uddin N. Developments in fiber-reinforced polymer (FRP) composites for civil engineering: Elsevier, 2013.

[19] Awad ZK, Aravinthan T, Zhuge Y, Gonzalez F. A review of optimization techniques used in the design of fibre composite structures for civil engineering applications. Materials & design. 2012;33:534-44.
[20] Monaldo E, Nerilli F, Vairo G. Basalt-based fiber-reinforced materials and structural applications in civil engineering. Composite Structures. 2019;214:246-63.
[21] Scholz M-S, Blanchfield JP, Bloom L, Coburn BH, Elkington M, Fuller JD, et al. The use of composite materials in modern orthopaedic medicine and prosthetic devices: A review. Composites Science and Technology. 2011;71:1791-803.
[22] Sun LN, Deng Z. The carbon fiber composite materials application in sports equipment. Advanced Materials Research: Trans Tech Publ; 2012. p. 173-6.
[23] Uddin N, Vaidya U, Abro AM. Design and Analysis of Thermoplastic Composite Bridge Superstructures. University Transportation Center for Alabama; 2007.
[24] Nolan L. Carbon fibre prostheses and running in amputees: a review. Foot and ankle surgery. 2008;14:125-9.
[25] Chen X, Taylor LW, Tsai L-J. An overview on fabrication of three-dimensional woven textile preforms for composites. Textile Research Journal. 2011;81:932-44.
[26] Ansar M, Xinwei W, Chouwei Z. Modeling strategies of 3D woven composites: A review. Composite Structures. 2011;93:1947-63.
[27] Khokar N. 3D fabric-forming processes: distinguishing between 2D-weaving, 3D-weaving and an unspecified non-interlacing process. Journal of the Textile Institute. 1996;87:97-106.
[28] Khokar N. 3D-weaving: theory and practice. Journal of the Textile Institute. 2001;92:193-207.
[29] Gokarneshan N, Alagirusamy R. Weaving of 3D fabrics: A critical appreciation of the developments. Textile Progress. 2009;41:1-58.
[30] Bilisik K. Multiaxis three-dimensional weaving for composites: a review. Textile Research Journal. 2012;82:725-43.
[31] Bilisik K. Multiaxis three dimensional (3D) woven fabric. Advances in modern woven fabrics technology. 2011:79-106.
[32] Yan S, Zeng X, Long A. Experimental assessment of the mechanical behaviour of 3D woven composite T-joints. Composites part B: Engineering. 2018;154:108-13.

[33] Umair M, Shaker K, Javaid MU, Hussain M, Kashif M, Nawab Y. Effect of weaving patterns on damage resistance of 3D woven jointless T and H shaped reinforcements. Mechanics of Advanced Materials and Structures. 2020:1-14.
[34] Marsh G. Aero engines lose weight thanks to composites. Reinforced Plastics. 2012;56:32-5.
[35] Chen X. Advances in 3D textiles: Elsevier, 2015.
[36] Behera B, Dash B. An experimental investigation into structure and properties of 3D-woven aramid and PBO fabrics. The Journal of The Textile Institute. 2013;104:1337-44.
[37] Behera B, Dash B. Mechanical behavior of 3D woven composites. Materials & design. 2015;67:261-71.
[38] Zahid B, Chen X. Manufacturing of single-piece textile reinforced riot helmet shell from vacuum bagging. Journal of composite materials. 2013;47:2343-51.
[39] Mohamed M, Bogdanovich A. Comparative analysis of different 3D weaving processes, machines and products. Proceedings of the 17TH international conference on composite materials (ICCM-17)2009. p. 27-31.
[40] Rudov-Clark S, Mouritz A, Lee L, Bannister M. Fibre damage in the manufacture of advanced three-dimensional woven composites. Composites Part A: Applied Science and Manufacturing. 2003;34:963-70.
[41] Yu B, Bradley R, Soutis C, Hogg P, Withers P. 2D and 3D imaging of fatigue failure mechanisms of 3D woven composites. Composites Part A: Applied Science and Manufacturing. 2015;77:37-49.
[42] Labanieh AR, Legrand X, Koncar V, Soulat D. Development in the multiaxis 3D weaving technology. Textile Research Journal. 2016;86:1869-84.
[43] Mahadik Y, Hallett S. Effect of fabric compaction and yarn waviness on 3D woven composite compressive properties. Composites Part A: Applied Science and Manufacturing. 2011;42:1592-600.
[44] Green S, Matveev M, Long A, Ivanov D, Hallett S. Mechanical modelling of 3D woven composites considering realistic unit cell geometry. Composite Structures. 2014;118:284-93.
[45] Dahale M, Neale G, Lupicini R, Cascone L, McGarrigle C, Kelly J, et al. Effect of weave parameters on the mechanical properties of 3D woven glass composites. Composite Structures. 2019;223:110947.

[46] Neale G, Dahale M, Yoo S, Toso N, McGarrigle C, Quinn J, et al. Improved crush energy absorption in 3D woven composites by pick density modification. Composites part B: Engineering. 2020;192:108007.
[47] Rudov-Clark Sa, Mouritz A. Tensile fatigue properties of a 3D orthogonal woven composite. Composites Part A: Applied Science and Manufacturing. 2008;39:1018-24.

Chapter 2 Development of glass/aramid fiber hybrid 3D woven composites

2.1 Introduction

For many years, FRP composites have been widely used in automobile, aerospace, civil, and many other fields owing to their light weight, excellent mechanical performance, and easy manufacturing. Traditional laminated composites have a weak inter-laminar connection when subjected to transversal loading, and, as such, fiber or yarn is introduced in the through-thickness direction to improve out-of-plane mechanical strength. 3D textile structures with an additional yarn group in the through-thickness direction can be used to improve both the through-thickness strength and delamination resistance of composites. In essence, 3D textiles are defined as textiles with a 3D shape or with 3D inner-fiber interlacement [1]. Based on the latter, 3D woven structures can be classified into several structure groups, i.e., orthogonal, angle interlock, multilayer, through thickness, and layer-to-layer, and they can be fabricated with a conventional or modified weaving loom as well as with a 3D weaving loom. Unfortunately, manufacturing 3D woven textiles has several limitations due to the problems associated with weaving technologies, fiber properties, and textile structures [2, 3]. Various 3D woven structures have been manufactured based on a variety of weaving looms. In some research [4, 5], 3D woven textiles were manufactured on a traditional weaving loom, and, as such, yarn selection, density, and whole textile thickness and structure were limited. With respect to structure, TTOW textiles are mostly fabricated with a 3D weaving loom, whereas angle-interlock woven textiles are mostly fabricated with a traditional or modified weaving loom owing to their relative structural complexity. Research is currently lacking concerning angle-interlock woven structures fabricated with a 3D weaving loom because of weaving technology limitations.

In this chapter, a new weaving technology with a modified heddle position system based on a self-built 3D weaving loom is designed and proposed, and four typical 3D woven textile structures with different binder-yarn paths and undulations are designed and manufactured based on the said weaving technology for the first time.

2.2 3D woven textile manufacturing

2.2.1 Three-dimensional weaving loom

In a conventional 2D weaving process, as shown in **Fig. 2-1 (a)**, the warp yarn runs in the direction of the weaving loom, passes through the heddle eyes, and moves upwards or downwards with the heddle frames to form the shed, whereas the weft yarn runs transversely from one side to the other side of the loom and passes through the shed to interlace with the warp yarn to form a 2D textile. Only one shed is opened in each shedding process, and one group of weft yarn passes through in each weft insertion process. In contrast, for a traditional 3D weaving process, as shown in **Fig. 2-1 (b)**, the warp yarn and binder yarn run in the loom direction, and the weft yarn runs transversely from one side to the other side of the loom; the binder yarn passes through the heddle eyes and moves upwards or downwards with the heddle frames to form sheds. During the shedding process, the warp yarn is stable; moreover, there are several warp-yarn layers, and, as such, several sheds can be formed simultaneously. In the weft insertion process, weft yarn passes through the sheds to form a 3D textile.

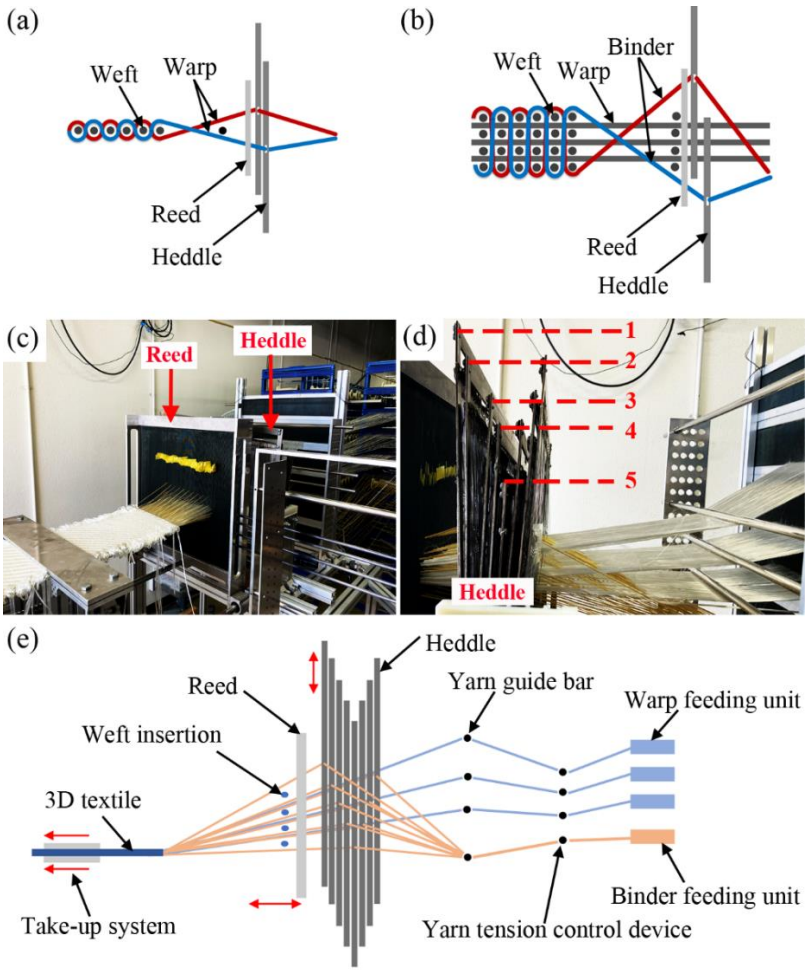

Fig. 2-1. Illustration of **(a)** two-dimensional and **(b)** three-dimensional weaving. **(c)** Self-built 3D weaving loom and **(d)** heddles in different positions in the modified heddle position system. **(e)** Schematic view of the self-built 3D weaving loom.

On a traditional 3D weaving loom without heddle position modification, the heddle frames only have two statuses, i.e., lifted and nonlifted, which correspond to the same two positions in the shedding process of a 2D weaving loom. In this weaving system, only parts of 3D woven structures can be manufactured owing to the limitations associated with heddle-frame positioning. For the present study, a modified heddle-frame position system based on a self-built 3D weaving loom was developed, which is shown in **Fig. 2-1 (c)** and **(d)**. The schematic view of the 3D weaving loom is depicted in **Fig. 2-1 (e)**, eight heddle frames were used, and the frames could stop at five positions to form four sheds in each shedding process for the designed 3D woven structures, four layers of weft yarn could pass through the sheds at the same time and allow the binder yarns to bind several layers of weft yarns to form different woven structures. The

weaving technology for the TTAIW structure is shown in **Fig. 2-2**. The eight heddle frames were in different positions in each shedding process to ensure that the eight binder-yarn groups were layered appropriately. Different from the traditional weaving technology, which is based on a weave diagram that defines the warp- and weft-yarn interlacing, heddle position information is required for 3D weaving to define the binder-yarn position in each shedding process. For a TTAIW structure, the heddle position information of eight shedding in one weave repeat is listed in **Table 2-1**.

Table 2-1. Heddle position information in one weave repeat of a through-thickness angle-interlock woven.

Shedding	Heddle 1 position (Binder 1)	Heddle 2 position (Binder 2)	Heddle 3 position (Binder 3)	Heddle 4 position (Binder 4)	Heddle 5 position (Binder 5)	Heddle 6 position (Binder 6)	Heddle 7 position (Binder 7)	Heddle 8 position (Binder 8)
First	1	2	3	4	5	4	3	2
Second	2	1	2	3	4	5	4	3
Third	3	2	1	2	3	4	5	4
Fourth	4	3	2	1	2	3	4	5
Fifth	5	4	3	2	1	2	3	4
Sixth	4	5	4	3	2	1	2	3
Seventh	3	4	5	4	3	2	1	2
Eighth	2	3	4	5	4	3	2	1

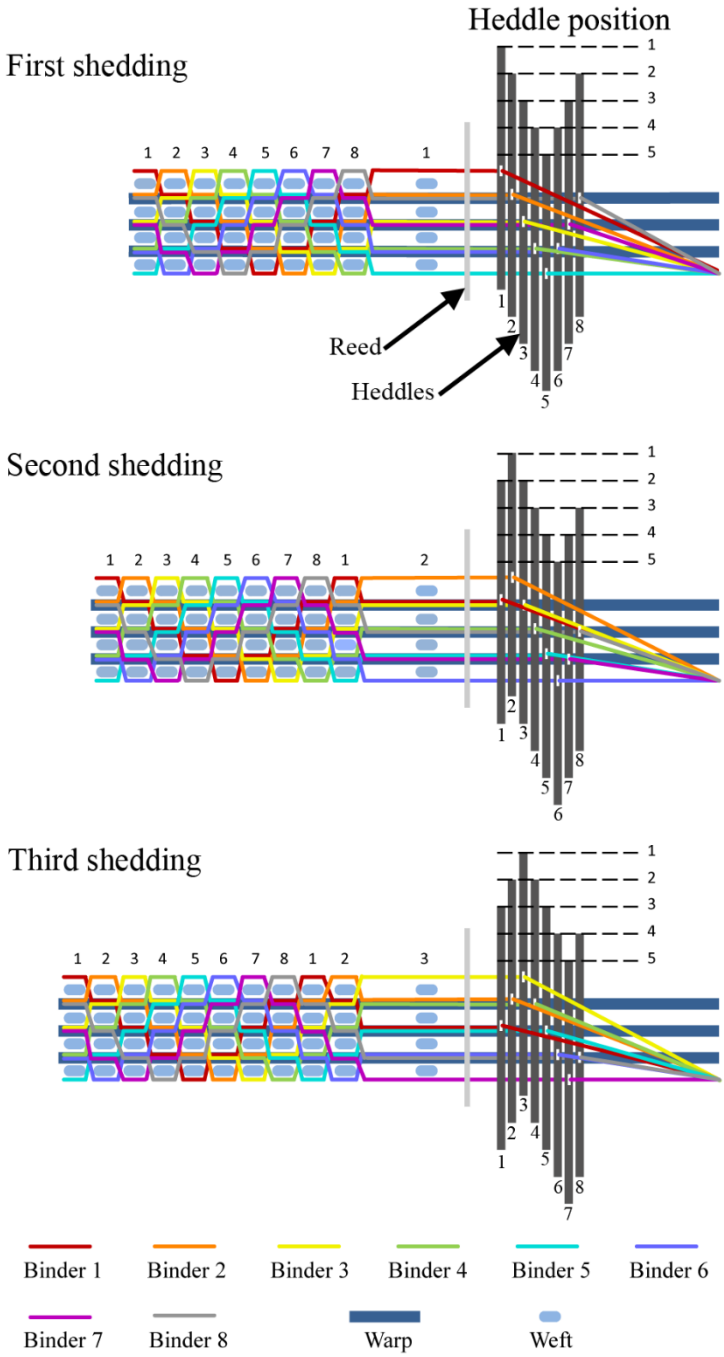

Fig. 2-2. Heddle position in the first three shedding processes for through-thickness angle-interlock woven.

There are several advantages for the proposed modified heddle position system. More types of 3D woven structures can be effectively and efficiently manufactured. It provides possibilities for manufacturing complex 3D woven textiles such as textile preforms for composite fan blade applications based on the modified heddle position system. Compared with Jacquard weaving technology, the modified 3D weaving may be

more suitable for manufacturing 3D woven textiles with greater thickness and larger structural integrity due to its primary 3D weaving benefits. In a traditional weaving loom, warp yarn passes through the heddle eyes and moves upwarps and downwards to form the shed for angle-interlock and layer-to-layer structure manufacturing, but, in the modified weaving system, it is not necessary for the warp yarn to pass through the heddle eyes and the warp yarns keep stable in weaving process for all designed woven structures, and thus, yarn damage/degradation decreases, especially for brittle yarn such as glass or carbon fiber. Moreover, compared with traditional weaving system, less heddle frames are needed based on this modified weaving system to weave complicated structures such as angle-interlock structures and layer-to-layer structures, due to that the warp yarns do not need to pass through the heddle eyes during weaving as mentioned previously.

2.2.2 Three-dimensional textile structures

Six woven structures, i.e., LLOW-1, LLOW-2, TTOW, LLAIW-1, LLAIW-2, and TTAIW, were fabricated under similar weaving conditions (such as warp-, weft-, and binder-yarn tension) and with a comparable yarn density. For all designed 3D woven structures, there are three layers of warp yarn and four layers of weft yarn, and the yarn arrangement in the warp direction is three warp yarns (one warp yarn in each layer) followed by one binder yarn. In orthogonal-woven structures, the binder yarn is perpendicular to the warp and weft yarn theoretically, and, in angle-interlock woven structures, binder yarns have an angle smaller than 90 degrees from the warp direction as designed. Moreover, in through-thickness woven structures, all four weft-yarn layers are bounded from the top to the bottom layer by the binder yarn, whereas, in layer-to-layer woven structures, two or three weft-yarn layers are bounded. Accordingly, in this study, for the layer-to-layer woven structures, both layer numbers are used: two adjacent weft-yarn layers are bonded together for LLOW-1 and LLAIW-1, and three adjacent weft-yarn layers are bonded together for LLOW-2 and LLAIW-2. **Fig. 2-3** shows 3D models, weft-z and warp-z diagrams in one unit cell of the six 3D woven textiles. The unit cell sizes vary because of structural differences. For instance, there are 24 warp yarns, 32 weft yarns, and 8 binder yarns in one unit for TTAIW and 6 warp yarns, 8 weft yarns, and 2 binder yarns in one unit for TTOW. E-glass fiber (1150tex, RS 110 QL-520, Nitto Boseki Co., Japan) was used for the warp and weft yarn, and aramid

fiber (330tex, Kevlar® 29, Du Pont-Toray Co., Japan) was used for the binder yarn. The 3D hybrid woven textiles were produced with comparable yarn density and textile-area density; the warp-yarn density is roughly 3.5 ends/cm/layer, the binder-yarn density is roughly 3.5 ends/cm, and the weft-yarn density is roughly 2.0–3.6 picks/cm/layer. Surface top-view photographs of the six 3D woven textiles are shown in **Fig. 2-4.**

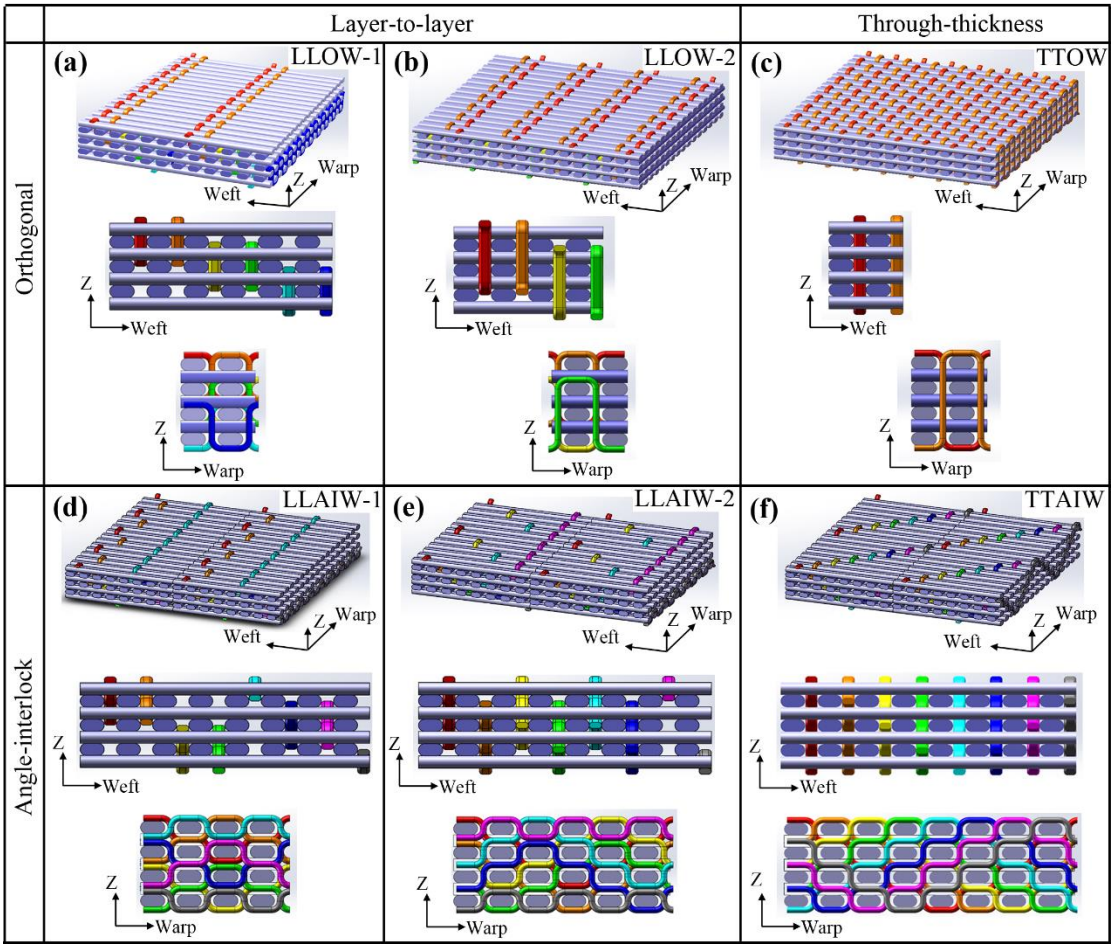

Fig. 2-3. Three-dimensional models, weft-z and warp-z schematic diagrams: **(a)** LLOW-1, **(b)** LLOW-2, **(c)** TTOW, **(d)** LLAIW-1, **(e)** LLAIW-2, and **(f)** TTAIW.

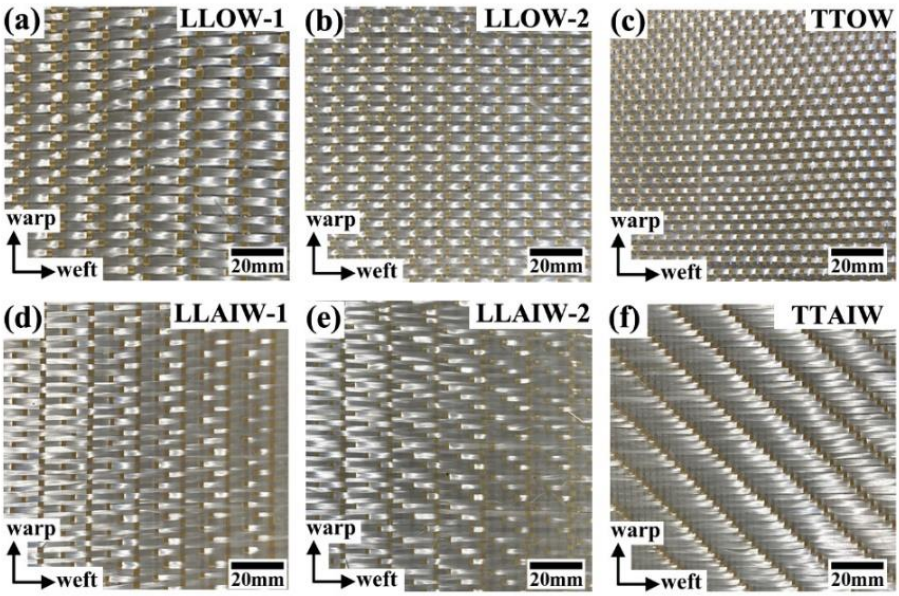

Fig. 2-4. Surface top-view photographs of **(a)** LLOW-1, **(b)** LLOW-2, **(c)** TTOW, **(d)** LLAIW-1, **(e)** LLAIW-2, and **(f)** TTAIW.

2.3 3D woven composite fabrication

Thermoset epoxy resin and a hardener (DENATITE XNR6815 and DENATITE XNH6815, Nagase ChemteX Co., Japan) were used for the composite matrix. The textiles were infused within a vacuum bag using VARTM technology. The schematic and experimental set-up of VARTM technology is depicted in **Fig. 2-5**. The epoxy resin and hardener were heated separately at 40°C in an oven and then mixed with a weight ratio of 100:27. The mixed resin was pumped into the vacuum bag with a vacuum pump, and the pressure was about one bar. After infusion, the composite was cured within the sealed vacuum bag for 24 h at room temperature. The normalized parameters of the six 3D woven textiles and textile-reinforced composites are summarized in **Table 2-2**. The composite fiber volume fraction was calculated by a resin burn-off method.

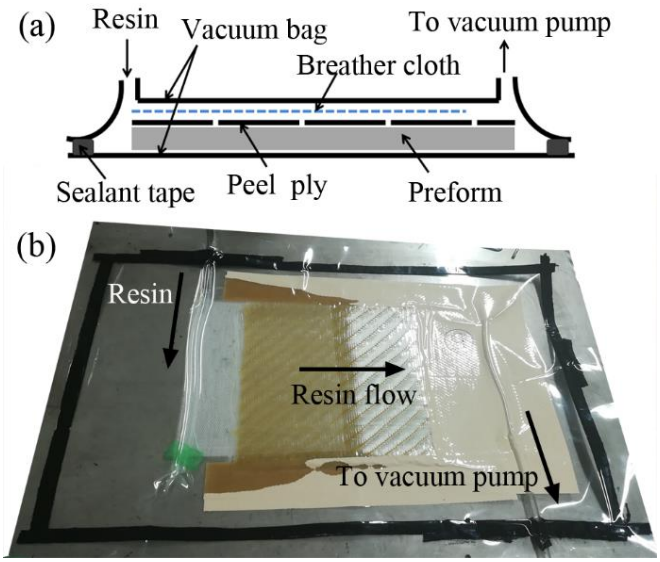

Fig. 2-5. (a) Schematic and **(b)** experimental set-up of VARTM technology.

Table 2-2. Normalized parameters of the three-dimensional woven textiles and reinforced composites.

Textile group	**LLOW**		**TTOW**	**LLAIW**		**TTAIW**
Textile ID	**LLOW-1**	**LLOW-2**	**TTOW**	**LLAIW-1**	**LLAIW-2**	**TTAIW**
Dry textile thickness (mm)	3.26	3.04	2.72	2.98	3.25	3.20
Dry textile areal density (kg/m^2)	3.00	2.53	2.49	3.32	3.51	3.24
No. of warp yarn in one repeat unit	18	12	6	24	24	24
No. of binder yarn in one repeat unit	6	4	2	8	8	8
No. of weft yarn in one repeat unit	8	8	8	16	24	32
Composite thickness (mm)	2.73	2.73	2.83	2.40	2.71	2.49
Composite fiber volume fraction	0.40	0.36	0.34	0.48	0.49	0.47

2.4 Internal geometry of 3D woven composites

Internal geometry of the 3D woven composites is shown in **Figs. 2-6** and **2-7**. Obvious geometrical differences can be observed for the following parameters: binder-yarn path, undulation angle, and cross-section shape; warp- and weft-yarn waviness, distribution, and cross-section shape; and resin-pocket shape and distribution. All woven structures have relative uniform weft-yarn distribution. This is mainly because the binder yarn is perpendicular to the weft yarn, and, therefore, the weft yarn does not exhibit large shifting, at the same time, binder yarn is parallel to the warp yarn, and adjacent warp yarns shift and attach to each other easily if there is no binder yarn between them in layer-to-

layer woven group. The warp-yarn shift has an influence on the weft-yarn straightness. For instance, for LLOW and LLAIW, the weft yarn, especially the central two layers, has an obvious waviness owing to warp-yarn shifting. It should be noted that the binder yarn also influences the weft-yarn waviness, particularly at the interlaced part. Among all woven structures, the through-thickness woven structures have relative uniform warp- and weft-yarn distribution and cross-section shape, which is mainly because the binder yarn has a consistent path in these 3D woven textile systems: it moves in the through-thickness direction and binds weft-yarn layers from top to bottom, thereby securing structural uniformity.

As shown in **Fig. 2-6**, the binder-yarn peak span corresponds to one unit cell along the warp direction (Lx) in each woven structure. In **Fig. 2-7**, the arrows correspond to one unit cell along the weft direction (Ly) in each woven structure. The binder-yarn weave length (L) and height (h), the undulation degree is measured, in which undulation degree of binder-yarn is defined as the largest angle form warp direction in this study; a larger angle means a larger binder yarn undulation. **Table 2-3** shows the internal geometry of the six 3D woven composites, from which it is evident that the TTAIW structure has the largest real unit cell size, followed by LLAIW, LLOW, and TTOW. Moreover, the TTOW structure has the largest binder-yarn undulation, followed by LLOW-2, TTAIW, LLOW-1, LLAIW-2, and LLAIW-1. For both LLOW and LLAIW, the binder yarn that binds three weft-yarn layers has a larger undulation than has the binder yarn binding two weft-yarn layers.

The angle-interlock woven structures have the largest weft-yarn density values and thus exhibit a larger composite fiber volume fraction than do the orthogonal-woven structures, which can be attributed to structural differences and weaving condition limits. For TTOW, the binder yarn binds weft-yarn layers from top to bottom, and two adjacent binder yarns move in opposite directions in each shedding process, which means it undergoes the largest tension during the weaving process, and, as such, it is difficult to obtain a large weft-yarn density. Alternatively, for layer-to-layer and angle-interlock structures, the binder yarn binds two or three adjacent weft-yarn layers in two continuous shedding processes, which reduces the binder-yarn tension and increases the weft-yarn density. The angle-interlock woven structures have a weft-yarn density that is roughly 1.5 times larger than that of orthogonal-woven structures, as well as a

composite fiber volume fraction that is roughly 1.3 times larger. The effective binding density is defined as the number of interlaced parts between the effective binder yarn (binding two or more weft yarn layers) and the surface-weft yarn per unit area. The effective binding density is used to compare the binding condition among the woven structures. For LLAIW-1 and LLAIW-2, there are two binder yarns only interlacing the surface-weft yarn layers in one repeat unit for the necessary structural design, which is expected as it is not going in the through-thickness direction and is defined as ineffective binder yarn. The angle-interlock group has a smaller effective binding density than has the orthogonal group, as shown in **Fig. 2-4** and **Table 2-3**. This means that angle-interlock woven structures have less effective binder/surface-weft yarn binding parts than have the orthogonal woven structures.

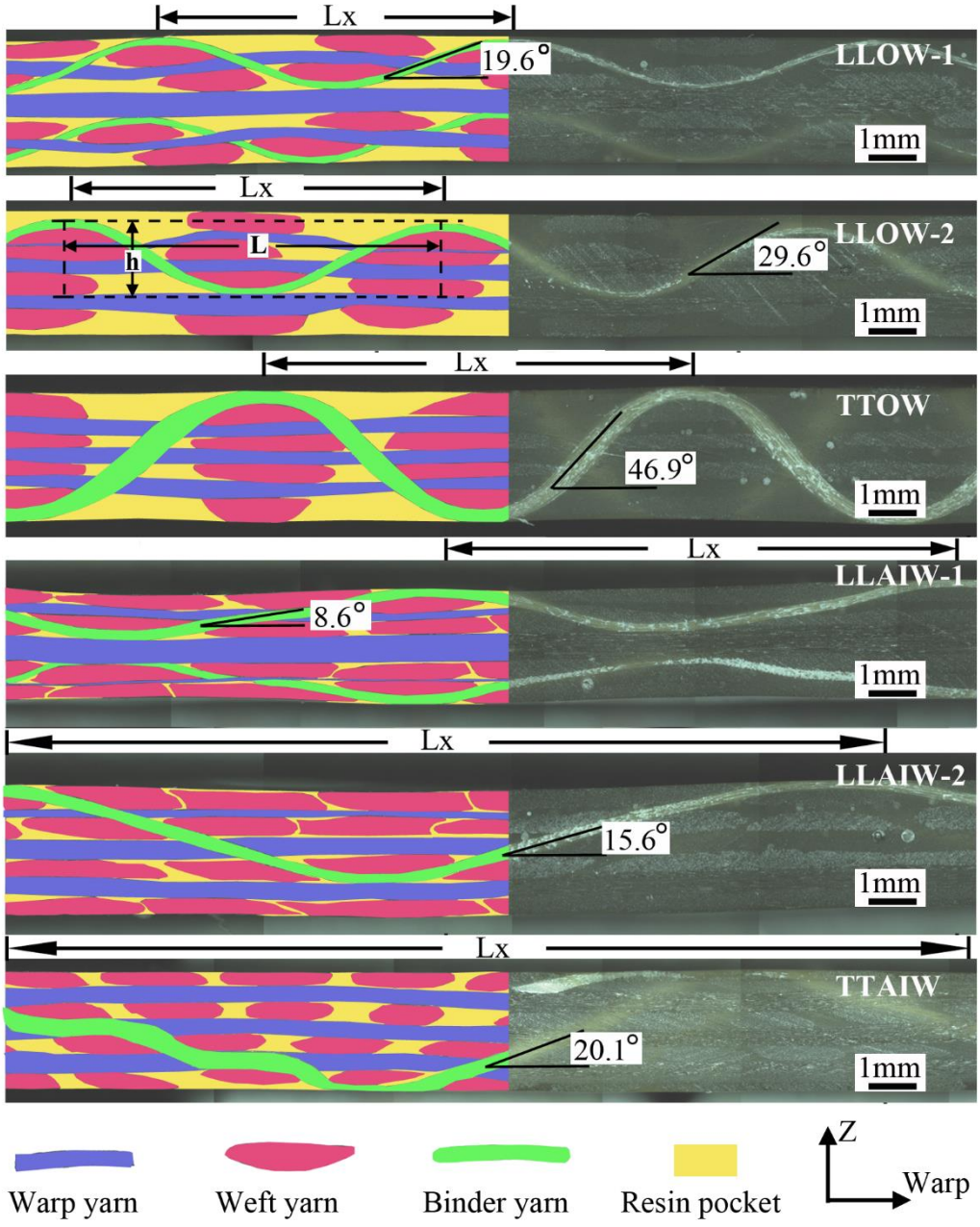

Fig. 2-6. Internal geometry of three-dimensional woven composites (parallel to the warp direction).

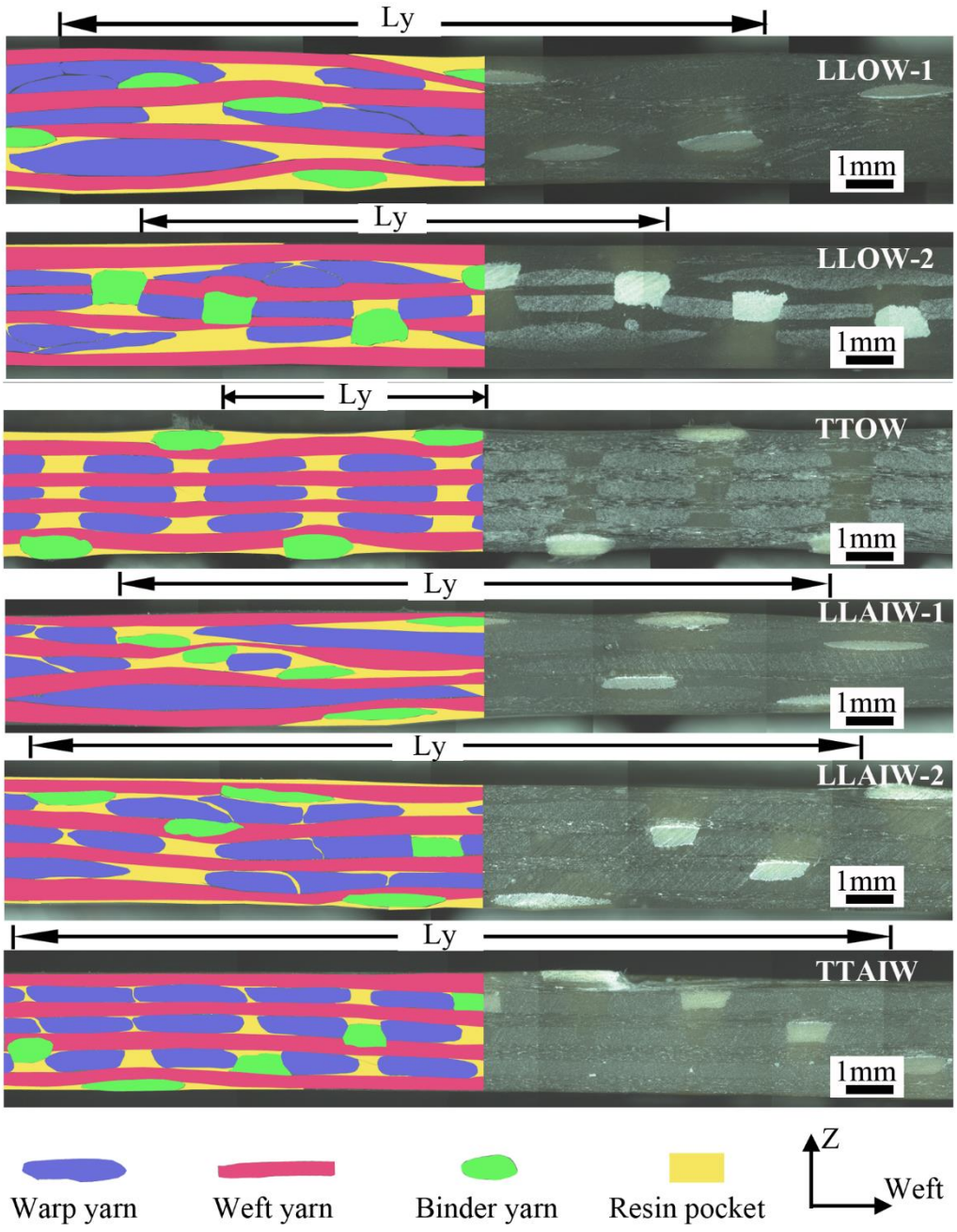

Fig. 2-7. Internal geometry of three-dimensional woven composites (parallel to the weft direction).

Table 2-3. Internal geometry information of three-dimensional woven composites.

Textile group	**LLOW**		**TTOW**	**LLAIW**		**TTAIW**
Textile ID	**LLOW-1**	**LLOW-2**	**TTOW**	**LLAIW-1**	**LLAIW-2**	**TTAIW**
Warp-yarn density (ends/cm/layer)	3.6	3.5	3.5	3.5	3.6	3.6
Binder-yarn density (ends/cm)	3.6	3.5	3.5	3.5	3.6	3.6
Weft-yarn density (picks/cm/layer)	2.8	2.4	2.0	3.6	3.6	3.4
Real unit size (mm^2)	7.1 × 16.6	8.2 × 11.3	9.8 × 5.6	11.2×22.8	16.5 × 22.4	23.5 × 22.3
Binder-yarn weave length (mm)	7.1	8.2	9.8	11.2	16.5	23.5
Binder-yarn weave height (mm)	1.2	2.0	2.8	1.0	2.2	2.5
Binder-yarn undulation angle	19.6°	29.6°	46.9°	8.6°	15.6°	20.1°
Effective binding density (cm^{-2})	1.68	2.75	3.51	0.77	1.13	1.62

Overall, LLAIW-1, LLAIW-2, and TTAIW have the smallest binder-yarn undulation angle and the largest composite fiber volume fraction, and, as such, compared with those of LLOW-1, LLOW-2, and TTOW.

2.5. Conclusions

In this chapter, a new weaving technology with heddle position modification based on a self-built 3D weaving loom was designed and introduced to develop four typical 3D woven structures: LLOW, TTOW, TTAIW, and LLAIW. The new weaving technology has great potential for manufacturing various 3D woven structures effectively and efficiently. VARTM was applied to fabricate the designed glass/aramid fiber hybrid 3D textile-reinforced epoxy-resin composites. Internal geometry of the 3D woven composites was observed by an optical microscopy. Based on the proposed weaving system, the angle-interlock woven structures have the largest weft-yarn density (roughly 1.5 times larger than that of the orthogonal structures) and composite fiber volume fraction (roughly 1.3 times larger than that of the orthogonal structures). The through-thickness woven structures have a relative uniform yarn distribution than have the layer-to-layer

woven structures. In particular, the TTAIW is the optimal design based on this weaving system, and this structure could achieve larger weft-yarn density and has a uniform warp, weft, and binder yarn distribution at the same time. A further modification is needed to achieve higher weft-yarn density for orthogonal woven structures based on this weaving system.

References

[1] Chen X, Taylor LW, Tsai L-J. An overview on fabrication of three-dimensional woven textile preforms for composites. Textile Research Journal. 2011;81:932-44.

[2] Khokar N. 3D-weaving: theory and practice. Journal of the Textile Institute. 2001;92:193-207.

[3] Chen X. Advances in 3D textiles: Elsevier, 2015.

[4] Behera B, Dash B. An experimental investigation into structure and properties of 3D-woven aramid and PBO fabrics. The Journal of The Textile Institute. 2013;104:1337-44.

[5] Zahid B, Chen X. Manufacturing of single-piece textile reinforced riot helmet shell from vacuum bagging. Journal of Composite Materials. 2013;47:2343-51.

Chapter 3 Quasi-static flexural performance of glass/aramid fiber hybrid 3D woven composites

3.1 Introduction

For 3D textile-reinforced composites, the flexural mechanical performance and failure mode are complex because of the anisotropic characteristics. Different failure modes can yield simultaneously or successively under various loadings until the composite structure fails. Out-of-plane loading is more likely than any other loading type to introduce delamination failure in fiber-reinforced composites, and thus it is important to study the transversal loading behavior and its failure modes on 3D woven-structure textile-reinforced composites.

Many researchers have examined the influence of design parameters on flexural performance and failure modes, such as reinforcement density, binder-yarn path and undulation, number of warp- and weft-yarn layers, and yarn arrangement. Pankow [1] studied the flexural response of 3D woven textile composite panels with two woven-structure types using the end notch flexural test and found that textile structure has a clear influence on crack propagation and failure mode under flexural loading. Turner [2] studied the effect of through-thickness reinforcement density on the collapse behavior of a 3D TTOW composite under out-of-plane bending. Gerlach [3] studied the effect of binder-yarn volume fraction on the through-thickness properties of a 3D TTAIW composite and found that a high binder-yarn volume fraction increases the delamination resistance under transversal loading. Behera [4, 5] studied the mechanical behavior of 3D woven composites and 2D laminated composites and found that the former has considerably superior out-of-plane mechanical properties; however, only 3D through-thickness angle-interlock and 3D through-thickness orthogonal structures were compared with their 2D laminate counterparts, and the layer-to-layer woven structure was not reported. Zhang [6] examined various hybrid structures with different percentages and layups of the constituent fibers in a 3D orthogonal-woven composite subjected to flexural loading. Other researchers [7, 8] have examined small sections of 3D woven structures to clarify the relationship between the woven structure and its mechanical properties under transversal loading. Many researchers have studied the flexural performance of 3D textile composites with various structure and weaving parameters, the results of which suggest that weaving pattern seriously influences mechanical

properties. Unfortunately, research is lacking concerning systematic comparisons of the four typical 3D woven structures, i.e., LLOW, LLAIW, TTOW, and TTAIW, and the flexural properties and failure modes under transversal loading among the four main 3D woven structures both need to be clarified. In this chapter, the quasi-static flexural properties of the hybrid glass/aramid 3D woven textile-reinforced epoxy-resin composites are systematically investigated as well as the relationship between woven structure, flexural mechanical performance, and failure mode.

3.2 Materials and experiments

3.2.1 Materials

The 3D woven textile-reinforced composites, i.e., LLOW-1, LLOW-2, TTOW, LLAIW-1, LLAIW-2, and TTAIW, which are developed in Chapter 2, were used to test their quasi-static flexural performance.

3.2.2 Three-point bending test

The 3D woven textile-reinforced composite specimens underwent three-point bending tests at room temperature, the schematic and experimental setup of which are shown in **Fig. 3-1**. The beam specimens had a length of 110 mm, a width of 25 mm, and a thickness of roughly 2.4–2.8 mm. Three warp-direction beam specimens were tested as well as three weft-direction beams for each textile-structure composite. A universal testing machine (AG-20kND, Shimadzu Co., Japan) with a 20-kN load cell was used. The support span was 80 mm long with a loading-nose diameter of 10 mm, and a loading-nose displacement speed of 5 mm/min was applied until beam failure occurred. Optical microscopy was applied to observe and analyze internal structural failure after flexural testing.

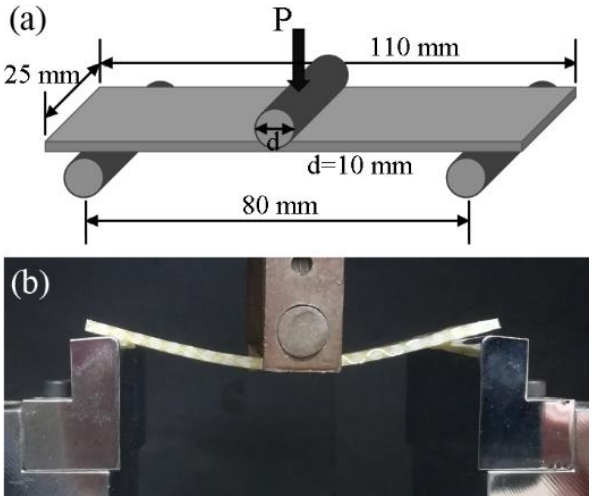

Fig. 3-1. (a) Schematic and **(b)** experimental setup for three-point bending test.

3.3 Results and discussion

3.3.1 Mechanical properties

In this study, the support span-to-thickness ratio of the beam specimens was greater than 16, and the deflection was larger than 10% of the support span. Stress was calculated by Eq. (3-1) to correct the end forces at the support noses, and strain was calculated by Eq. (3-2) in accordance with ASTM D790 [9]:

$$\sigma = (3PL/2bd^2)[1 + 6(\delta/L)^2 - 4(d/L)(\delta/L)] \quad (3\text{-}1)$$

$$\varepsilon = 6\delta d/L^2 \quad (3\text{-}2)$$

where σ denotes the stress on the outer surface at the midspan, P denotes the applied force, L denotes the support span, b denotes the beam width, d denotes the beam thickness, ε denotes the maximum strain in the outer surface, and δ denotes the midspan deflection.

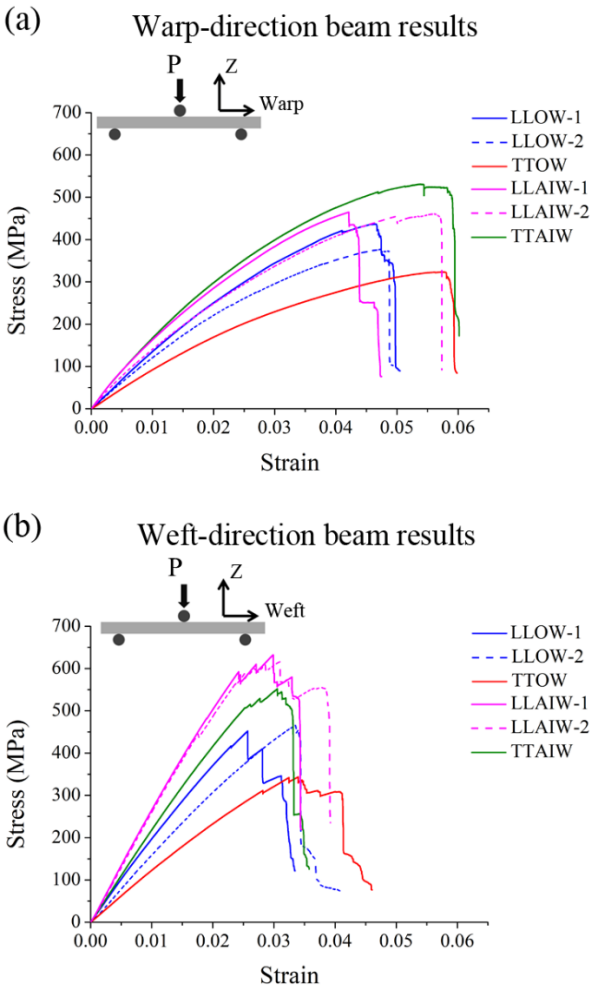

Fig. 3-2. Representative flexural stress–strain curves of three-dimensional woven composites under three-point bending: **(a)** warp-direction beam results and **(b)** weft-direction beam results.

Fig. 3-2 shows representative flexural stress–strain curves of the six 3D woven composites along warp and weft directions. It is evident that all types of 3D woven composites exhibit linear stress–strain behavior at the beginning of loading; nonlinear behavior can be observed after a strain of roughly 0.005 and 0.02 for specimens along the warp and weft directions, respectively. Warp-direction beams exhibit ductile behavior, whereas weft-direction beams exhibit brittle behavior. This may be due to geometrical differences between the warp- and weft-direction beams. In the warp-direction composite beam shown in **Fig. 3-3 (a)**, three layers of warp and binder yarns are in the beam length direction, and four layers of weft yarn are in the beam width direction. In the weft-direction composite beam shown in **Fig. 3-3 (b)**, four layers of weft yarn are in the beam length direction, and three layers of warp and binder yarns are in the beam width

direction. During three-point bending, yarns in the beam length direction mainly carry tensile load at outer layers and carry compression load at inner layers, yarns in the beam width direction mainly carry shear load. Compared with the warp-direction beam, the weft-direction beam has an additional yarn layer in the beam length direction, at the same time, two of the beam-length yarn layers are on the beam surface where the maximum stress and strain occurred, and, as such, it has an enhanced load-carrying ability, especially for bending loads.

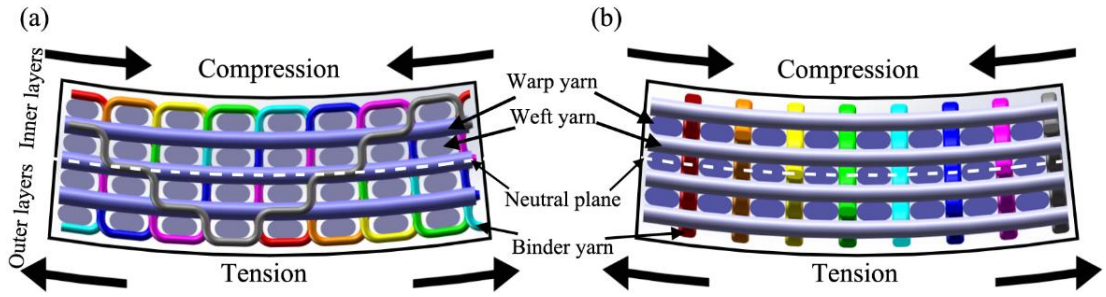

Fig. 3-3. TTAIW composite beam model under three-point bending test: **(a)** warp-direction beam and **(b)** weft-direction beam.

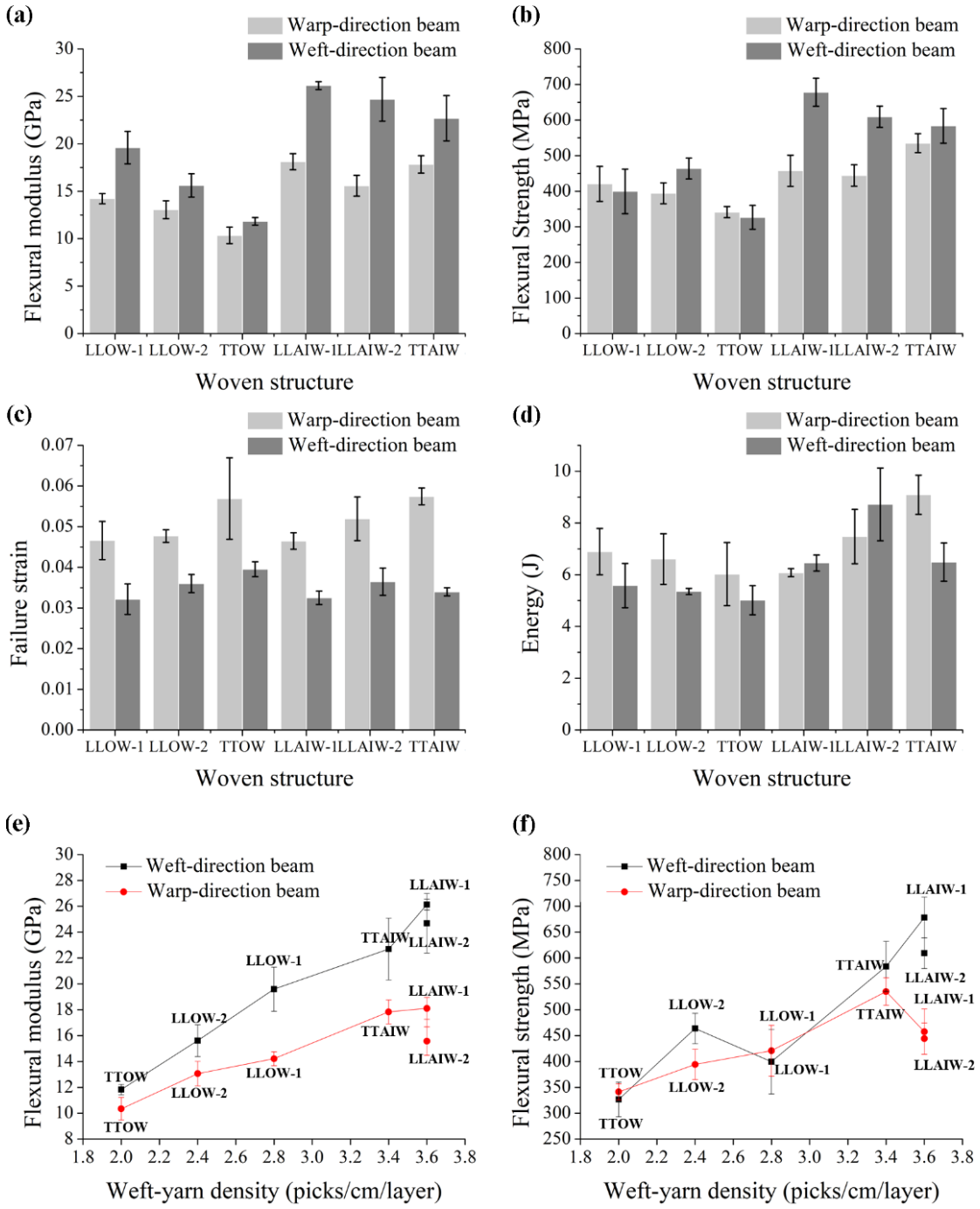

Fig. 3-4. Flexural property information under three-point bending: **(a)** flexural modulus, **(b)** flexural strength, **(c)** failure strain, **(d)** deformation energy, **(e)** relationship between flexural modulus and weft-yarn density, and **(f)** relationship between flexural strength and weft-yarn density.

The flexural modulus is the modulus at the initial loading stage, during which the beam undergoes minimal deflection, and the yarns in composite beam length direction may contribute more to the modulus. The weft-direction composite beams have a larger

flexural modulus than have the warp-direction composite beams for all woven structures, which can be attributed to geometrical differences between the warp- and weft-direction beams as mentioned previously. The angle-interlock woven structures have a larger flexural modulus than have the orthogonal-woven structures for both warp- and weft-direction beams, as shown in **Fig. 3-4 (a)**, and this is mainly due to that there is a larger weft yarn density and fiber volume fraction accordingly for angle-interlock woven structures. As shown in **Fig. 3-4 (e)**, the flexural modulus increases with an increase in weft-yarn density for both weft- and warp-direction beams; this tendency is more evident for the orthogonal-woven structures. For weft-direction beams, a higher weft-yarn density corresponding to the increased number of load-bearing yarns in the beam length direction, increases the flexural modulus. For warp-direction beams with a similar warp-yarn density, the increased weft-yarn density corresponds to the increased composite fiber volume fraction and enhances the flexural modulus. In angle-interlock woven group, LLAIW-1 and LLAIW-2 have similar weft-yarn density and composite fiber volume fraction, but LLAIW-1 has a larger flexural modulus, which can be attributed to its superior structure, and the binder yarn may also play a key role. The binder yarn for LLAIW-1 has a smaller undulation angle (8.6°) compared with LLAIW-2 (15.6°), which means that the binder yarn for LLAIW-1 is in more laying in in-plane direction and undergoes increased tension during bending.

The flexural strength is the largest load-carrying ability until beam failure occurs, at which the beam undergoes relatively large deflection, and all yarn layers may contribute to the flexural strength. A similar failure mechanism was observed during the three-point bending test for fiber-reinforced composites: compression-side yarn kink-band failure developed first, followed by fiber-tow rupture failure in the tension side, where yarn kink-band failure refers to small load drops and tensile-side fiber-tow rupture failure refers to a final large load drop [10]. There are several obvious small load drops before the final large load drop for weft-direction composites, as shown in **Fig. 3-2 (b)**; this may because of that in a weft-direction beam, two of the weft yarn layers are on the beam surface, inner surface weft-yarn kinking failures happened first and then followed by the outer surface weft-yarn cracking failure. For warp-direction beams, three layers of warp yarn and binder yarn are in the beam length direction, and the warp yarn is not on the beam surface, which means that yarn kink-band failure is unlikely compared with weft-direction beams, and, thus, there are no obvious small load drops before

the final load drop in the flexural stress–strain figures shown in **Fig. 3-2 (a)**. The angle-interlock woven structures have a larger flexural strength than have the orthogonal-woven structures, perhaps owing to the higher weft-yarn density and structural superiority. As shown in **Fig. 3-4 (f)**, there is no clear tendency between flexural strength and weft-yarn density, especially for weft-direction beams; thus, the woven structure may contribute more to the flexural strength.

The energy required for beam failure is referred to as the composite-failure resistance and was calculated from the area under the load–deflection curves. The warp-direction beams exhibit a smaller bending load but larger deflection than do weft-direction beams for all structures, and accordingly larger failure strain for warp-direction beams, as shown in **Fig. 3-4 (c)**. Basically, angle-interlock woven structures have larger deformation energy than have orthogonal woven structures, as shown in **Fig. 3-4 (d)**. TTAIW has the largest composite-failure resistance along warp direction.

Overall, LLAIW-1, LLAIW-2, and TTAIW have the smallest binder-yarn undulation angle and the largest composite fiber volume fraction, and, as such, compared with those of LLOW-1, LLOW-2, and TTOW, their flexural strength and modulus are larger by 50% and 40%, respectively. The flexural modulus is more sensitive to weft-yarn density and composite fiber volume fraction, whereas the flexural strength is more sensitive to woven structure. Indeed, a smaller binder-yarn undulation angle may have increased the tensile strength for warp-direction composites during three-point bending [11].

3.3.2 Failure modes

Fig. 3-5 shows strong-light background photographs of warp- and weft-direction beam specimens of six woven types after flexural test. Sunlight was used as the strong-light source positioned behind the specimens and the concave surface of the composite beams was facing the camera. The transparent part is the area without failures, and the opaque part (dark part) is the area with failures due to the transparent characteristic of glass fiber and epoxy resin matrix as well as refraction and reflection of light. Failures such as yarn debonding and delamination will introduce serious refraction and reflection of light, corresponding to the dark pixels in strong-light background photographs, the darker pixels, the more serious failures. Obvious failures can be observed at the

center of the warp- and weft-direction beams for all woven types as shown in **Fig. 3-5 (a)**. This is expected as the beam center where was the contact area for the loading nose during the three-point bending test, and, as such, tensile and compressive stress are both at a maximum and failures easily occur. For the warp-direction composite beams, obvious propagating failures can be observed beyond the center areas, spreading along the weft-yarn direction (beam-width direction) as shown in **Fig. 3-5 (b)**; for weft-direction composite beams, the failures are mostly localized at the center area, beyond which there are no obvious propagating failures. On the one hand, the orthogonal-woven structures, which have a larger binder-yarn undulation angle and more interlaced parts between surface-layer weft and binder yarn, exhibit serious weft-yarn debonding failure (thick dark lines in **Fig. 3-5 (b)**). On the other hand, the angle-interlock woven structures, which have a smaller binder-yarn undulation angle and less interlaced parts between surface-layer weft and binder yarn, exhibit slight weft-yarn debonding failure (thin dark lines in **Fig. 3-5 (b)**). The different failures could be attributed to the internal geometrical differences: there is a relative homogeneous weft-yarn arragement in angle-interlock woven group, whereas the weft yarns have obvious gaps between two adjacent weft-insetions in orthogonal woven group, which could be observed in **Fig. 2-6**. Moreover, for warp-direction beams of orthogonal woven structures, propagating failures along weft yarns are more serious at the interlaced part of the binder and weft yarn (dark dots enclosed by red squares in **Fig. 3-5 (b)**). This is mainly owing to the binder-yarn load-transfer ability, thus woven structure with specific binder-yarn path has an influence in failure map.

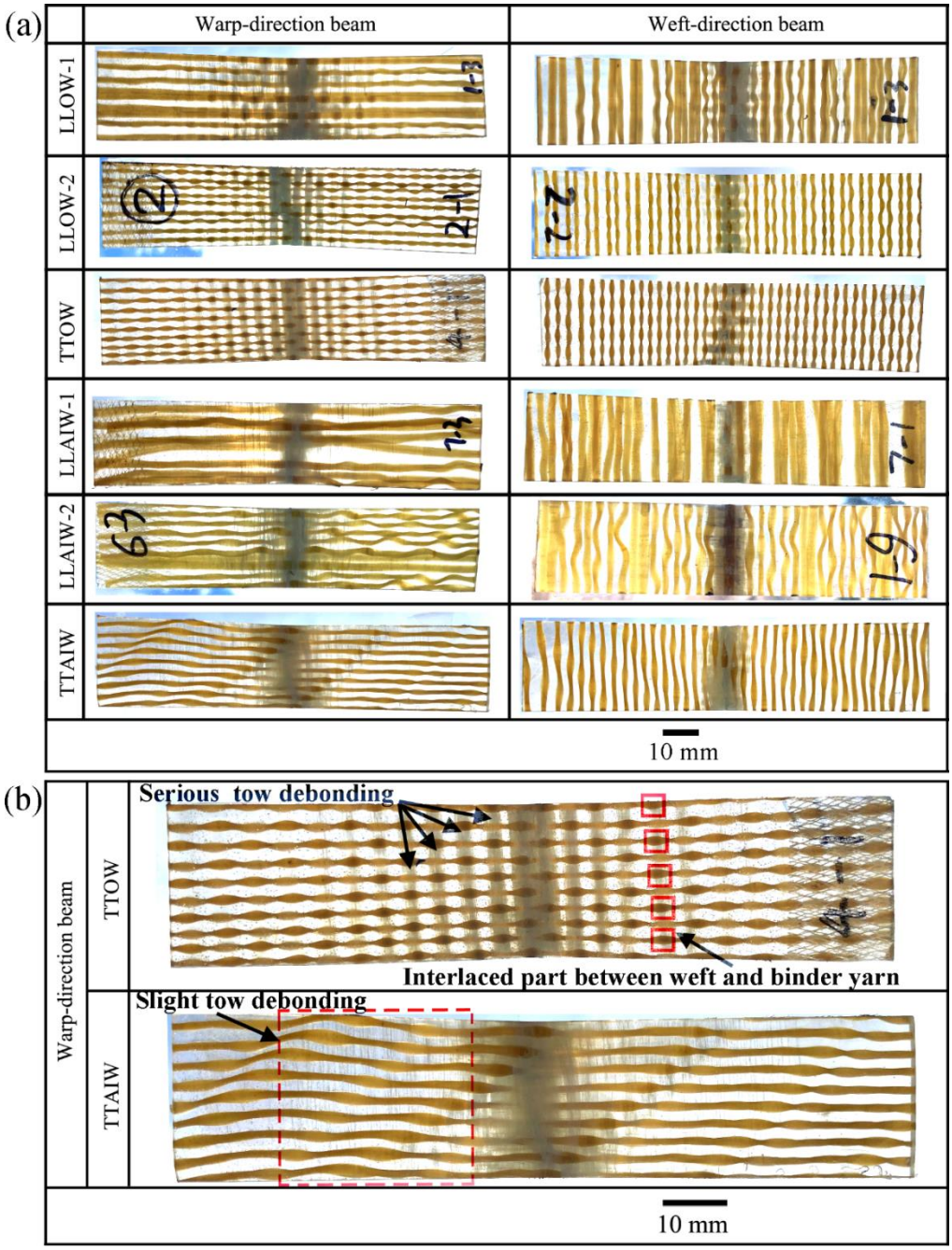

Fig. 3-5. (a) Strong-light background photographs of warp- and weft-direction beam specimens of six woven types after flexural test. **(b)** Comparation of warp-direction beams of TTOW and TTAIW structures. The transparent part is the area without failure, and the dark part is the area with failure.

A detailed failure map for the warp- and weft-direction beams of the TTAIW structure is shown in **Fig.3-6 (a)**, from which it is evident that the propagating-failure area and center-failure area in the warp direction are relatively large, which is similar for all other woven structures as shown in **Fig.3-5 (a)**. This may be because, for warp-direction

composite beams, the binder yarn runs in the beam length direction, which means it could transfer loads to adjacent weft yarn and thereby increase the weft-yarn debonding-failure area. There are similar failure modes for weft-direction beams among all six woven structures. For instance, in the center part of the beam for structure TTOW shown in **Fig. 3-6 (b)**, weft-yarn kink-band failure occurs at the inner surface (compression side) owing to compression loads, and warp-yarn tow-splitting failure mainly occurs at the outer layers (tension side) owing to shear loads; at the same time, delamination failure occurs mainly at the beam center for the outer yarn layers. This failure modes are associated with the structure of weft-direction beams, as four layers of weft yarn run in the beam length direction and two of these layers run on the beam surface, which mean that kink-band failure and fiber-breakage failure both likely occur. In contrast, for warp-direction beams, three layers of warp yarn run in the beam length direction, but none run at the beam surface, which means that warp-yarn kink-band failure and fiber-breakage failure rarely occur; rather, surface weft-yarn tow-splitting failure in the beam center-failure area more likely occurs, as shown in **Fig. 3-6 (a)**, due to the fact that the weft-yarn layers run in the beam width direction and thus bear large shear loads during bending.

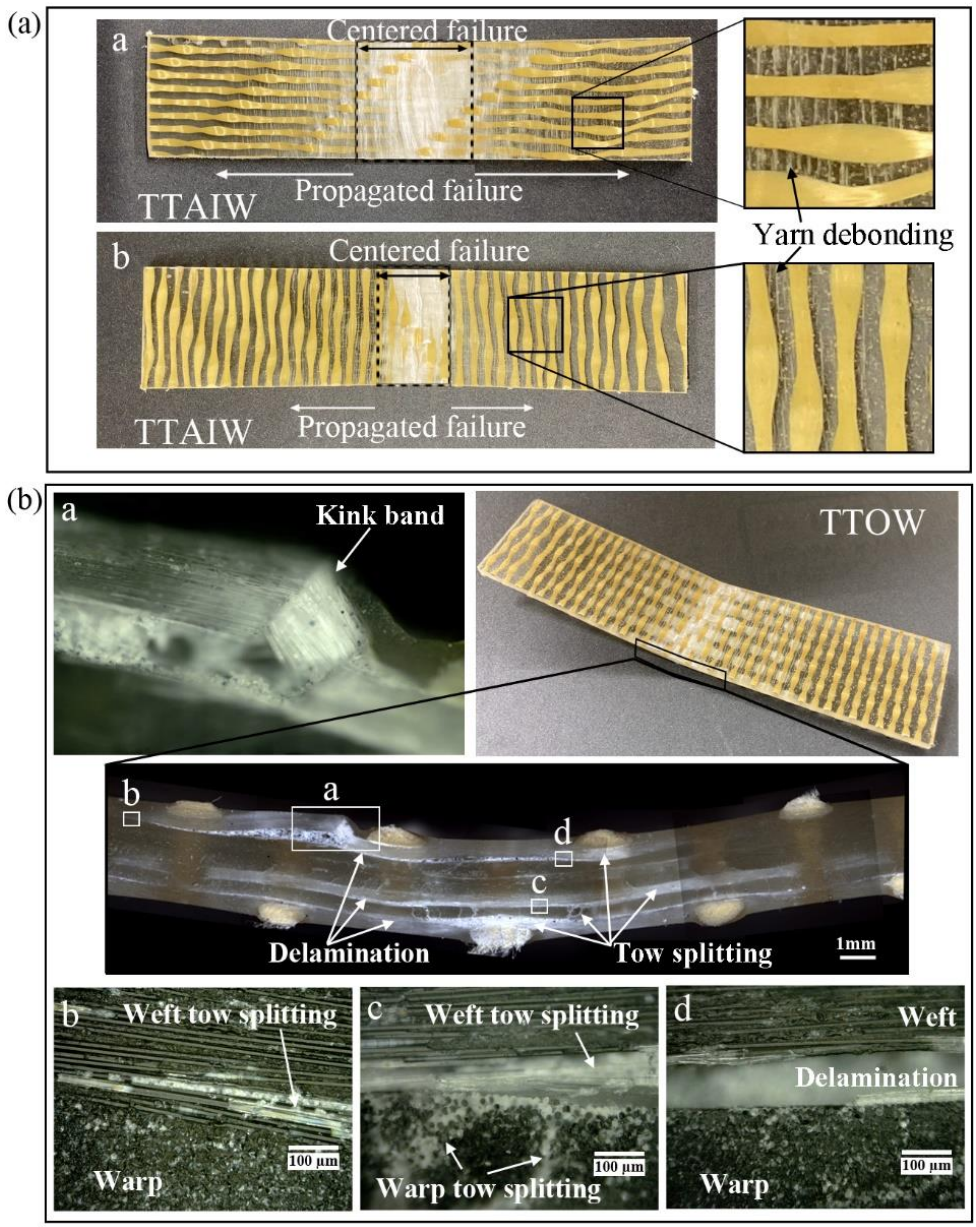

Fig. 3-6. Failure modes under flexural loading: **(a)** TTAIW in-plane failure map and **(b)** TTOW through-thickness failure map along the weft direction.

Overall, there are obvious differences in the failure modes of warp- and weft-direction beams for the six types of woven composites, and woven structure or binder-yarn path influences the failure map for warp-direction beams. In essence, for weft-direction beams, failure mainly occurred at the center part of the tested beams; for warp-direction beams, obvious propagating failures occurred because of the binder-yarn load-transfer ability. Yarn kink-band failure and fiber-breakage failure are likely for weft-direction beams, and surface-yarn tow-splitting failure is likely for warp-direction beams.

Moreover, the angle-interlock woven structures have slighter propagating weft-yarn debonding failure compared with orthogonal-woven structures.

3.4 Conclusions

In this chapter, the quasi-static flexural properties of the developed 3D woven composites were experimentally characterized with a three-point bending test, and optical microscopy was used to observe failures after bending. The conclusions outlined below can be drawn.

(1) Different mechanical behavior is shown along textile warp and weft directions for the designed 3D woven structures, weft-direction composite specimens have a higher flexural modulus but lower failure strain than have warp-direction composite specimens. Moreover, the angle-interlock woven structures have a larger flexural strength and modulus than that of orthogonal structures: 50% and 40% larger, respectively. The quasi-static flexural modulus of such 3D woven composites is more sensitive to fiber volume fraction and flexural strength is more sensitive to woven structure. In particular, the TTAIW structure along the warp direction has the best flexural-failure resistance among all composites.

(2) Woven structure or binder-yarn path has an obvious influence on the composite failures after three-point bending. For weft-direction beams, there is no obvious propagating failure beyond beam center, but for warp-direction beams, obvious propagating weft-yarn debonding failure can be observed beyond the center part, which can be attributed to binder yarn running in the beam length direction for warp-direction beams, which transfers loads to adjacent interlaced weft yarn. The angle-interlock woven structures have slight weft-yarn debonding failure in the propagating-failure area compared with the orthogonal-woven structures, because the binder-yarn undulation angle is smaller, and they have less interlaced parts between the surface weft- and binder-yarn layers.

(3) It should be noted that binder yarns not only improve the out-of-plane interlayer strength of such 3D woven composites, but also influence the in-plane failure mode, due to that the binder yarns are both in through-thickness and warp directions. Proper structural or binder-yarn path design of 3D woven composite is key issue to achieve better flexural performance.

References

[1] Pankow M, Salvi A, Waas A, Yen C, Ghiorse S. Resistance to delamination of 3D woven textile composites evaluated using End Notch Flexure (ENF) tests: Experimental results. Composites Part A: Applied Science and Manufacturing. 2011;42:1463-76.

[2] Turner P, Liu T, Zeng X. Collapse of 3D orthogonal woven carbon fibre composites under in-plane tension/compression and out-of-plane bending. Composite Structures. 2016;142:286-97.

[3] Gerlach R, Siviour CR, Wiegand J, Petrinic N. In-plane and through-thickness properties, failure modes, damage and delamination in 3D woven carbon fibre composites subjected to impact loading. Composites Science and Technology. 2012;72:397-411.

[4] Behera Ba, Dash B. Mechanical behavior of 3D woven composites. Materials & design. 2015;67:261-71.

[5] Behera B, Dash B. An experimental investigation into the mechanical behaviour of 3D woven fabrics for structural composites. Fibers and Polymers. 2014;15:1950-5.

[6] Zhang D, Waas AM, Yen C-F. Progressive damage and failure response of hybrid 3D textile composites subjected to flexural loading, part I: Experimental studies. International Journal of Solids and Structures. 2015;75:309-20.

[7] Umer R, Alhussein H, Zhou J, Cantwell W. The mechanical properties of 3D woven composites. Journal of Composite Materials. 2017;51:1703-16.

[8] Zhang D, Waas A, Pankow M, Yen C, Ghiorse S. Flexural behavior of a layer-to-layer orthogonal interlocked three-dimensional textile composite. Journal of Engineering materials and technology. 2012;134.

[9] ASTM S. Standard test methods for flexural properties of unreinforced and reinforced plastics and electrical insulating materials. ASTM D790. Annual book of ASTM Standards. 1997.

[10] Cox B, Dadkhah M, Morris W, Flintoff J. Failure mechanisms of 3D woven composites in tension, compression, and bending. Acta metallurgica et materialia. 1994;42:3967-84.

[11] Stegschuster G, Pingkarawat K, Wendland B, Mouritz A. Experimental determination of the mode I delamination fracture and fatigue properties of thin 3D woven composites. Composites Part A: Applied Science and Manufacturing. 2016;84:308-15.

Chapter 4 Low-velocity impact performance of glass/aramid fiber hybrid 3D woven composites

4.1 Introduction

FRPs are of interest as structural components which may be subjected to low-velocity impact, owing to their high mechanical performance and low weight, and as an alternative for metallic materials for saving energy and cost. The failure of fiber-reinforced composite materials has always been a hot research area because of its critical influence on the health and lifespan of such composite materials. Fiber/matrix interface deboning, and delamination failure are critical failure modes in FRP composites, especially for laminated structures, and are easily introduced under out-of-plane low-velocity impact, such as tool drop. This differs from high-velocity impact, which leaves a visible perforation, as low-velocity impact always leaves a barely visible indent on the structural component surface and damage inside the structure, which induces a large decrease in residual strength. Thus, it is important to study the low-velocity impact performance of FRP composite materials. To improve interlaminar strength and delamination resistance, various techniques have been applied to FRP composites, such as improving the fiber/matrix interfacial combination strength [1-4] or introducing fiber or yarn in the through-thickness direction [5-10]. In particular, 3D woven textile-reinforced composites have been developed and have drawn much attention in recent decades as an effective way to improve composite impact resistance and delamination resistance [11-17].

3D woven textile-reinforced composites with three groups of yarn (warp, weft, and binder yarns) in three perpendicular directions exhibit superior out-of-plane mechanical performance compared to 2D laminated composites. The binder yarn in the composite through-thickness direction improves the through-thickness strength and delamination resistance. Many researchers have focused on the low-velocity impact properties of 3D woven composites with orthogonal structure [18-27]. Baucom et al. [26, 27] studied low-velocity impact damage propagation among 3D orthogonal woven, biaxially warp-knit, and 2D laminated glass fiber-reinforced composites. They found that the 3D woven textile composite had the largest penetration resistance and energy absorbability. Seltzer et al. [19] studied mechanical performance and damage micro-mechanisms in 3D orthogonal woven and 2D laminated composites under low-velocity impact and

found that the 3D woven composite had better energy absorption capacity and structural integrity. Hart et al. [21] studied the mechanisms of impact damage in 2D laminated and 3D orthogonal woven composites and found that the 3D orthogonal composite had good delamination resistance. All above research indicates that 3D orthogonal woven composites exhibit superior low-velocity impact resistance than 2D laminated counterparts. Researchers have also studied low-velocity impact properties of 3D woven composites with other specific structures [28-36]. Elias et al. [28] studied low energy/velocity impact damage generated in 3D woven composites with specific LLAIW structure. Zhang et al. [29] studied low-velocity impact and the mechanism of compression after impact damage for 3D woven composites with a multilayer angle-interlock structure. Cao et al. [31] studied low-velocity impact damage of 3D woven composites with a specific angle-interlock structure. Zhou et al. [33] studied low-velocity impact properties of 3D auxetic textile composites, and Dau et al. [36] studied the soft impact performance of 3D woven composites with TTAIW structure. Bandaru et al. [34] and Behera et al. [30] carried out studies on the low-velocity impact response of 2D and 3D woven composites with two or three types of 3D textile structures: TTOW, TTAIW, and multilayer woven. There are many types of composite reinforcements, especially 3D woven structures, and the reinforcement structure has an obvious influence on out-of-plane mechanical performance. In the studies of Bandaru and Behera, the 3D woven textiles were all fabricated based on a traditional weaving loom. There are weaving limitations for angle-interlock woven manufacturing on a traditional weaving loom, such as yarn selection and structure design. Further studies are necessary for developing various 3D woven textile-reinforced composite structures to obtain better out-of-plane mechanical performance and to clarify the failure process in engineering applications.

In this chapter, impact performance and failure modes of the six developed 3D woven composites namely, LLOW-1, LLOW-2, TTOW, LLAIW-1, LLAIW-2, and TTAIW, were studied comprehensively by low-velocity drop-weight impact tests, and the effect of the woven structure on its impact performance was analyzed. An optimal structural design based on this new weaving system is obtained, and the composite is expected as a promising impact-resistance material to specific engineering applications.

4.2 Materials and experiments

4.2.1 Materials

The 3D woven textile-reinforced composites, i.e., LLOW-1, LLOW-2, TTOW, LLAIW-1, LLAIW-2, and TTAIW, which are developed in Chapter 2, were used to test their dynamic flexural performance.

4.2.2 Low-velocity drop-weight impact test

Low-velocity impact tests were conducted on an Instron Dynatup 9250HV drop-weight impact testing apparatus with a hemispherical steel impactor tup (12.7-mm diameter, 7.07-kg drop weight, and a 22-kN load cell). The setup of the low-velocity drop-weight impact test apparatus and specimen-holding platform is shown in **Fig. 4-1**. The force history was measured by a load cell located in the impactor, and the displacement and velocity history of the impactor tup was measured by the testing apparatus. Impact energy values of 10, 20, and 30 J were tested to clarify the penetration energy and to produce different damage levels of the designed composites. The energy was adjusted by changing the height of the drop weight, corresponding to 1.68, 2.38, and 2.91 m/s nominal impact velocities, for 10-, 20-, and 30-J impact energies, respectively. Three specimens of each woven structure were tested at each impact energy level. The composite specimens were held by two rigid square jaw platforms with a circular free zone with a diameter of 70 mm, to avoid slippage during test. The dimensions of the composite specimens were 100 × 100 mm^2.

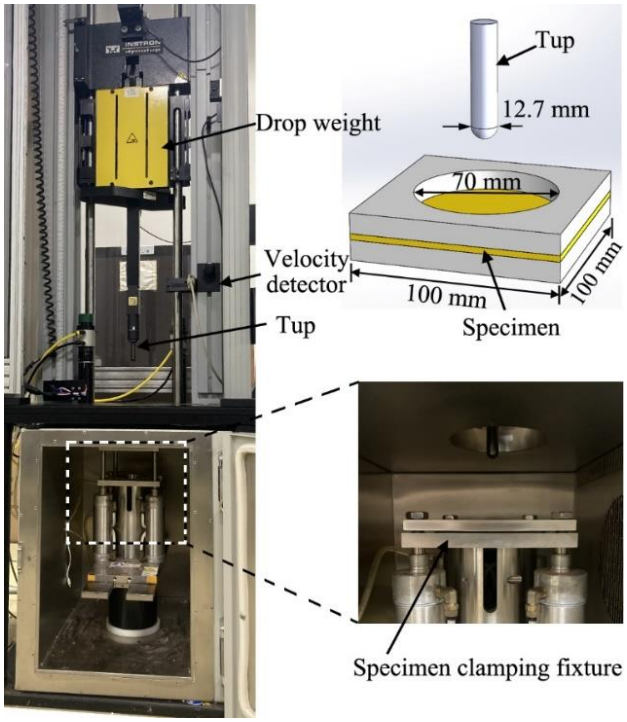

Fig. 4-1. Experimental setup of the low-velocity drop-weight impact test.

4.3 Results and discussion

4.3.1 Impact responses under different impact energy levels

The penetration energy of the LLOW-1 composites and their impact response under impact energy levels of 10, 20, and 30 J are discussed as an example of the 3D woven textile-reinforced composites. Typical load–deflection, load–time, and energy–time curves of LLOW-1 under the three impact energy levels are plotted in **Fig. 4-2**. Relatively smooth load–deflection and load–time curves are exhibited for the composite under a 10-J impact, as shown in **Fig. 4-2 (a1**, **a2)**. The load increases with the increase of composite deflection (or impactor contact time) until a peak load appears. The peak load is followed by a smooth reduction in load, which corresponds to the impactor rebounding phase. It should be noted that the small load undulation at the initial loading phase corresponds to small damage formation, such as matrix cracking and yarn debonding, which is mostly located at the contact area between the impactor and composite. In this case, a large deflection recovery of the composite (84% of peak deflection) and a typical hysteresis loop, as shown in **Fig. 4-2 (a1)**, and a large rebound energy (also called elastic energy), which is 59% of the impact energy, in the energy–time

curve, as shown in **Fig. 4-2 (a3)**, indicate that elastic deformation in the impacted composite dominates and, thus, less damage formation is expected under the 10-J impact.

There is a small load drop after the peak load under the 20-J impact, as shown in **Fig. 4-2 (b1**, **b2)**. This small load drop is expected as the major failure onset; failures, such as yarn debonding and delamination beyond the contacted area, start to propagate beyond this point. In this case, a small deflection recovery (30% of peak deflection), as shown in **Fig. 4-2 (b1)**, and a small rebound energy (less than 10% of the impact energy), as shown in **Fig. 4-2 (b3)**, indicate that major failure occurs. It is expected that 20 J is a quasi-penetration energy, which means that an impact energy over 20 J will introduce penetration failure.

For the 30-J impact, there is a sudden large load drop after the peak load that is followed by multiple small load drops and a zigzag unloading curve, as shown in **Fig. 4-2 (c1**, **c2)**. This corresponds to the development of multiple failures and impactor/composite friction; a larger failure is expected compared with that in the 20-J impact case. In the 30-J impact case, no deflection recovery is exhibited, as shown in **Fig. 4-2 (c1)**, and all impact energy was absorbed by the composite specimen, as shown in **Fig. 4-2 (c3)**, which indicates that penetration occurred.

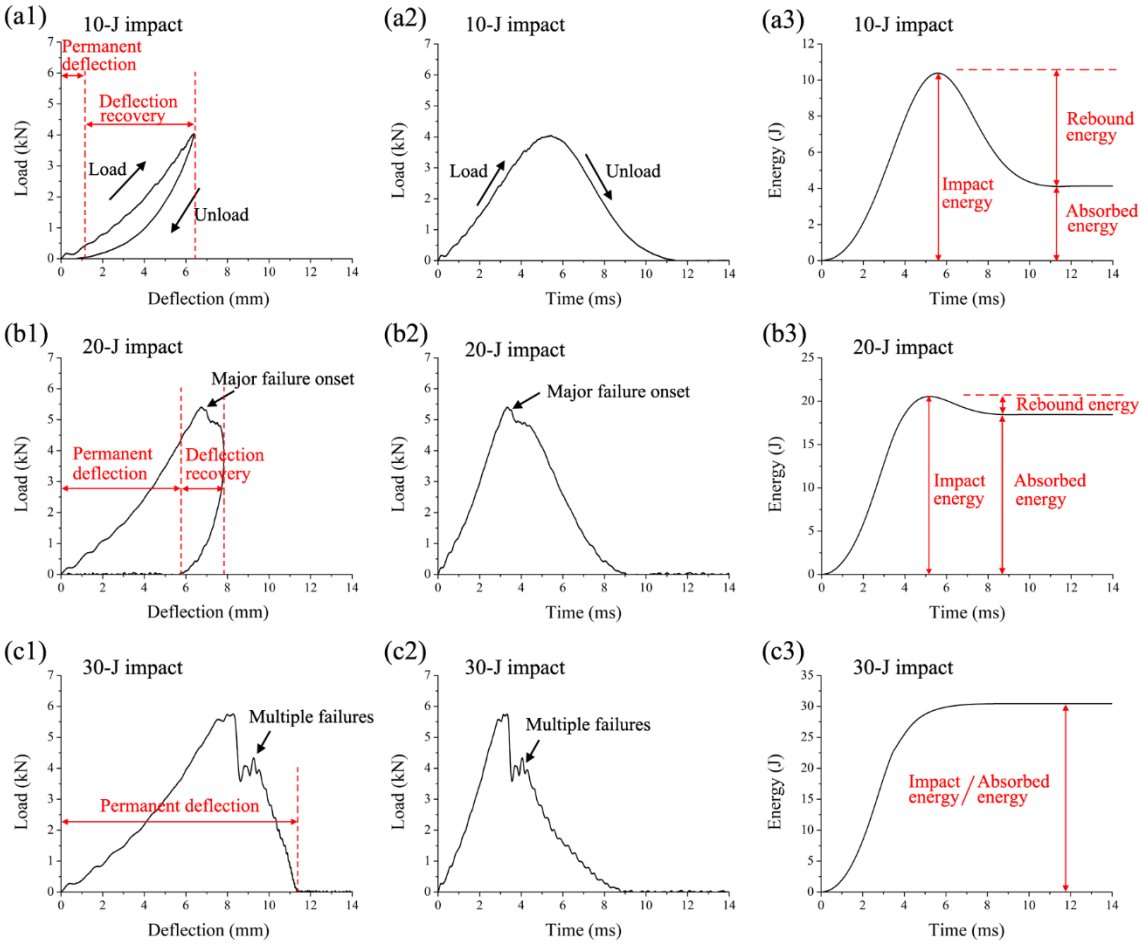

Fig. 4-2. Typical load–deflection, load–time, and energy–time curves for the LLOW-1 composite under three impact energy levels: **(a1, a2, a3)** 10-J impact; **(b1, b2, b3)** 20-J impact; and **(c1, c2, c3)** 30-J impact.

4.3.2 Impact resistance of the six designed 3D woven composites

The six designed 3D woven composites were investigated to clarify the influence of woven structure on impact resistance from the perspective of load bearing capacity, deflection characteristics, and energy characteristics during an impact event. Peak load is a key indicator of the load bearing capacity and impact resistance of composites. Representative load–time curves, peak load versus impact energy curves, and peak load versus composite fiber volume fraction curves for the six 3D woven composites under low-velocity impact testing are plotted in **Fig. 4-3**. There are similar load–time curves for the 10-J impact, as shown in **Fig. 4-3 (a)**, but there is a big difference in curves for the 20-J and 30-J impacts among the six woven composites, as shown in **Figs. 4-3 (b)** and **(c)**. This may be due to the low susceptibility of the composites subjected to 10-J

impact energy, at which less failure occurred, and the higher susceptibility to 20- and 30-J impact energies, at which major failure occurred, as discussed earlier. The angle-interlock woven group has larger peak loads of 4.16, 5.84, and 6.10 kN, for impact values of 10, 20, and 30 J, respectively, compared to the orthogonal group peak loads of 4.00, 4.93, and 5.28 kN (correspondingly 4%, 18.5%, and 15.5% larger), respectively. This may be mainly due to the larger fiber volume fraction of the angle-interlock group compared with that of the orthogonal group. A larger fiber volume fraction contributes a larger peak load, and this tendency is clearer in the orthogonal group for 20- and 30-J impacts. LLOW-1 exhibits the largest peak loads, followed by LLOW-2 and TTOW, as shown in **Figs. 4-3 (d)** and **(e)** and **Table 4-1**. By contrast, for the angle-interlock group composite with a similar fiber volume fraction, TTAIW exhibits the largest peak loads for 20- and 30-J impacts, followed by LLAIW-2 and LLAIW-1. The structural difference may play a key role in this case. TTAIW is expected to have structural superiority as each binder yarn has the same path, goes in the through-thickness direction, and appears at the composite surface, thus transferring the load evenly. Binder yarn appearing at the composite surface, where the largest stress happened under the out-of-plane impact, has the ability to transfer the load to adjacent bounded weft yarn layers. LLAIW-1 and LLAIW-2, wherein only part of the binder yarns appear at the composite surface, has limited load transferring capacity. LLAIW-2 exhibits a larger peak load than does LLAIW-1, which may contribute by a larger composite thickness for LLAIW-2 and the structural difference between these two structures. Binder yarn in LLAIW-2 binds one more weft yarn layer (three layers) and exhibits a larger undulation angle of 15.6° than does that in LLAIW-1, wherein the binder yarn binds two adjacent weft yarn layers and has a smaller undulation angle of 8.6°. A larger binder yarn undulation angle means that binder yarn lies more in through-thickness direction of the composites, and, thus, has more delamination-resistance ability when subjected to out-of-plane impact.

Moreover, the orthogonal group exhibits more multiple failures in the load–time curves than does the angle-interlock group subjected to 20- and 30-J impacts and a more obvious difference for the 30-J impact. This may also mainly be due to fiber volume fraction and woven structural differences between the two groups. Low fiber volume fraction contributes to the low load bearing capacity of the composite and likely introduces

multiple failures. The structural difference in the two woven groups introduces the different failure modes.

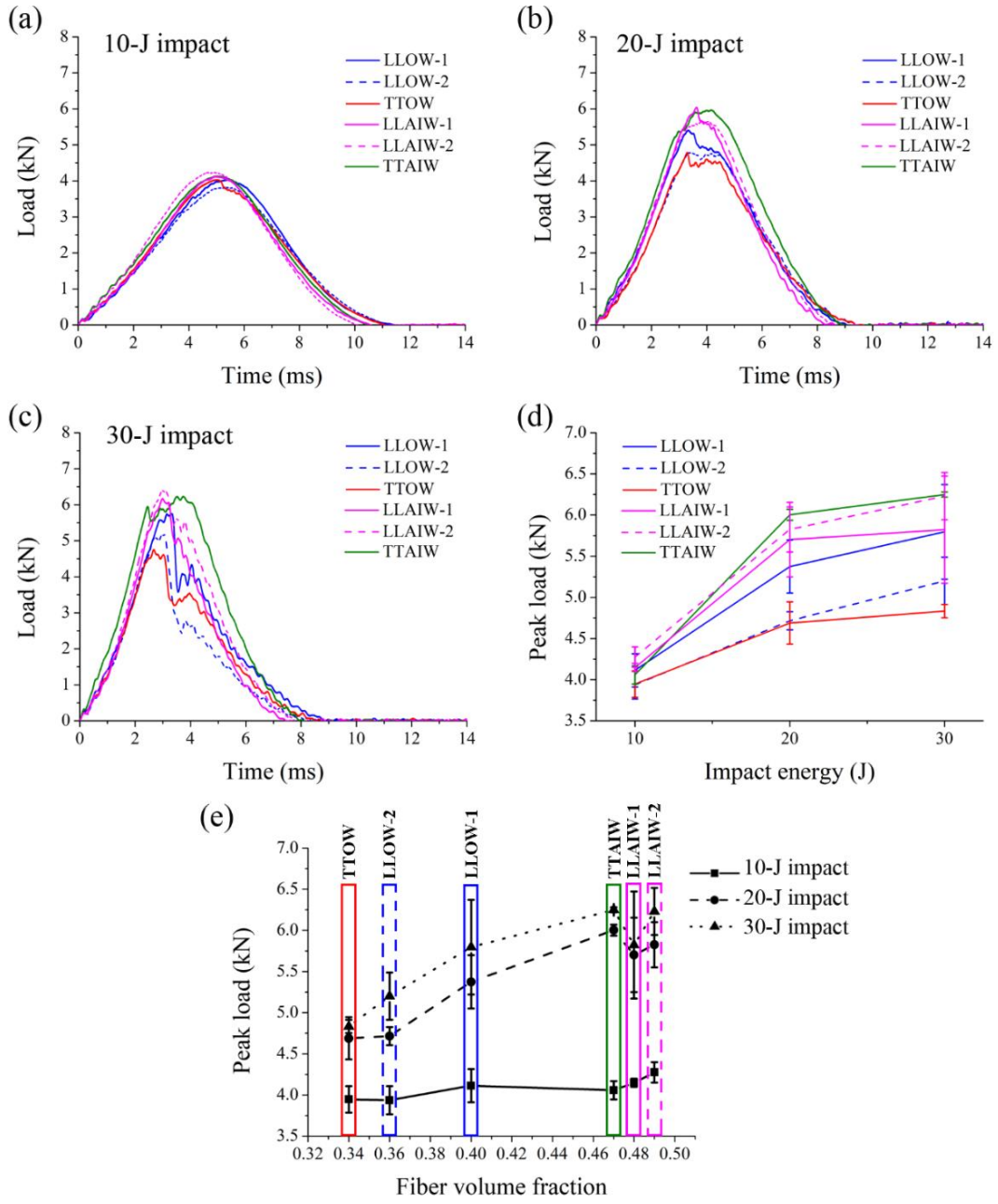

Fig. 4-3. Representative load–time curves of low-velocity drop-weight impact for six 3D woven composites subjected to three impact energy levels: **(a)** 10, **(b)** 20, and **(c)** 30 J. **(d)** Peak load versus impact energy curves and **(e)** peak load versus fiber volume fraction curves.

Table 4-1. Peak loads of six 3D woven composites under the low-velocity drop-weight impact test.

Textile group		Orthogonal			Angle-interlock		
		Layer-to-layer		Through-thickness	Layer-to-layer		Through-thickness
Textile ID		LLOW-1	LLOW-2	TTOW	LLAIW-1	LLAIW-2	TTAIW
Peak load (kN)	10-J impact	4.11	3.94	3.95	4.15	4.28	4.06
	20-J impact	5.37	4.72	4.69	5.70	5.83	6.00
	30-J impact	5.80	5.20	4.83	5.82	6.23	6.25

Deflection characteristics, such as maximum deflection (D_{max}), permanent deflection (D_{per}), and deflection recovery during an impact event, are indicators of the impact resistance of composites. Maximum deflection refers to the deflection ability or failure situation of the impacted composite, and permanent deflection is mainly caused by composite failure after impact. A larger permanent deflection indicates that larger failure occurred for the composite. Deflection recovery is the phase where the impactor rebounded from the composite, and, in this phase, energy is transferred from the deflected composite to the impactor. Here, the deflection recovery ratio (DRR), which is the ratio of deflection recovery to maximum deflection as shown in Eq. (4-1), is introduced to compare the deflection recoverability among the six 3D woven composites.

$$DRR = \frac{D_{max} - D_{per}}{D_{max}} \tag{4-1}$$

A larger recovery ratio means that larger elastic energy is stored in the impacted composite and, thus, larger impact resistance is expected. Representative load–deflection curves, maximum deflection, permanent deflection, and the DRR versus impact energy curves for the six 3D woven composites under low-velocity impact test are plotted in **Fig. 4-4**.

Typical hysteresis loop curves are exhibited for composites subjected to a 10-J impact, as shown in **Fig. 4-4 (a)**, and indicate that less failure occurred. There is similar maximum deflection, permanent deflection, and DRR values for composites under the 10-J impact, as listed in **Table 4-2**. This indicates a low susceptibility to the 10-J impact for these composites. There is an obvious difference in deflection behavior among

composites subjected to 20- and 30-J impacts, as shown in **Figs. 4-4 (b)** and **(c)**. The angle-interlock group exhibits a higher stiffness, which is the slope of the load–deflection curves in the loading phase, compared to the orthogonal group subjected to 20- and 30-J impacts. For a 20-J impact, all woven structures exhibit impactor rebound behavior. In this case, TTAIW has the smallest maximum and permanent deflection, as well as the largest DRR, followed by LLAIW-2, LLOW-1, LLAIW-1, LLOW-2, and TTOW, as shown in **Figs. 4-4 (d)**, **(e)**, and **(f)**, as well as in **Table 4-2**. The angle-interlock group has a roughly 8.7% smaller maximum deflection, 28.3% smaller permanent deflection, and 88.1% larger DRR than has the orthogonal group for the 20-J impact. For the 30-J impact, TTAIW has a slight DRR of roughly 0.1, whereas the other structures exhibit penetration performance and no deflection recovery and have the same value between maximum and permanent deflection, as shown in **Figs. 4-4 (c)** and **(f)**. In this case, TTAIW has the smallest permanent deflection, followed by LLAIW-2, LLOW-1, LLAIW-1, TTOW, and LLOW-2. Furthermore, the angle-interlock group has a roughly 21.3% smaller permanent deflection than has the orthogonal group.

The angle-interlock group has better impact resistance than has the orthogonal group from the perspective of deflection performance owing to its higher fiber volume fraction and structural superiority. It should be noted that TTAIW has excellent deflection recoverability than has the other structures, which may be due to its structural superiority, as discussed before. LLOW-1 has much higher impact resistance performance than have the other orthogonal woven structures and is even higher than LLAIW-1. This may mainly be due to the higher fiber volume fraction and smaller effective binding density of LLOW-1 compared to LLOW-2 and TTOW, as listed in **Table 2-3**, as well as its special failure mode, which will be discussed later.

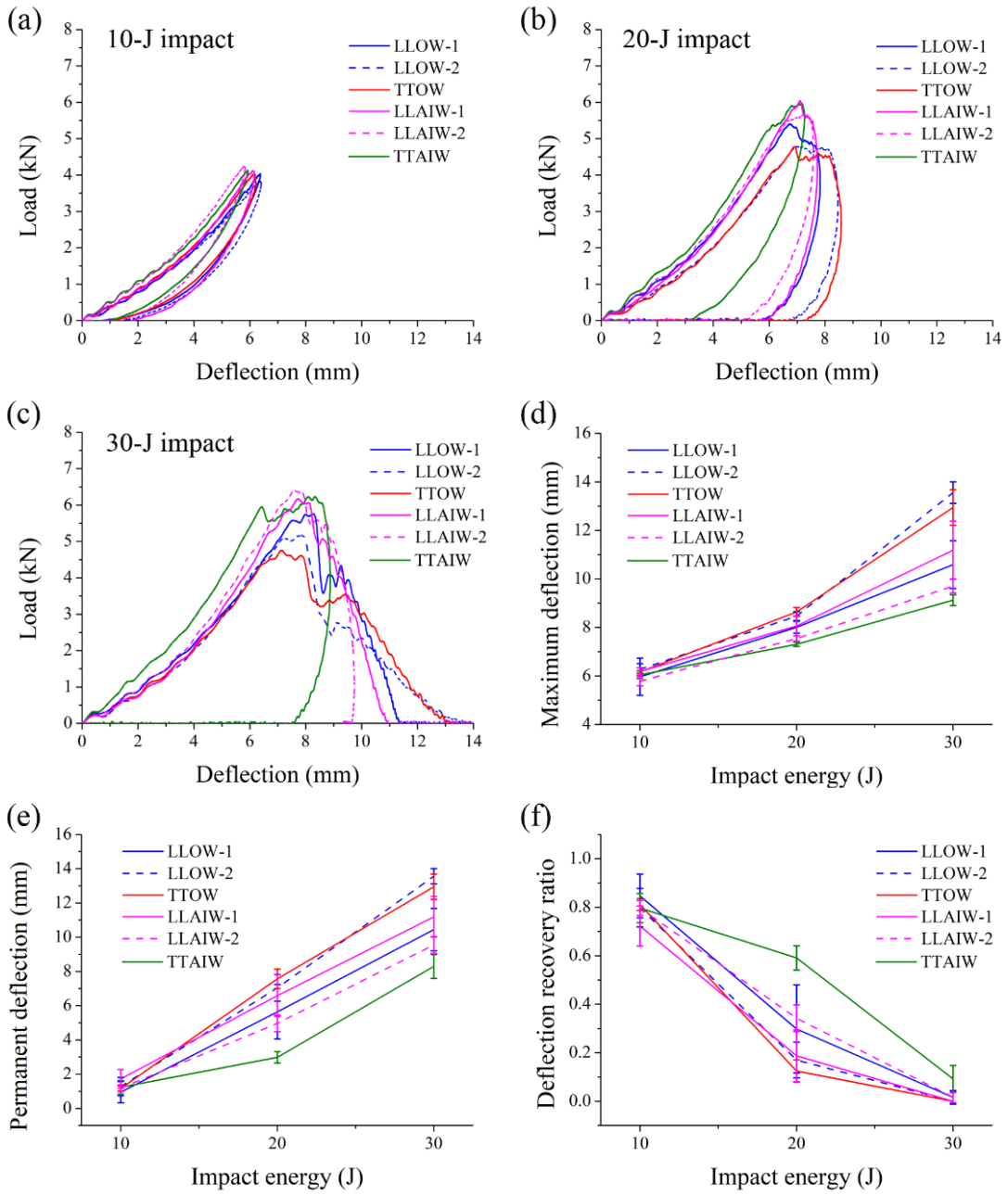

Fig. 4-4. Representative load–deflection curves for low-velocity drop-weight impact for six 3D woven composites subjected to three impact energy levels: **(a)** 10, **(b)** 20, and **(c)** 30 J. **(d)** Maximum deflection, **(e)** permanent deflection, and **(f)** DRR versus impact energy curves.

Table 4-2. Deflection characteristics of the six 3D woven composites under low-velocity drop-weight impact tests.

Textile group		Orthogonal			Angle-interlock		
		Layer-to-layer		Through-thickness	Layer-to-layer		Through-thickness
Textile ID		LLOW-1	LLOW-2	TTOW	LLAIW-1	LLAIW-2	TTAIW
Maximum deflection (mm)	10-J impact	5.96	6.27	6.16	6.18	5.78	6.04
	20-J impact	8.00	8.47	8.64	8.06	7.54	7.30
	30-J impact	10.59	13.56	12.95	11.19	9.70	9.12
Permanent deflection (mm)	10-J impact	0.95	1.27	1.17	1.72	1.18	1.23
	20-J impact	5.64	7.04	7.57	6.58	4.96	2.98
	30-J impact	10.44	13.56	12.95	11.19	9.55	8.29
Deflection recovery ratio	10-J impact	0.85	0.80	0.81	0.72	0.80	0.80
	20-J impact	0.30	0.17	0.12	0.18	0.34	0.59
	30-J impact	0.02	0	0	0	0.02	0.09

Energy characteristics, including absorbed energy (E_{abs}), rebounded energy (E_{reb}), energy absorbed to peak load, and impact resistance index (*IRI*), are compared for the six woven composites. Energy absorbed by a composite during an impact event is equal to the area enclosed by the load–deflection curve and is utilized in damage and failure creation in an impacted composite. Energy-to-peak load is the energy absorbed before major failure occurs, and a higher value means that more energy is needed to induce major failure in a composite, thus suggesting higher impact resistance. The IRI is a parameter defined as the ratio of rebounded energy to absorbed energy, as shown in Eq. (4-2), to indicate the impact resistance for composites in an impact event [37]. A higher value of *IRI* means that more energy is rebounded to the impactor during an impact event and thus a better composite impact resistance.

$$IRI = \frac{E_{reb}}{E_{abs}} \tag{4-2}$$

Representative energy–time curves, absorbed energy, energy-to-peak load, and IRI versus impact energy curves for the six 3D woven composites under low-velocity impact test are plotted in **Fig. 4-5**. Over 50% of the impact energy is rebounded to the impactor for composites subjected to a 10-J impact, as shown in **Fig. 4-5 (a)** and **Table 3**, which indicates that a typical impactor rebounding case dominates and less failure is expected. For the 20-J impact, TTAIW exhibits the largest rebounded energy of 6.97 J, over 30% of the impact energy, whereas the other structures leave less rebounded energy, as

shown in **Fig. 4-5 (b)**. It is expected that composites have a quasi-penetration energy of 20 J, except for TTAIW. For the 30-J impact, TTAIW has a rebound energy of 0.74 J, and the other structures exhibit penetration behavior with no rebound energy, as shown in **Fig. 4-5 (c)**, which indicates that TTAIW has a quasi-penetration energy of 30 J.

The relationship between absorbed energy of the six woven composites and impact energy is depicted in **Fig. 4-5 (d)**. Absorbed energy increases with impact energy; in the 10- and 30-J impacts, there is no obvious difference among the six woven composites owing to the low susceptibility to the 10-J impact and the penetration case for the 30-J impact of composites, as discussed earlier. It should be noted that there is an obvious difference in energy absorption under the 20-J impact. TTAIW absorbed the least energy of 13.35 J, whereas other structures absorbed more energy, as listed in **Table 4-3**. Moreover, the angle-interlock group absorbed roughly 13.5% less energy than did the orthogonal group, which means more energy is rebounded to the impactor and thus better impact resistance for angle-interlock structures.

The relationship between absorbed energy-to-peak load of the six woven composites and impact energy is depicted in **Fig. 4-5 (e)**. The absorbed energy-to-peak load increases with impact energy. For the 10-J impact, there is no major failure for the composites, and the energy-to-peak load equals the impact energy. Thus, the same energy-to-peak loads are exhibited for the six woven composites. For a 20-J impact, TTAIW exhibits the largest energy-to-peak load, followed by LLAIW-2, LLAIW-1, LLOW-1, LLOW-2, and TTOW, as listed in **Table 4-3**. Moreover, the angle-interlock group has a 17.5% larger energy-to-peak load than has the orthogonal group. For the 30-J impact, TTAIW and LLOW-1 exhibit the largest energy-to-peak load, followed by LLAIW-2, LLAIW-1, LLOW-2, and TTOW. The angle-interlock group has a 9% larger value of energy-to-peak load than has the orthogonal group. More energy is needed to introduce major failure for the angle-interlock group than for the orthogonal group, but the LLOW-1 exhibiting higher energy-to-peak load may be due to higher fiber volume fraction and good deflection performance discussed earlier. The relationship between IRI and impact energy is depicted in **Fig. 4-5 (f)**. There is no clear trend between the angle-interlock and orthogonal groups under a 10-J impact owing to the low susceptibility of the composites. It should be noted that TTAIW has a higher value (0.52) than

have the other structures when subjected to the 20-J impact and has a value of 0.03 when subjected to the 30-J impact, whereas the other structures have a value of zero due to the occurrence of penetration. This indicates that TTAIW has excellent impact resistance ability among the six woven composites.

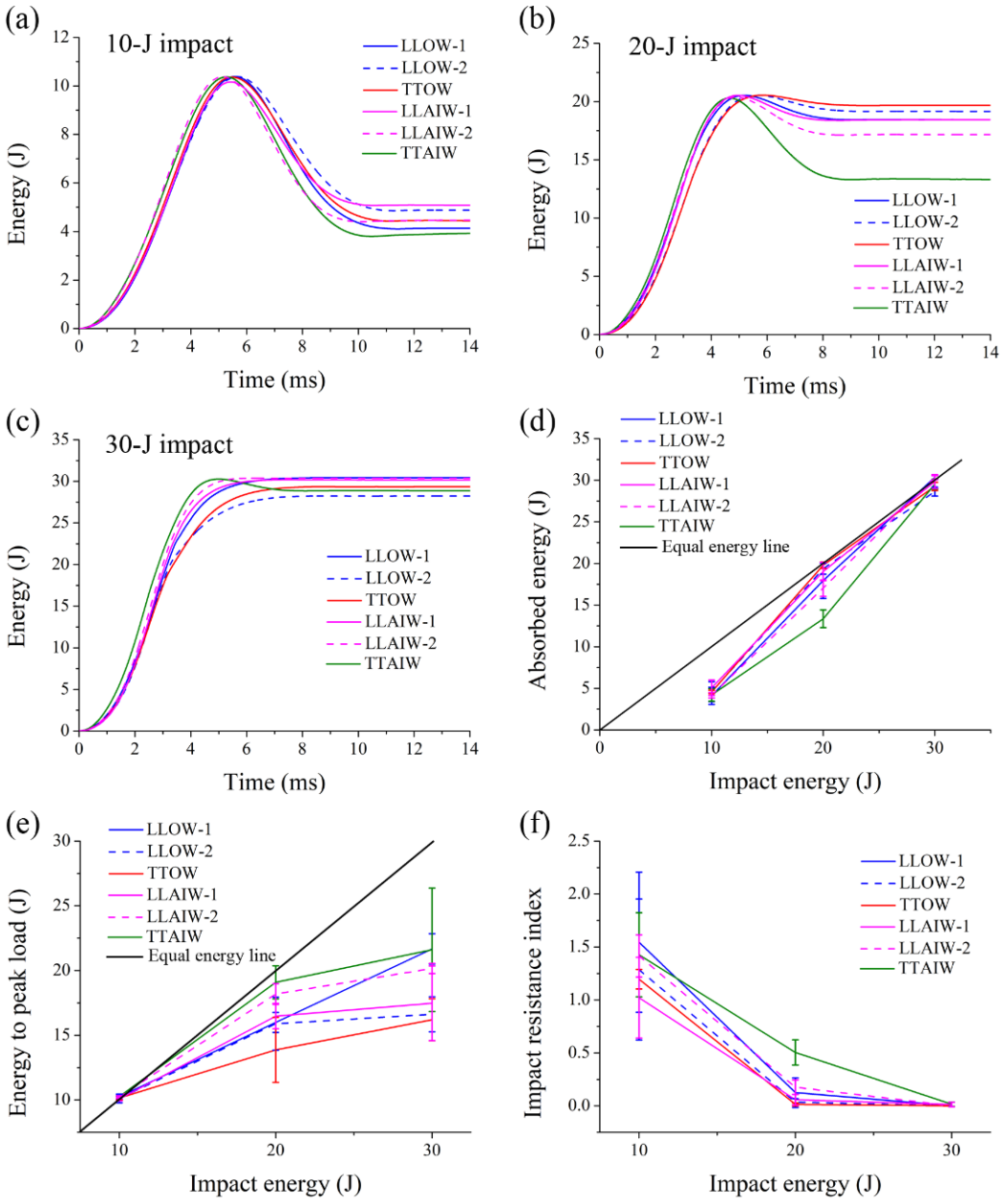

Fig. 4-5. Representative energy–time curves of low-velocity drop-weight impacts for the six 3D woven textile composites subjected to three impact energy levels: **(a)** 10, **(b)** 20, and **(c)** 30 J. **(d)** Absorbed energy, **(e)** energy-to-peak load, and **(f)** impact resistance index versus impact energy curves.

Table 4-3. Energy characteristic results for the six 3D woven composites under low-velocity drop-weight impact tests.

Textile group		Orthogonal			Angle-interlock		
		Layer-to-layer		Through-thickness	Layer-to-layer		Through-thickness
Textile ID		LLOW-1	LLOW-2	TTOW	LLAIW-1	LLAIW-2	TTAIW
Absorbed energy (J)	10-J impact	4.11	4.60	4.56	5.06	4.16	4.20
	20-J impact	17.95	19.36	19.79	19.04	17.04	13.35
	30-J impact	30.36	28.64	29.27	29.85	30.32	29.53
Rebounded energy (J)	10-J impact	6.18	5.80	5.84	5.27	6.22	6.17
	20-J impact	2.54	1.14	0.73	1.52	3.41	6.97
	30-J impact	0.01	0.02	0	0	0.09	0.74
Energy-to-peak load (J)	10-J impact	10.24	10.12	10.16	10.08	10.24	10.28
	20-J impact	15.99	15.89	13.87	16.48	18.18	19.09
	30-J impact	21.67	16.62	16.20	17.47	20.16	21.60
Impact resistance index	10-J impact	1.50	1.26	1.28	1.04	1.50	1.47
	20-J impact	0.14	0.06	0.04	0.08	0.2	0.52
	30-J impact	0	0	0	0	0	0.03

Overall, from the perspectives of load-carrying ability, deflection performance, and energy characteristics, the angle-interlock group has better impact resistance ability than has the orthogonal woven group owing to its higher fiber volume fraction and structural superiority. In particular, TTAIW, with a uniform structure, exhibits the best and excellent impact resistance performance among the developed 3D woven composites.

4.3.3 Failure modes

Internal damage of an impacted composite specimen can be visually identified using a back-lighting method owing to the transparent properties of glass fiber and epoxy resin. Back-lighting photographs of the impacted composites were taken with sunlight as the background. **Fig. 4-6** illustrates the localized failure region of the six impacted composite specimens, wherein the dark pixel is localized failure that is enclosed by a red line. The warp-direction length (L_x), weft-direction length (L_y), and area of the failure region are measured and summarized in **Table 4-4**. L_x, L_y, and failure area increase with increase of impact energy for all woven structures. The orthogonal group (**Fig. 4-6 (a)**) has a smaller and localized failure area than has the angle-interlock group (**Fig. 4-6 (b)**) under each impact energy level. At the same time, the orthogonal group exhibits a circle-like failure region, whereas the angle-interlock group exhibits an ellipse-like failure region with a longer side in the weft direction. The difference in failure area may be

due to the structural difference of the two woven groups. For the orthogonal group, the binder yarn binds two adjacent weft yarns and has more interlaced parts with surface-weft yarns per unit area (higher effective binding density). For the angle-interlock group, the binder yarn is not binding two adjacent weft yarns and has fewer interlaced parts with surface-weft yarns; the more interlaced parts or higher effective binding density restrict the failure propagation along weft yarn; thus, a smaller failure area is exhibited for orthogonal woven structures. It should be noted that LLOW-1 has the smallest effective binding density (1.68 cm^{-2}) compared to LLOW-2 (2.75 cm^{-2}) and TTOW (3.51 cm^{-2}) in the orthogonal group. LLOW-1 also has a similar value as that of TTAIW (1.62 cm^{-2}); thus, LLOW-1 has a larger failure area and exhibits a more ellipse-like failure area. The failure region in the angle-interlock group is more developed in the weft direction than in the warp direction. This is mainly because two weft yarn layers are at the composite surface, where the largest stress happens when the composite is subjected to out-of-plane loading. The two weft yarn layers carry large load under impact loading and are likely to induce failure. At the same time, the binder yarn lies in the warp direction and has the ability to transfer load to bounded weft yarns, restricting the failure development in the warp direction.

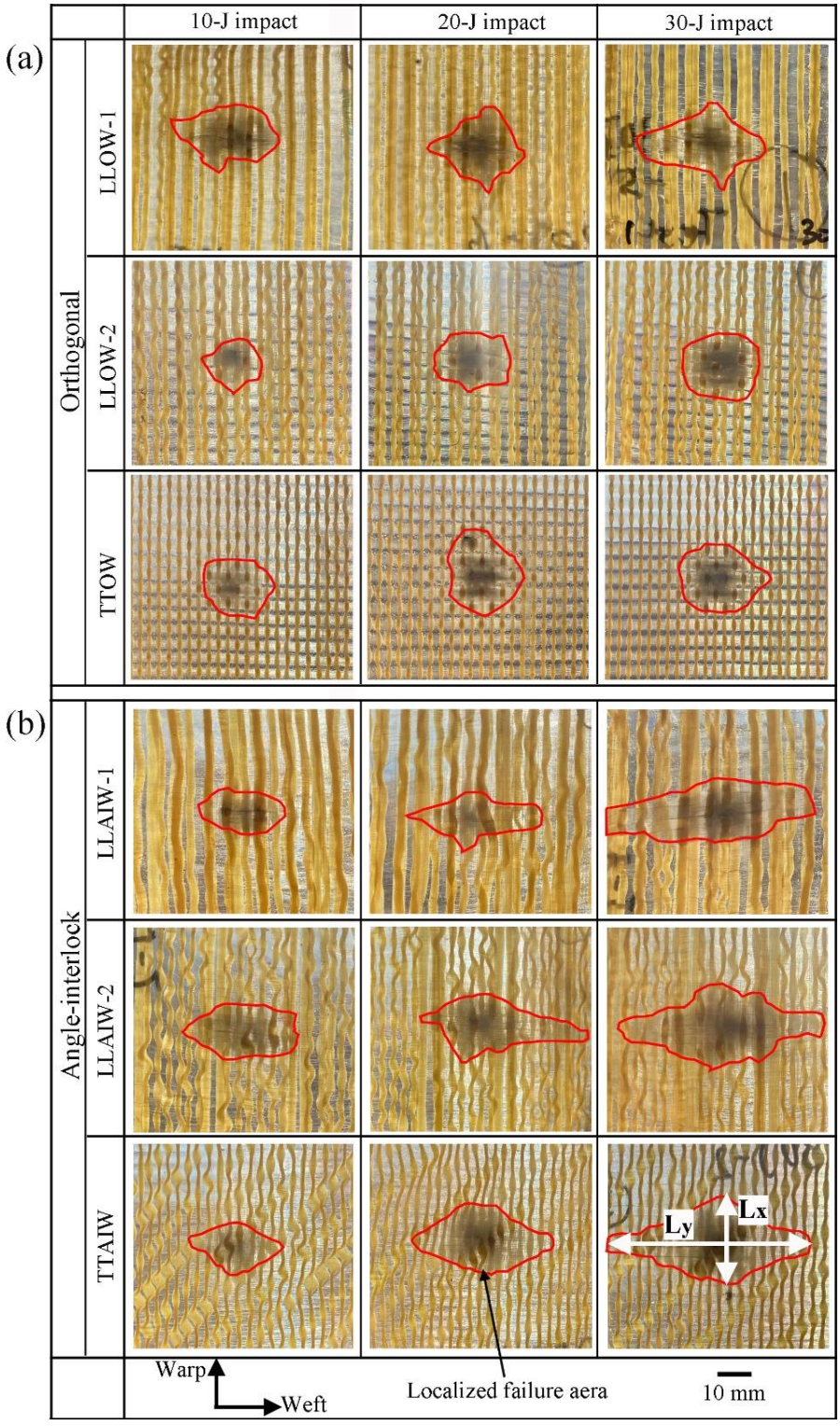

Fig. 4-6. Sunlight back-lighting photographs of six impacted woven composites: **(a)** orthogonal woven group and **(b)** angle-interlock woven group.

Table 4-4. Parameters of localized failure regions for the six impacted woven composites.

Textile group		Orthogonal			Angle-interlock		
		Layer-to-layer		Through-thickness	Layer-to-layer		Through-thickness
Textile ID		LLOW-1	LLOW-2	TTOW	LLAIW-1	LLAIW-2	TTAIW
10-J impact	Lx (mm)	24	18	19	16	19	18
	Ly (mm)	34	20	24	19	40	22
	Area (mm^2)	500	250	400	350	550	300
20-J impact	Lx (mm)	30	19	29	20	24	24
	Ly (mm)	22	25	24	44	56	47
	Area (mm^2)	450	350	500	600	550	700
30-J impact	Lx (mm)	30	22	23	24	30	30
	Ly (mm)	43	26	31	56	70	68
	Area (mm^2)	550	450	500	900	900	1100

Detailed failure at the composite front (impacted) and rear (unimpacted) faces for TTOW and TTAIW is shown in **Fig. 4-7**. There is a larger failure area at the rear face than at the front face in TTOW (**Fig. 4-7 (a)**) and TTAIW (**Fig. 4-7 (b)**) after impact. This is also the same for the other woven structures owing to their bending properties. During impact, the impacted face of the composite plate undergoes the largest compression and the unimpacted face undergoes the largest tension, owing to composite plate deflection. Failure is likely introduced and propagated initially at the unimpacted side [38]. It should be noted that TTOW has obvious fiber fracture failure at the rear face, even under the 10-J impact. TTAIW has no obvious fiber fracture failure, even under the 30-J impact, and limited delamination at the rear face is exhibited for TTAIW under all impact energy levels.

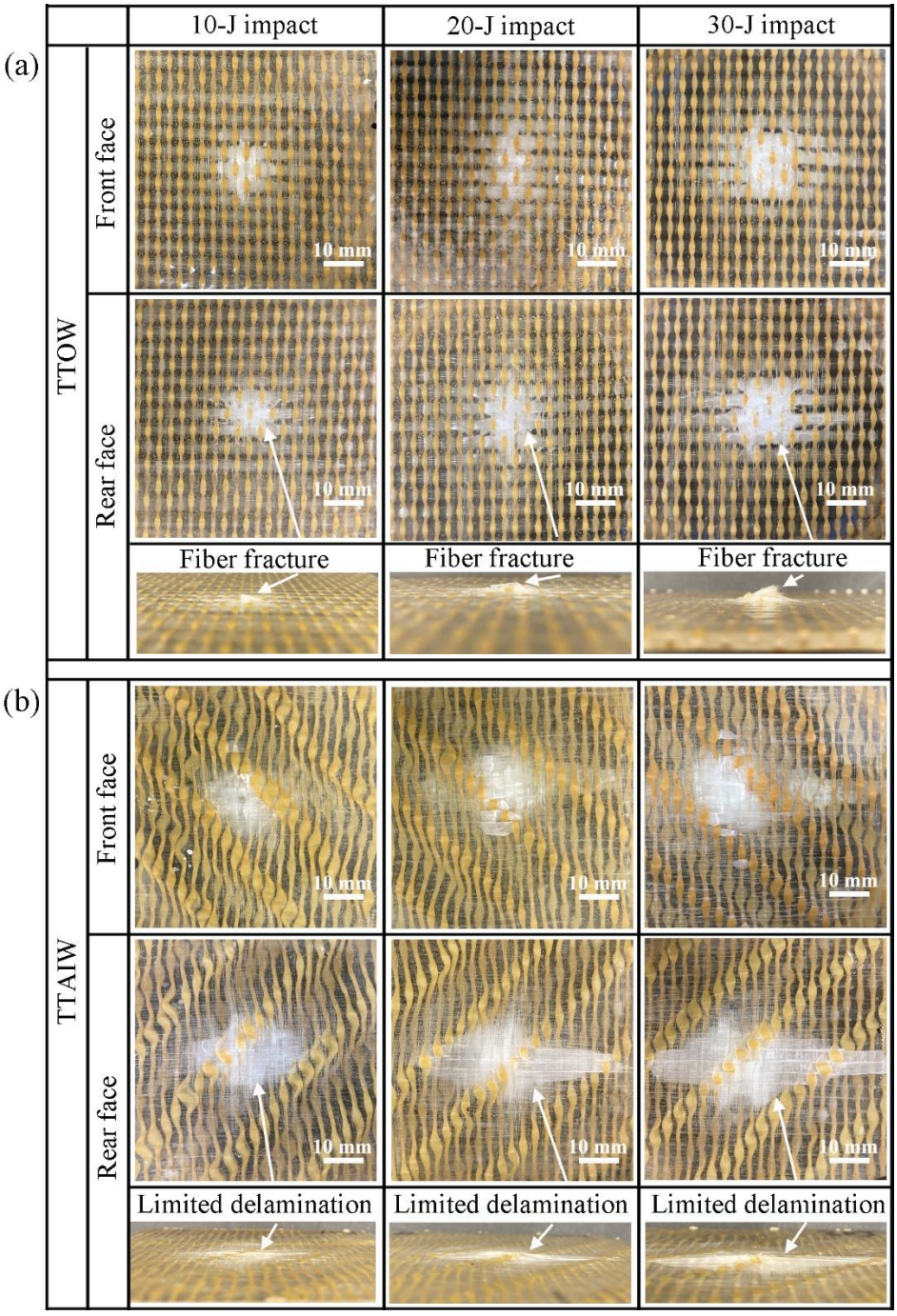

Fig. 4-7. Front and rear face photographs for **(a)** TTOW and **(b)** TTAIW composites after low-velocity drop-weight impact tests.

A detailed failure map in the through-thickness direction at the center of TTOW and TTAIW specimens subjected to quasi-penetration energy impact is shown in **Fig. 4-8**. Weft yarn debonding failure was observed in both structures. In the TTOW composite, serious fiber fracture failure was observed at both impacted and unimpacted sides, as shown in **Fig. 4-8 (a)**. This is due to the compression load at the impacted side and the

tensile load at the unimpacted side. At the same time, fiber fracture failure is also observed in the other orthogonal structures. For the TTAIW composite, there is large-scale limited delamination failure, which is marked by the red dashed line in **Fig. 4-8 (b)**, instead of serious fiber fracture failure, and the limited delamination failure is also observed for other angle-interlock structures. The obvious difference in failure mode between the two typical woven groups is mainly due to the structural difference.

Detailed 3D models of TTOW and TTAIW are shown in **Fig. 4-8 (c)** and **(d)**, as representative structures of the two typical woven groups. As shown in **Fig. 4-8 (c)**, each surface-weft yarn is bound by binder yarn, and a large effective binding density is exhibited for TTOW. However, there is a large unbounded area between the warp- and weft yarn layers of TTAIW, which is the free area enclosed by black dashed lines in **Fig. 4-8 (d)**. There is a larger free area for the angle-interlock woven structures, and the energy absorbed by the composite during the impact is likely utilized to create a new surface in the composite. This is due to lower interlaminar strength between the warp- and weft yarn layers in the free area than the tensile strength of the glass fiber. Thus, limited delamination failure is likely introduced in the free area for angle-interlock woven structures. On the other hand, orthogonal woven structures with higher effective binding density, which is more binder/surface-weft yarn interlaced parts per unit area or less or no free area, exhibit delamination resistance ability but likely leave serious fiber fracture failure. The fiber fracture failure is expected to likely introduce perforation in a composite when subjected to a larger impact energy. It should be noted that TTOW-1, with smaller effective binding density and larger free area compared with other orthogonal structures, also exhibits limited delamination failure at the free area, which is the same as other angle-interlock structures. Thus, woven structural design has an obvious influence on the failure mode for textile-reinforced composites and plays a key role for specific engineering applications.

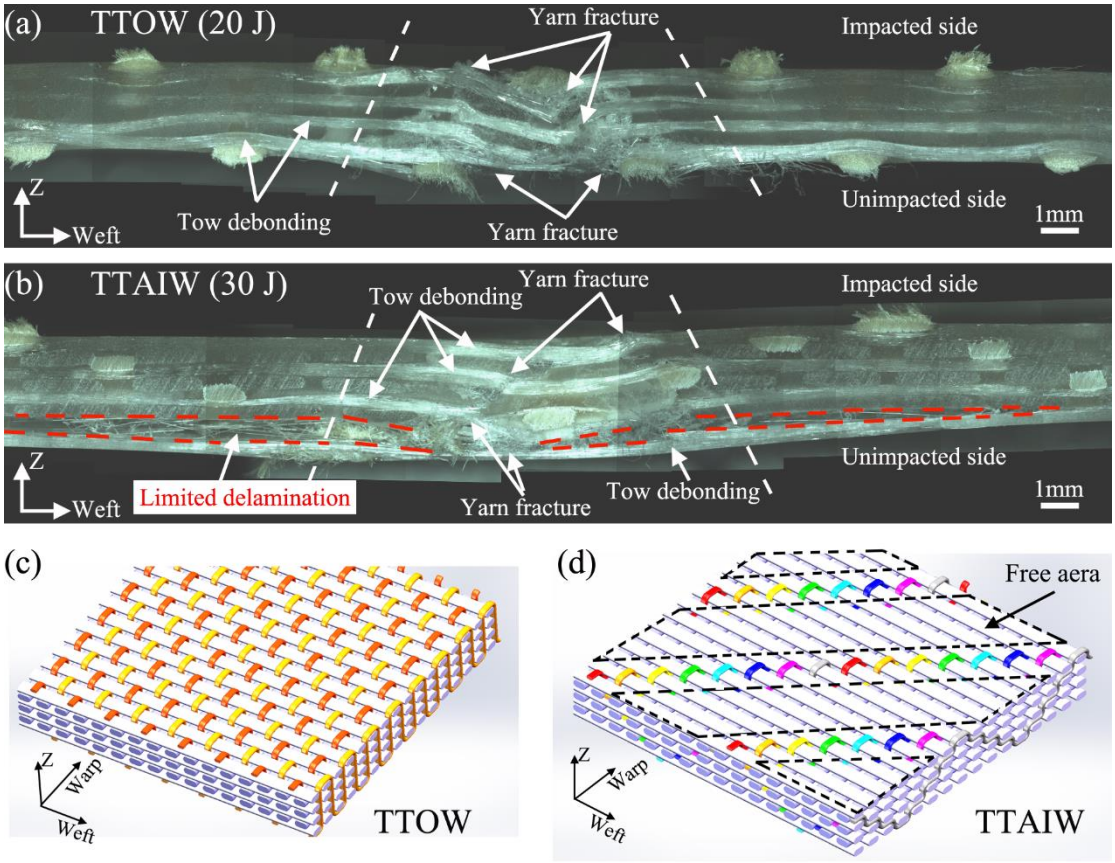

Fig. 4-8. Through-thickness failure map of composites under quasi-penetration energy impact for **(a)** TTOW and **(b)** TTAIW. Images of the free area without binder yarn between warp and weft yarn layers in 3D models for **(c)** TTOW and **(d)** TTAIW.

4.4 Conclusions

Low-velocity drop-weight impact tests of the six developed 3D woven composites were conducted under 10, 20, and 30 J impact energy levels. The effect of woven structure and impact energy on impact performance of such 3D woven composites was comprehensively studied. The failure mode of the composites was analyzed and discussed systematically. The main conclusions are as follows:

(1) The developed composites are not sensitive to low energy impact (10 J and lower energy), but sensitive to higher impact energies (20 and 30 J). The 3D woven composites exhibit a quasi-penetration energy of 20 J except the TTAIW which exhibits a quasi-penetration energy of 30 J. TTAIW with the largest fiber volume fraction and a uniform binder yarn path, is the optimal structural design among the developed composites for specific engineering application that may be subjected to low-velocity

impact.

(2) Fiber volume fraction has an obvious influence on the impact resistance of these 3D woven composites subjected to low-velocity impact. The angle-interlock group has a better impact resistance than has the orthogonal group from the perspectives of load-carrying ability, deflection characteristics, and energy characteristics. This is mainly due to angle-interlock group composites being capable of achieving a 31% higher fiber volume fraction in this weaving system compared with the orthogonal group composites. Achieving high fiber volume fraction is a top consideration for 3D woven composites to develop impact-resistance materials.

(3) Woven structure design is also a key parameter to improve impact-resistance ability for these 3D woven composites. In the angle-interlock group which has a nominal same fiber volume fraction, TTAIW composite with a uniform structure exhibits the largest peak load, DRR, energy-to-peak load, and IRI. Binder yarn path plays an important role in composite when subjected to out-of-plane low-velocity impact.

(4) Woven structure has an obvious influence on failure mode of the composites. The angle-interlock group has larger localized failure area than has the orthogonal group under all impact energy levels owing to the binder yarn path difference between the two groups. The failures in angle-interlock woven structures are more limited delamination failures and leaving of structural completeness. However, serious glass fiber fracture failure in warp and weft yarns is likely introduced for orthogonal woven structures. It is expected that perforation is likely induced for orthogonal woven structures subjected to higher impact energy due to its fiber fracture failure mode.

References

[1] Godara A, Gorbatikh L, Kalinka G, Warrier A, Rochez O, Mezzo L, et al. Interfacial shear strength of a glass fiber/epoxy bonding in composites modified with carbon nanotubes. Composites Science and Technology. 2010;70:1346-52.

[2] Valadez-Gonzalez A, Cervantes-Uc J, Olayo R, Herrera-Franco P. Effect of fiber surface treatment on the fiber–matrix bond strength of natural fiber reinforced composites. Composites Part B: Engineering. 1999;30:309-20.

[3] George J, Sreekala M, Thomas S. A review on interface modification and characterization of natural fiber reinforced plastic composites. Polymer Engineering & Science. 2001;41:1471-85.

[4] Drescher P, Thomas M, Borris J, Riedel U, Arlt C. Strengthening fibre/matrix interphase by fibre surface modification and nanoparticle incorporation into the matrix. Composites Science and Technology. 2013;74:60-6.
[5] Mouritz A. Review of z-pinned composite laminates. Composites Part A: applied science and manufacturing. 2007;38:2383-97.
[6] Cartié DD, Dell'Anno G, Poulin E, Partridge IK. 3D reinforcement of stiffener-to-skin T-joints by Z-pinning and tufting. Engineering Fracture Mechanics. 2006;73:2532-40.
[7] Nanayakkara A, Feih S, Mouritz A. Improving the fracture resistance of sandwich composite T-joints by z-pinning. Composite Structures. 2013;96:207-15.
[8] Dell'Anno G, Treiber J, Partridge I. Manufacturing of composite parts reinforced through-thickness by tufting. Robotics and Computer-Integrated Manufacturing. 2016;37:262-72.
[9] Bortoluzzi DB, Gomes GF, Hirayama D, Ancelotti AC. Development of a 3D reinforcement by tufting in carbon fiber/epoxy composites. The International Journal of Advanced Manufacturing Technology. 2019;100:1593-605.
[10] Martins A, Aboura Z, Harizi W, Laksimi A, Khellil K. Analysis of the impact and compression after impact behavior of tufted laminated composites. Composite Structures. 2018;184:352-61.
[11] Kamiya R, Cheeseman BA, Popper P, Chou T-W. Some recent advances in the fabrication and design of three-dimensional textile preforms: a review. Composites Science and Technology. 2000;60:33-47.
[12] Gerlach R, Siviour CR, Wiegand J, Petrinic N. In-plane and through-thickness properties, failure modes, damage and delamination in 3D woven carbon fibre composites subjected to impact loading. Composites Science and Technology. 2012;72:397-411.
[13] Mouritz AP, Bannister MK, Falzon P, Leong K. Review of applications for advanced three-dimensional fibre textile composites. Composites Part A: applied science and manufacturing. 1999;30:1445-61.
[14] Khokar N. 3D-weaving: theory and practice. Journal of the Textile Institute. 2001;92:193-207.
[15] Chen X, Taylor LW, Tsai L-J. An overview on fabrication of three-dimensional woven textile preforms for composites. Textile Research Journal. 2011;81:932-44.

[16] Chen X. Advances in 3D textiles: Elsevier, 2015.
[17] Cheng X, Zhou H, Wu Z, Hu X. An investigation into self-sensing property of hat-shaped 3D orthogonal woven composite under bending test. Journal of Reinforced Plastics and Composites. 2019;38:149-66.
[18] Wang X, Hu B, Feng Y, Liang F, Mo J, Xiong J, et al. Low velocity impact properties of 3D woven basalt/aramid hybrid composites. Composites Science and Technology. 2008;68:444-50.
[19] Seltzer R, González C, Muñoz R, LLorca J, Blanco-Varela T. X-ray microtomography analysis of the damage micromechanisms in 3D woven composites under low-velocity impact. Composites Part A: applied science and manufacturing. 2013;45:49-60.
[20] Miao H, Wu Z, Ying Z, Hu X. The numerical and experimental investigation on low-velocity impact response of composite panels: Effect of fabric architecture. Composite Structures. 2019;227:111343.
[21] Hart KR, Chia PX, Sheridan LE, Wetzel ED, Sottos NR, White SR. Mechanisms and characterization of impact damage in 2D and 3D woven fiber-reinforced composites. Composites Part A: applied science and manufacturing. 2017;101:432-43.
[22] Wu Z, Zhang L, Ying Z, Ke J, Hu X. Low-velocity impact performance of hybrid 3D carbon/glass woven orthogonal composite: Experiment and simulation. Composites Part B: Engineering. 2020;196:108098.
[23] Saleh MN, El-Dessouky HM, Saeedifar M, De Freitas ST, Scaife RJ, Zarouchas D. Compression after multiple low velocity impacts of NCF, 2D and 3D woven composites. Composites Part A: applied science and manufacturing. 2019;125:105576.
[24] Hao A, Sun B, Qiu Y, Gu B. Dynamic properties of 3-D orthogonal woven composite T-beam under transverse impact. Composites Part A: applied science and manufacturing. 2008;39:1073-82.
[25] Muñoz R, Martínez-Hergueta F, Gálvez F, González C, LLorca J. Ballistic performance of hybrid 3D woven composites: experiments and simulations. Composite Structures. 2015;127:141-51.
[26] Baucom J, Zikry Ma, Rajendran A. Low-velocity impact damage accumulation in woven S2-glass composite systems. Composites Science and Technology. 2006;66:1229-38.

[27] Baucom JN, Zikry M. Low-velocity impact damage progression in woven E-glass composite systems. Composites Part A: applied science and manufacturing. 2005;36:658-64.
[28] Elias A, Laurin F, Kaminski M, Gornet L. Experimental and numerical investigations of low energy/velocity impact damage generated in 3D woven composite with polymer matrix. Composite Structures. 2017;159:228-39.
[29] Zhang D, Gu Y, Zhang Z, Jia M, Yue S, Li G. Effect of off-axis angle on low-velocity impact and compression after impact damage mechanisms of 3D woven composites. Materials & Design. 2020;192:108672.
[30] Behera Ba, Dash B. Mechanical behavior of 3D woven composites. Materials & Design. 2015;67:261-71.
[31] Cao W, Zhang J, Sun B, Gu B. X-ray tomography and numerical study on low-velocity impact damages of three-dimensional angle-interlock woven composites. Composite Structures. 2019;230:111525.
[32] Umer R, Alhussein H, Zhou J, Cantwell W. The mechanical properties of 3D woven composites. Journal of Composite Materials. 2017;51:1703-16.
[33] Zhou L, Zeng J, Jiang L, Hu H. Low-velocity impact properties of 3D auxetic textile composite. Journal of materials science. 2018;53:3899-914.
[34] Bandaru AK, Chavan VV, Ahmad S, Alagirusamy R, Bhatnagar N. Low velocity impact response of 2D and 3D Kevlar/polypropylene composites. International Journal of Impact Engineering. 2016;93:136-43.
[35] Bandaru AK, Patel S, Sachan Y, Alagirusamy R, Bhatnagar N, Ahmad S. Low velocity impact response of 3D angle-interlock Kevlar/basalt reinforced polypropylene composites. Materials & Design. 2016;105:323-32.
[36] Dau F, Dano M-L, Duplessis-Kergomard Y. Experimental investigations and variability considerations on 3D interlock textile composites used in low velocity soft impact loading. Composite Structures. 2016;153:369-79.
[37] Bhudolia SK, Joshi SC. Low-velocity impact response of carbon fibre composites with novel liquid Methylmethacrylate thermoplastic matrix. Composite Structures. 2018;203:696-708.
[38] Naik NK, Sekher YC, Meduri S. Damage in woven-fabric composites subjected to low-velocity impact. Composites Science and Technology. 2000;60:731-44.

Chapter 5 Flexural performance of carbon fiber 3D woven composites developed based on traditional weaving technology

5.1 Introduction

Nowadays, carbon fiber-reinforced plastic/polymer (CFRP) materials have a wide application in aerospace, automobile, sports, etc., due to their superior mechanical properties, low weight compared to metal materials. Traditional CFRPs with laminated structures are easily introduced delamination failures when subjected to out-of-plane loadings, due to their low interlayer strength since there is no fiber reinforcement in the through-thickness direction. Out-of-plane loadings, especially low-velocity impact loading which may be introduced by tool-drop during maintenance, always leave a barely visible indent on the CFRP component surface but decrease the residual strength dramatically, and, thus, it is important to improve the interlayer strength of these materials. Many techniques have been applied to improve interlayer strength of the laminated composites by modifying fiber/matrix interface [1-3], as well as introducing fiber reinforcement in composite through-thickness direction [4-6]. 3D textiles have been introduced since decades ago as the reinforcement in CFRP materials to improve delamination resistance ability. 3D textile is defined as the textile with a whole 3D structure or with inner yarn interlacement in three perpendicular directions [7]. Particularly, 3D woven textiles which are manufactured based on the weaving technology have attracted much attention from researchers.

There are several weaving technologies to manufacture carbon fiber textile preforms. Traditional weaving loom, Jacquard weaving loom, 3D weaving loom, specially designed loom or machine could be used to manufacture carbon fiber 3D woven textiles with some modifications, due to the conductive property and brittle character of carbon fiber. In a complex net-shaped 3D woven textile-reinforced composite component, such as composite engine fan blade, different woven structures are needed in different sections of the component to meet the specific mechanical requirements, thus, it is important to study the mechanical performance of the composites with various reinforcement structures.

In this chapter, four carbon fiber 3D woven textiles with special structural design (weft interlock) having same warp-yarn density, weft-insertion density, and textile areal

density, as well as different woven structures with specific weft-to-binder yarn ratios, were manufactured based on a traditional weaving technology successfully. The textile reinforced CFRP composites with same composite fiber volume fraction and different reinforcement structures were developed via VARTM technique. Three-point bending tests and low-velocity drop-weight impact tests were conducted on the 3D woven CFRP composites to study the effect of woven structure on their out-of-plane mechanical performance. The failure mode of these CFRP materials were studied with ultrasonic C-scan and X-ray micro computed tomography (μCT) techniques, and the failure mechanism is clarified for the engineering application.

5.2 Materials and experiments

5.2.1 Three-dimensional woven textiles

Three 3D orthogonal woven textiles namely 3D-a, 3D-b, and 3D-c, and one multilayer woven textile namely 2.5D, were manufactured based on a carbon fiber dobby sample weaving loom (Orika TNY101A-20T, Toyoshima Business System Corp., Japan), as shown in **Fig. 5-1 (a)**. Carbon fiber (T300B-3000, Torayca®, Toray Corp., Japan) with 3K filaments per bundle was used to manufacture these woven structures. The textile structural design and the weaving diagram for four textiles are shown in **Fig. 5-1 (b)**, **(c)**, **(d)**, and **(e)**. There are eight layers of warp yarn for all woven structures, and seven layers of weft yarn for 3D orthogonal woven and eight for 2.5D woven. There are 14, 6 and 2 binder yarns for 3D-a, 3D-b, 3D-c structures in one repeat unit, the binder yarns bind adjacent two, four, and all eight warp-yarn layers, respectively. 2.5D structure has a similar structural design with 3D-a structure, in which the binder yarns have same path, and both bind adjacent two warp-yarn layers. Moreover, for 2.5D structure, the weft yarn at each layer has an interlacement with warp yarn at same layer, but for the 3D woven structures, there is no interlacement between weft and warp yarns.

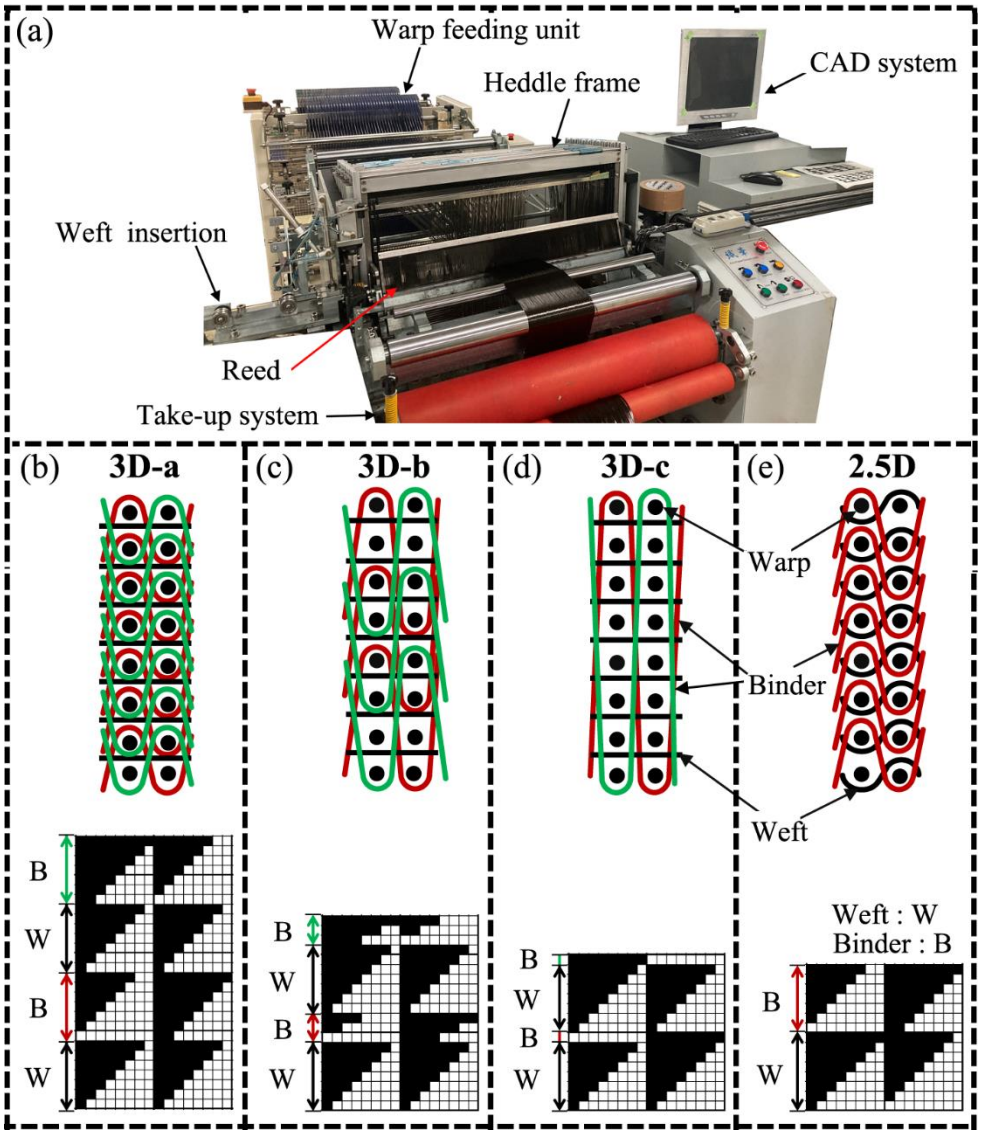

Fig. 5-1. **(a)** Carbon fiber dobby sample weaving loom. Textile architecture and weave diagram for four woven textiles: **(b)** 3D-a, **(c)** 3D-b, **(d)** 3D-c and **(e)** 2.5D.

The textile preform specifications are listed in **Table 5-1**. Top view surface photographs of the four woven textiles are shown in **Fig. 5-2**. During weaving process, same warp-yarn density of 20 ends/cm (2.5 ends/cm/layer) and same weft-insertion density of 47 picks/cm were set for the four woven structures to acquire same textile areal density and same composite fiber volume fraction. The low warp-yarn density is due to the limitation of amount of warp yarns based on the sample weaving loom. The weft insertions both served as weft yarns and binder yarns, and the ratio of weft-yarn to binder-yarn is different for the four woven structures, for example, 3D-a has a value of 7:7, which meaning that half of the weft insertions are served as binder yarns and half as

weft yarns. It should be noted that for the 3D-c with a highest weft-to-binder yarn ratio among all woven structures, which means that the largest amount of the weft insertion served as weft yarn, however, weft yarns are squeezed to have a zigzag waviness in weft direction in this case, which is marked with a red line as shown in **Fig. 5-2 (c)**, whereas other structures have a straight weft-yarn alignment. The relationship between weft-to-binder yarn ratio and weft-/binder-yarn density for the four woven textiles is depicted in **Fig. 5-3**, a larger weft-to-binder yarn ratio in the textiles, a larger weft-yarn density could be achieved, and a smaller binder-yarn density is exhibited. For instance, 3D-c structure with the largest weft-to-binder yarn ratio has the largest weft-yarn density (41.3 picks/cm), followed with 3D-b, 2.5D, and 3D-a structures (32.9, 24.8, and 23.8 picks/cm, respectively). The special structural design in which arranging binder yarns in weft direction instead of warp direction during weaving process has many advantages: less heddle frames are needed to developed 3D woven structures, especially structures with more yarn layers. For instance, if weaving 3D-a structures with traditional warp-interlock structural design, 28 heddle frames are needed, but with the special weft-interlock structural design, only 16 heddle frames are needed; There is no need to rearrange warp yarns when developing more types of woven structures, especially the structures with different binder-yarn ratios; No more warp-yarn feeding system modification is needed based on traditional weaving loom to manufacture 3D woven structures since the binder yarn lies in weft direction; It has great potential to develop complex woven structures with different woven structures in different sections.

Table 5-1. Specifications of four woven fabrics.

Woven structure	**3D-a**	**3D-b**	**3D-c**	**2.5D**
Thickness (mm)	2.0	2.0	2.1	2.0
Areal density (g/m^2)	1276	1276	1276	1276
Warp yarn density (ends /cm/layer)	2.5	2.5	2.5	2.5
Weft yarn density (picks /cm/layer)	3.4	4.7	5.9	3.1
Binder yarn density (picks /cm/layer)	3.4	4.7	5.9	3.1
No. of warp-yarn layers	8	8	8	8
No. of weft-yarn layers	7	7	7	8
No. of binder-yarn layers	7	3	1	7
Weft-to-binder yarn ratio	7/7	7/3	7/1	8/7

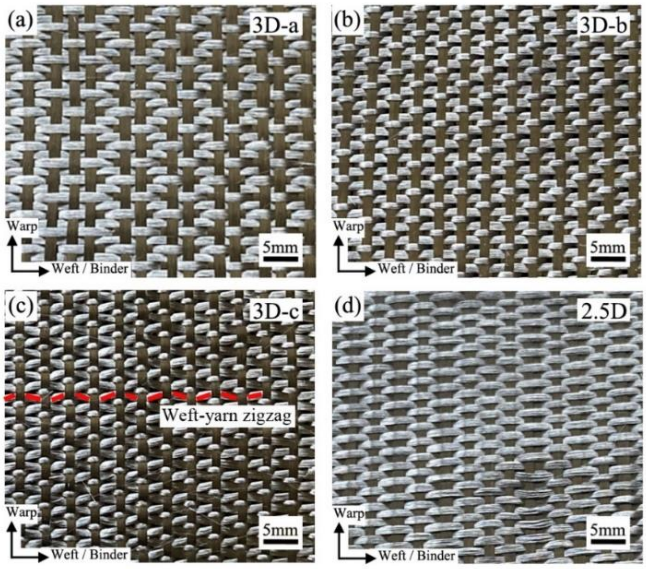

Fig. 5-2. Textile surface photographs of four woven structures: **(a)** 3D-a, **(b)** 3D-b, **(c)** 3D-c, and **(d)** 2.5D.

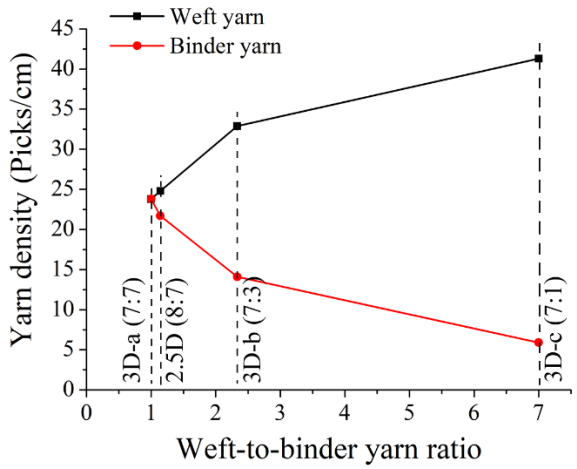

Fig. 5-3. Relationship between weft-to-binder yarn ratio and weft- and binder-yarn density for four woven textiles.

5.2.2 Three-dimensional woven composites

Carbon fiber 3D woven composites were fabricated using VARTM technology same to that of glass/aramid fiber hybrid 3D woven composites developed in Chapter 2.

The internal geometry of binder yarn in each woven structure is shown in **Fig. 5-4**. Composites specifications and internal geometry parameters of binder yarn in 3D/2.5D woven composites are summarized in **Table 5-2**. It should be noted that 3D-a and 2.5D multilayer have similar binder yarn path and waviness owing to the structural similarity,

in which same binder path exhibits. Binder-yarn waviness degree (2A/L) is defined as the ratio of binder-yarn double amplitude to wavelength, a large valve of 2A/L means that binder yarn has a larger waviness and lies more in through-thickness direction in composite.

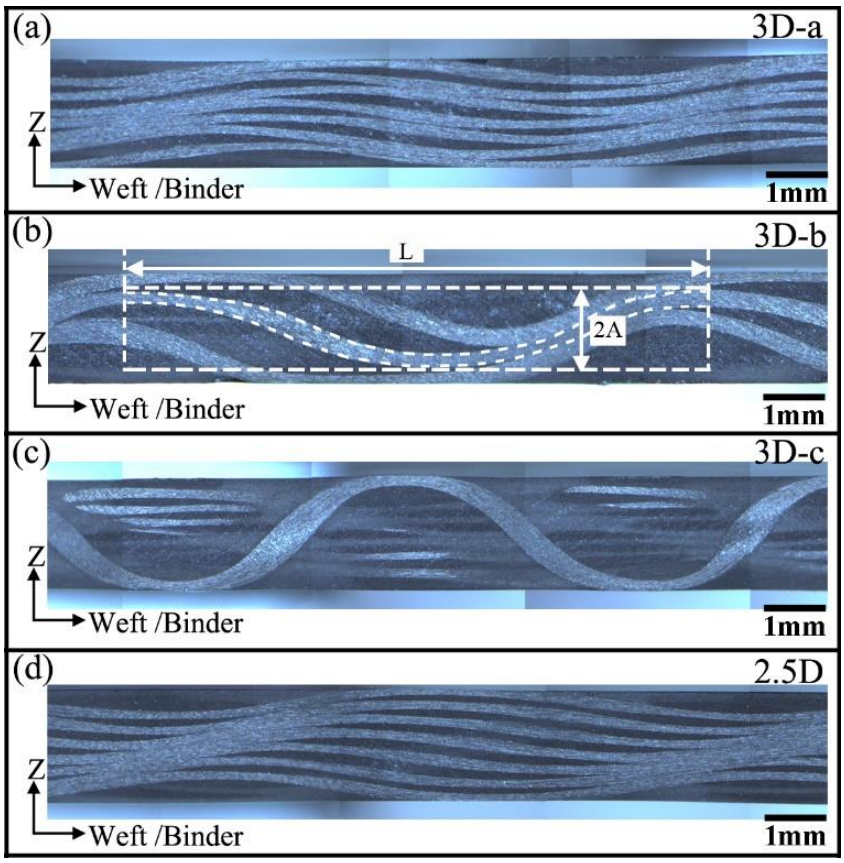

Fig. 5-4. Binder yarn path in four woven composites: **(a)** 3D-a, **(b)** 3D-b, **(c)** 3D-c, and **(d)** 2.5D. Section parallel to weft direction.

Table 5-2. Composite specifications and internal geometry parameters of binder yarn for four woven composites.

Woven structure	**3D-a**	**3D-b**	**3D-c**	**2.5D**
Composite thickness (mm)	1.74	1.71	1.95	1.72
Fiber volume fraction	0.38	0.38	0.37	0.38
Binder-yarn wavelength/ L (mm)	8.50	8.50	8.50	8.50
Binder-yarn amplitude/ A (mm)	0.23	0.61	0.98	0.23
Binder-yarn waviness degree (2A/L)	0.05	0.14	0.23	0.05

5.2.3 Three-point bending test

Three-point bending test was conducted on a universal material testing machine (AG-20kND, SHIMAZU Corp., Japan) with a 20kN load cell to study the quasi-static flexural performance of the composites. A loading nose of 10 mm diameter and loading rate of 5 mm/min were applied, support span was 60 mm long. Five warp- and five weft-direction beam specimens were tested, the beam specimens had a length of 80 mm, a width of 20 mm, and a thickness of 2 mm. In this study, flexural Stress and strain was calculated by Eq. (5-1) and Eq. (5-2), respectively, in accordance with ASTM D7264:

$$\sigma = 3PL/2bd^2 \tag{5-1}$$

$$\varepsilon = 6\delta d/L^2 \tag{5-2}$$

where σ denotes the stress on the outer surface at the midspan of the composite beam specimen, P denotes the applied force, L denotes the support span, b denotes the beam width, d denotes the beam thickness, ε denotes the maximum strain in the outer surface, and δ denotes the midspan deflection.

5.2.4 Low-velocity drop-weight impact test

Low-velocity impact test was conducted on an Instron Dynatup 9250HV drop-weight impact testing machine under 3-, 6- and 9-J impact energy levels to study the dynamic flexural performance of the composites. A hemispherical steel impactor of 12.7 mm in diameter, 7.07 kg in weight, and with a 22kN load cell was used in these tests. The force history is measured by a load cell located in the impactor; the displacement and velocity history of impactor is measured by the testing machine; impact energy was adjusted by changing the height of impactor drop weight. Three plate specimens for each impact energy level were tested for each woven structure. Specimen was held by two rigid square jaw platforms with a circular free zone of 70 mm diameter to avoid specimen slippage during test. The dimensions of tested composite plate specimens are 100×100 mm^2, the set-up of low-velocity drop-weight impact test and size of composite plate specimen are shown in **Fig. 5-5**.

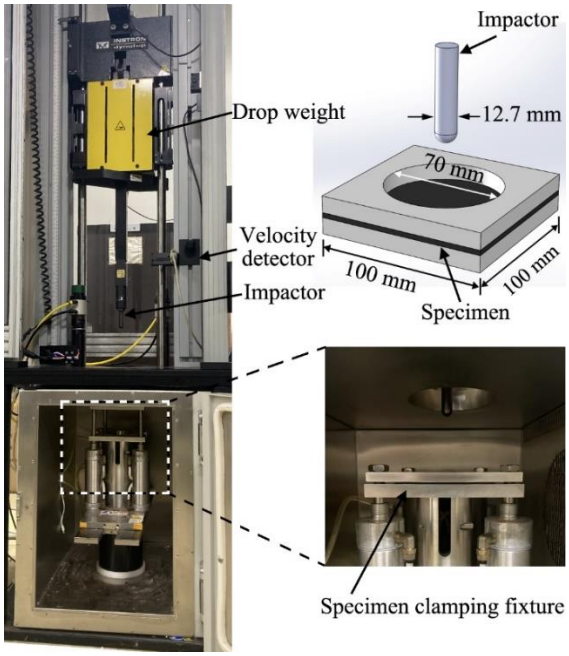

Fig. 5-5. Experimental set-up of low-velocity drop-weight impact testing machine.

5.2.5 Ultrasonic C-scan observation

Non-destructive ultrasonic C-scan (Fine SAT, Hitachi Corp., Japan) was applied to analyze the interlayer failures of the composite plate specimens after impact tests. A probe of PT1-15-17 with a frequency of 5 MHz, a focal distance of 17 mm was applied. 0.1 μs of focus gate width was selected and each gate has about 0.1 mm thickness in tested specimens. The schematic of the C-scan testing is depicted in **Fig. 5-6**, the upper, middle, and lower layers, which are about 0.5, 1.0 and 1.5 mm away from the composite impacted surface, are scanned to clarify the failure map in through-thickness direction.

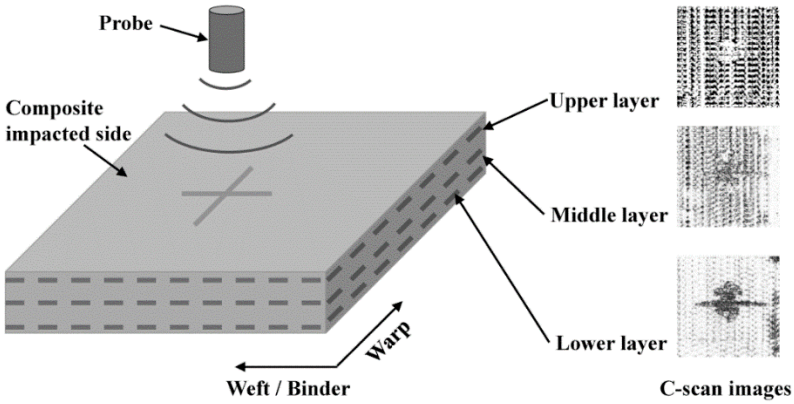

Fig. 5-6. Schematic of ultrasonic C-scan testing for composites after low-velocity drop-weight impact.

5.2.6 X-ray micro-CT inspection

Non-destructive X-ray μCT (Skyscan 1272, Bruker Corp., USA) was applied to characterize the internal failure mechanism of the composites after impact tests. The schematic illustration of the X-ray μCT scanning is depicted in **Fig. 5-7**, X-ray μCT relies on computational reconstruction of slice-by-slice projections under many different angles of illumination, and image contrast relies on attenuation differences of X-rays which path through the test specimen. 3D visual images could be obtained and each slice in the 3D images could be inspected. Test specimen (25×25 mm^2) is cut from impacted composite plate, and the impacted position is located at the center of the test specimen. Voxel size of 5 μm, specimen rotation step of 0.3°, 2 averaging frames at each angular position were set. X-ray bean energy of 50 kV and 200 μA and no filtering were applied.

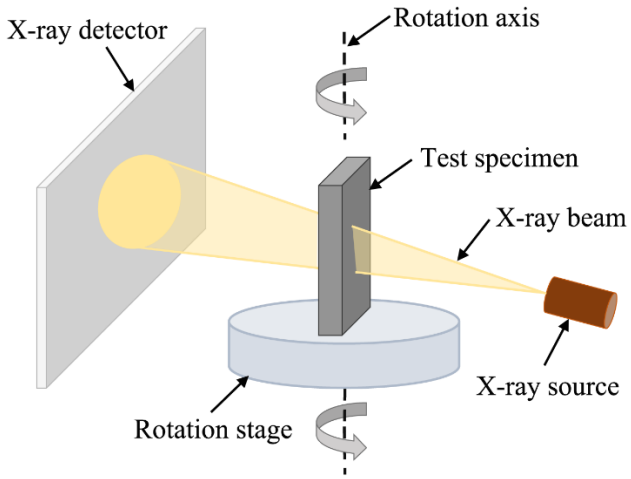

Fig. 5-7. Schematic illustration of X-ray μCT scanning for an impacted composite specimen.

5.3 Results and discussion

5.3.1 Quasi-static flexural performance

Representative flexural stress-strain curves and the flexural property figures for the four woven composites under three-point bending tests are plotted in **Fig. 5-8**. Weft- and warp-direction composite beams for each woven structure were conducted under three-point bending tests, and weft-direction composite specimens have about double higher flexural modulus and strength than have warp-direction specimens for all woven structures, as shown in **Fig. 5-8 (a)**, **(b)** and **(c)**, this is mainly due to that there is about

double higher yarn-density along weft direction than is along warp direction for the four woven textiles in the weaving process as mentioned previously. For weft-direction beams, weft and binder yarns are in beam-length direction and carry most load during bending event. 3D-a and 2.5D structures which have the smallest weft-to-binder yarn ratio of 7:7 and 8:7 as well as smallest weft-yarn density of 23.8 and 24.8 picks/cm, respectively, exhibit the largest weft-direction flexural modulus and strength, this mainly due to that binder yarn in the two structures has smaller waviness degree (2A/L = 0.05) and lies more in in-plane direction, and, thus, has more in-plane load-bearing capacity when subjected to out-of-plane loads. Moreover, for 3D-a and 2.5D structures, which have similar structural design, 3D-a exhibits a better flexural modulus and strength, this is mainly due to that 3D-a has straight weft-yarn alignment, whereas weft yarn in in 2.5D structure has a waviness due to the interlacement with warp yarn. Compared with 3D-a and 2.5D structures, 3D-b has a larger weft-to-binder yarn ratio of 7:3 and a larger weft-yarn density of 32.9 picks/cm, but exhibits a smaller flexural modulus and strength, this is mainly because that the binder yarn in 3D-b has a large waviness degree (2A/L = 0.14), and, thus, has less in-plane load-carrying ability. 3D-c structure with the largest weft-to-binder yarn ratio of 7:1 and the largest weft yarn density of 41.3 picks/cm, exhibits the smallest flexural modulus and strength, this mainly due to that weft-yarn waviness (zigzag) in in-plane direction, decreases the mechanical performance. For warp-direction beams which have same warp-yarn density and arrangement in beam-length direction, similar flexural modulus and strength trends exhibited with weft-direction beams, this indicate that yarn arrangement in weft direction both influence quasi-static flexural performance for weft-direction beams and warp-direction beams, due to the existence of binder yarn binding the structure into an integrity.

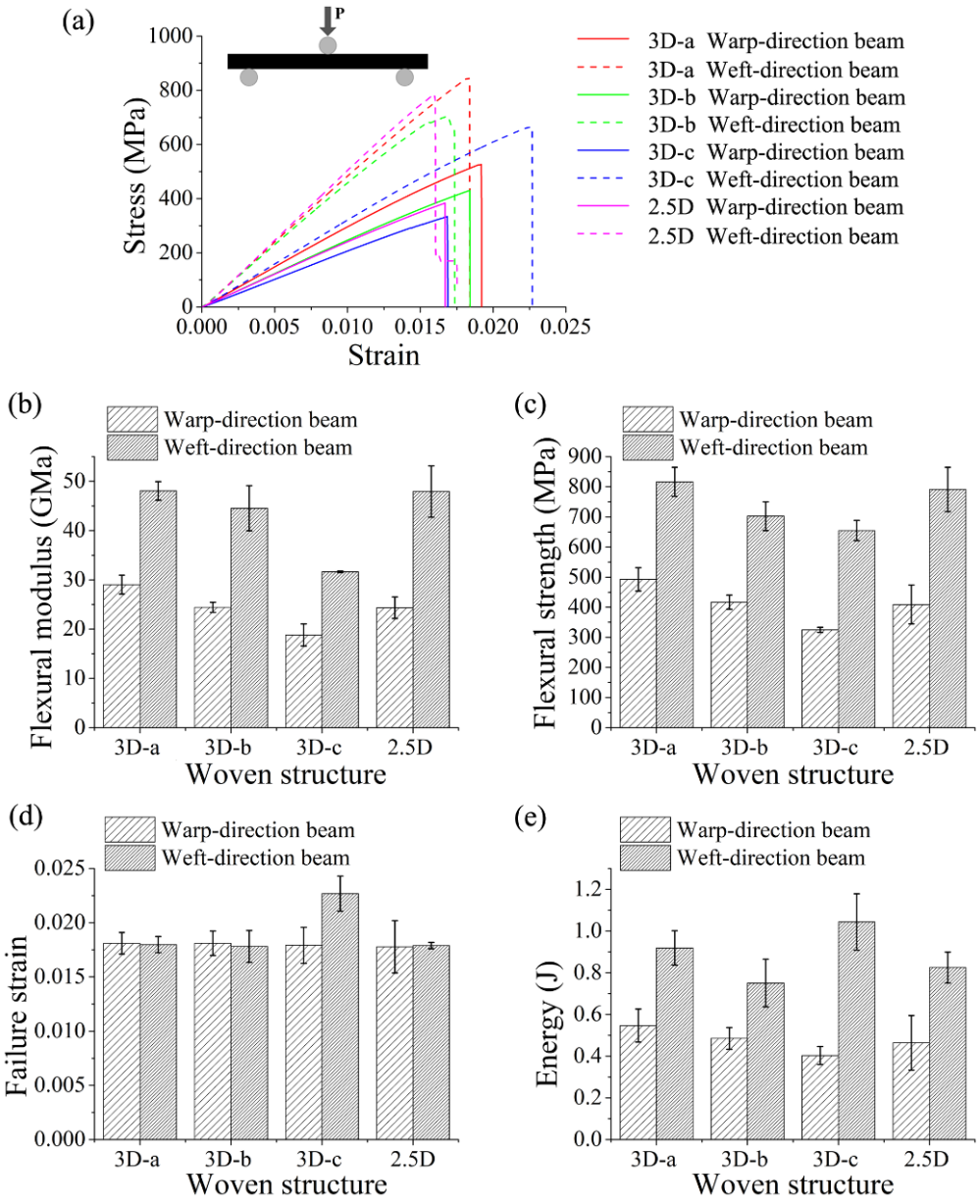

Fig. 5-8. **(a)** Representative flexural stress-strain curves for four woven composites under three-point bending tests. Flexural properties of the woven composites: **(b)** flexural modulus, **(c)** flexural strength, **(d)** failure strain, and **(e)** deformation energy.

Table 5-3. Three-point bending test results for the four woven composites.

Textile structure		**3D-a**	**3D-b**	**3D-c**	**2.5D**
Flexural modulus (GPa)	Warp-direction beam	29.03	24.41	18.82	24.34
	Weft-direction beam	48.05	44.52	31.63	47.92
Flexural strength (MPa)	Warp-direction beam	492.57	416.61	325.07	408.94
	Weft-direction beam	816.21	702.20	654.45	791.20
Failure strain	Warp-direction beam	0.018	0.018	0.018	0.018
	Weft-direction beam	0.018	0.018	0.023	0.018
Deformation energy (J)	Warp-direction beam	0.55	0.49	0.40	0.46
	Weft-direction beam	0.92	0.75	1.04	0.83

There are similar failure strains for all woven structures except for 3D-c in weft direction, as shown in **Fig. 5-8 (d)**, this may be attributed to the largest binder yarn undulation and the in-plane waviness (zigzag) of weft yarn in 3D-c structure, and the later may play a key role. Deformation energy during three-point bending is larger for weft-direction beams than is for warp-direction beams for all woven structures, as shown in **Fig. 5-8 (e)**, and this is due to that higher flexural modulus and strength of weft-direction specimens and higher yarn density in weft direction. 3D-c weft-direction beams have the largest of deformation energy, mainly due to the largest of failure strain.

Above all, weft-/binder-yarn ratio, binder yarn waviness degree as well as in-plane yarn waviness have an obvious influence on the quasi-static flexural performance of the woven composites. 3D-a and 2.5D have largest flexural modulus and strength, then followed with 3D-b and 3D-c.

5.3.2 Low-velocity impact mechanical response

In a low-velocity impact event, load-bearing ability, deflection characteristics and energy characteristics are vital parameters to clarity the impact performance of an impacted composite. Representative load-deflection and energy-time curves of low-velocity impact tests for four woven composites subjected to three impact energy levels: 3, 6, and 9 J, are depicted in **Fig. 5-9**. For 3-J impacts, four woven composites exhibit a similar mechanical behavior, as shown in **Fig. 5-9 (a1)** and (**a2)**. In this case, deflection recoveries and rebound energies are exhibited for the four composites in load-deflection curves and energy-time curves, respectively, which mean that the impactor rebounded from the impacted composites. For 6-J impacts, the composites exhibit a penetration or perforation failure except 3D-c. A penetration or perforation failure happens when there is no deflection recovery and rebound energy, as shown in **Fig. 5-9 (b1)** and **(b2)**. It should be noted that 3D-c structure exhibits a deflection recovery and a rebound energy, whereas other structures exhibit penetration or perforation failure, which means that 3D-c has a superior impact-resistance performance among these composites under 6-J impact. This may mainly be attributed to the woven structure of the 3D-c, in which these has a through-thickness binder yarn path and an in-plane weft yarn zigzag waviness. For 9-J impacts, all woven composites exhibit a penetration or perforation performance, which indicated by that there is no deflection recovery and no rebound energy in load-deflection curves and energy-time curves, respectively, as shown in **Fig. 5-9**

(c1) and **(c2)**. Above all, from the perspective of deflection characters and rebounding energy in the impact event, these 3D woven composites all survived from 3-J impacts; exhibit penetration or perforation failure under 6-J impacts except for 3D-c structure; and all failed under 9-J impacts. For 3-J and 9-J impacts, composites exhibit similar behavior due to that composite survive under 3-J impacts and perforate under 9-J impacts. For 6-J impact, 3D-c exhibit the largest peak load, and followed with 3D-b, 3D-a and 2.5D structures, at the same time, 3D-c has a deflection recovery ratio of 0.277 whereas other structures have a value of 0, all indicate that 3D-c exhibit the best impact performance.

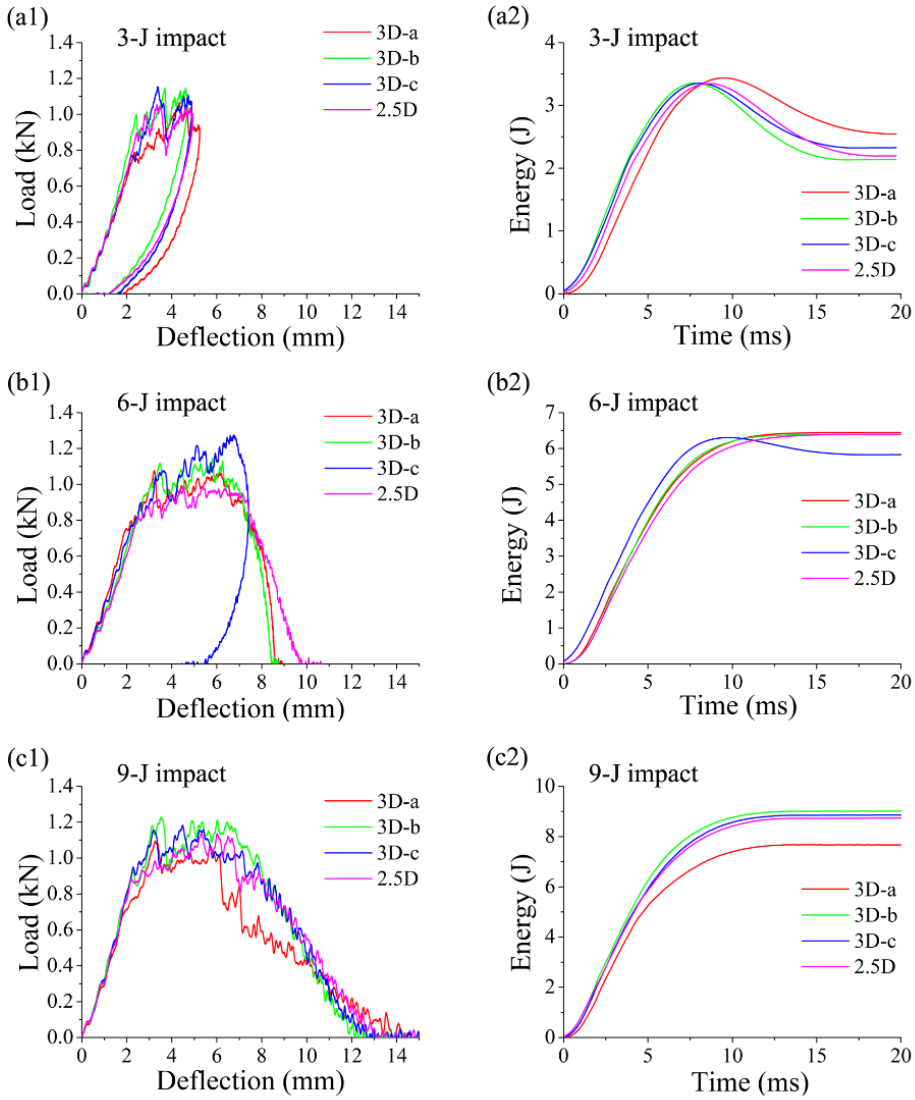

Fig. 5-9. Representative load-deflection and energy-time curves of low-velocity impact tests for four woven composites subjected to three impact energy levels: **(a1, a2)** 3, **(b1, b2)** 6, and **(c1, c2)** 9 J.

The peak load, DRR, energy-to-peak load, and IRI vasus impact energy for the four woven composites are depicted in **Fig. 5-10.** The low-velocity impact results of the composites are summarized in **Table 5-4**. Above all, 3D-c and 3D-b have larger peak loads than 3D-a and 2.5D in each impact energy level, as shown in **Fig. 5-10 (a)**. particularly, in 6-J impacts which is penetration or perforation threshold for the composites, 3D-c exhibits the largest peak load of 1.27 kN, and followed with 3D-b, 3D-a and 2.5D of 1.18, 1.10, and 1.01 kN, respectively. Under 6-J impact, the 3D-c has a DRR of 0.277, whereas other composites exhibit a value of 0, as shown in **Fig. 5-10 (b)**, which means that only 3D-b survives from 6-J impact, and other structures exhibit penetration or perforation. Energy-to-peak load characteristics, as shown in **Fig. 5-10 (c)**, show a similar result with peak load characteristics, especially in 6-J impact case. From the perspective of IRI, as shown in **Fig. 5-10 (d)**, 3D-c exhibits a value of 0.094, whereas other structures have a value of 0, which means that 3D-c has impact-resistance ability in 6-J impact case, and other woven structures failed. Overall, 3D-c exhibit the best impact resistance performance, and followed with 3D-b, 3D-a, and 2.5D structures.

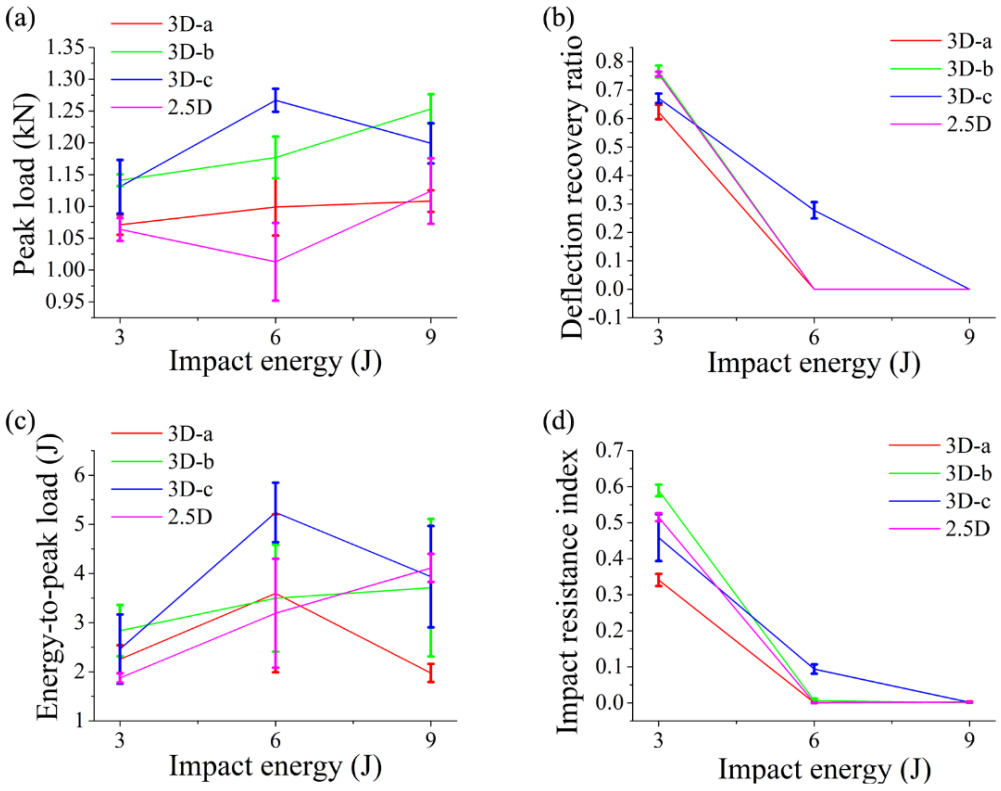

Fig. 5-10. Low-velocity impact test results for four woven structure composites: **(a)** peak load, **(b)** deflection recovery ratio, **(c)** energy-to-peak load, and **(d)** impact resistance index.

Table 5-4. Low-velocity impact test results for the four woven composites.

Textile structure		3D-a	3D-b	3D-c	2.5D
Peak load (kN)	3-J impact	1.07	1.14	1.13	1.06
	6-J impact	1.10	1.18	1.27	1.01
	9-J impact	1.11	1.25	1.20	1.12
Maximum deflection (mm)	3-J impact	5.19	4.70	4.93	4.82
	6-J impact	8.50	7.72	7.23	8.45
	9-J impact	13.80	12.32	12.79	12.96
Permanent deflection (mm)	3-J impact	1.95	1.10	1.62	2.00
	6-J impact	8.50	7.72	5.23	8.45
	9-J impact	13.80	12.32	12.79	12.96
Deflection recovery ratio	3-J impact	0.623	0.765	0.671	0.756
	6-J impact	0	0	0.277	0
	9-J impact	0	0	0	0
Absorbed energy (J)	3-J impact	2.55	2.10	2.30	2.21
	6-J impact	6.42	6.36	5.77	6.38
	9-J impact	7.72	9.11	8.86	8.56
Rebounded energy (J)	3-J impact	0.87	1.24	1.05	1.14
	6-J impact	0	0	0.54	0
	9-J impact	0	0	0	0
Energy-to-peak load (J)	3-J impact	2.26	2.84	2.46	1.87
	6-J impact	3.40	3.50	5.24	3.19
	9-J impact	1.97	3.71	3.94	4.11
Impact resistance index	3-J impact	0.341	0.590	0.459	0.515
	6-J impact	0	0	0.094	0
	9-J impact	0	0	0	0

5.3.3 Low-velocity impact failure modes

Ultrasonic C-scan images of the four woven composites after low-velocity drop-weight impact are depicted in **Figs. 5-11**, **5-12**, and **5-13**. It could be concluded that all woven composites exhibit an elliptical failure at upper and middle layers and a cross-shaped failure with hands along textile warp and weft directions at lower layers, and the failure aera (closed with red line) is larger at lower layer, where is the tensile side under out-of-plane deflection in the impact event. The failure area basically increases with the increasing of impact energy for each woven structure. These cross-shaped failures have a larger aera in hands along textile warp direction than have along textile weft direction, and, at the same time, a thinner and longer hand in weft direction. This may be attributed to that there is a roughly double higher yarn density in textile weft direction for these woven composites, and, thus, more load-bearing ability in weft direction, thus failures are different in warp and weft directions. The failure detected by C-scan is mainly the limited deflection and debonding failure which could introduce larger ultrasonic signals reflections, this limited delamination or debonding failures more easily develop along

textile warp direction for the developed 3D woven composites. Moreover, there is no obvious C-scan failure-areal difference among the four woven composites under each impact energy level since there is macrolevel structural similarity among the woven composites. A detailed failure mode inspection is needed with X-ray μCT scanning.

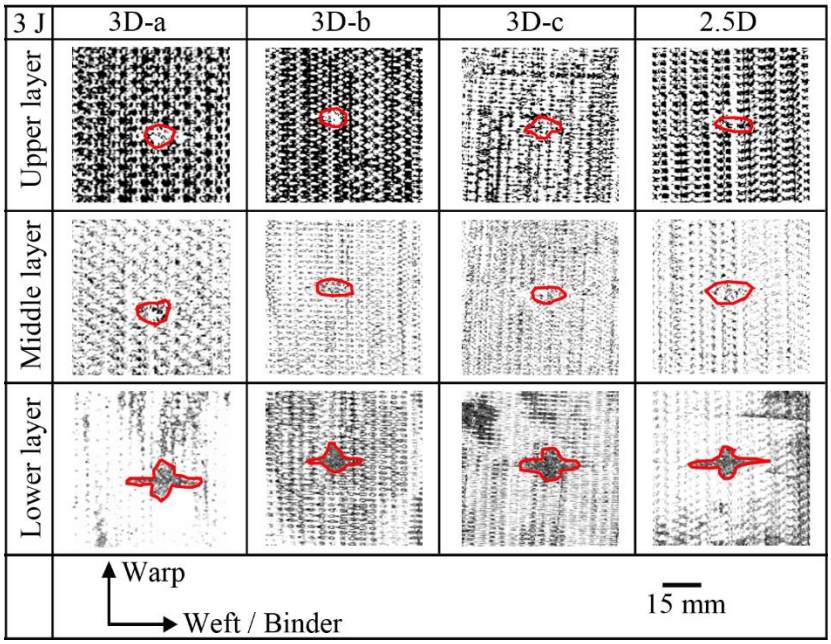

Fig. 5-11. Ultrasonic C-scan images of four woven composites under 3-J impact.

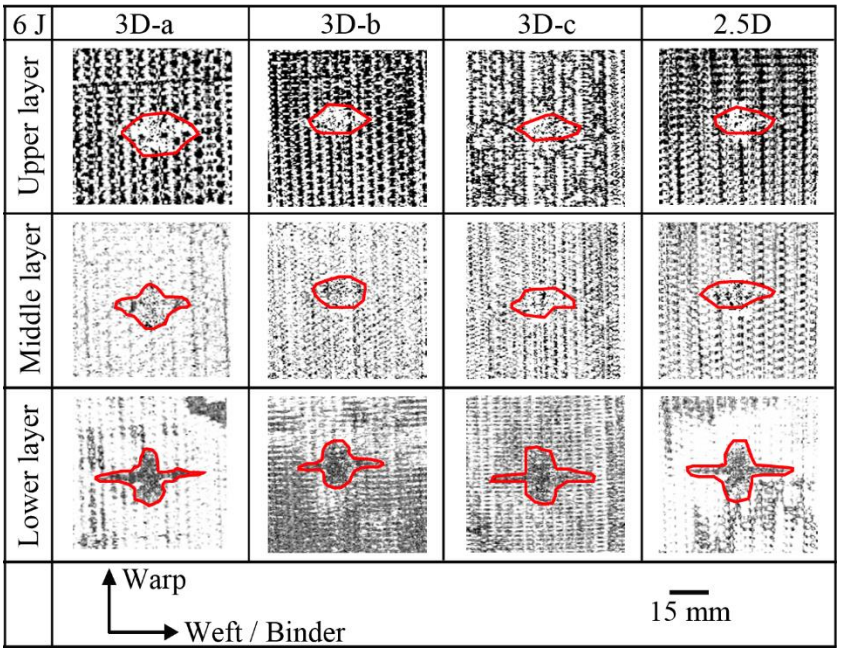

Fig. 5-12. Ultrasonic C-scan images of four woven composites under 6-J impact.

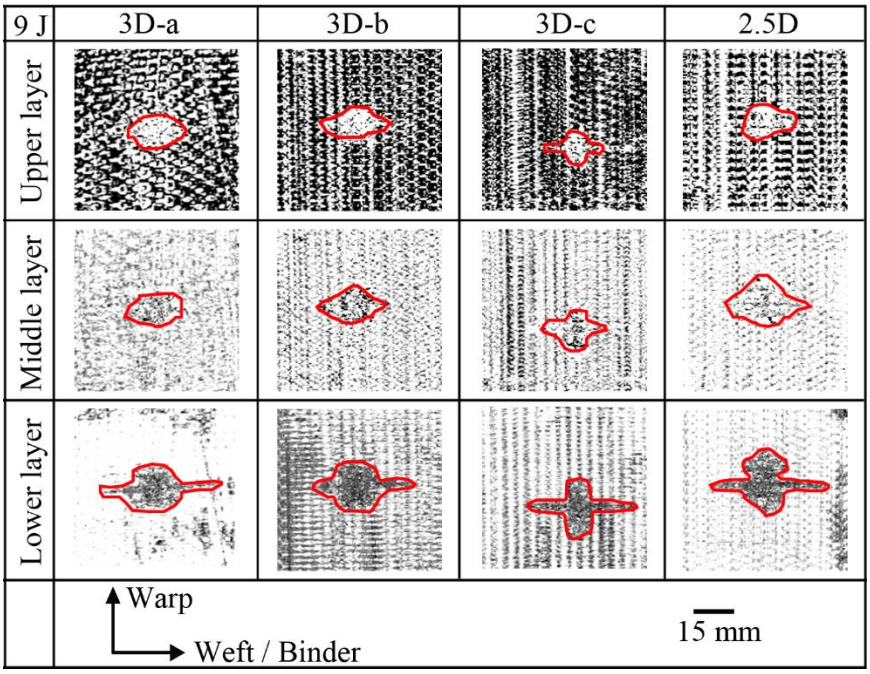

Fig. 5-13. Ultrasonic C-scan images of four woven composites under 9-J impact.

X-ray μCT scanning of the post-impact specimens of 3D-a and 3D-c under 6-J impact were conducted to clarify the effect of woven structure on the failure mechanism. X-ray μCT scanning images of post-impacted 3D-a composite are shown in **Fig. 5-14**. 3D image was reconstructed as shown in **Fig. 5-14 (a)**, and two slices which are parallel to textile warp (Slice a) and weft (Slice b) directions were inspected (**Fig. 5-14 (b)** and **(c)**). For the Slice a, there is a serious through-thickness crack at the center, and this crack exists at every slice parallel to the inspected Slice a, corresponding to the thinner and longer hand of cross-shaped failure in ultrasonic C-scan images (**Fig. 5-12**). At the same time, obvious through-thickness cracks exist away from the center part, and longitudinal cracks mainly located at the lower layers (**Fig. 5-14 (b)**). The through-thickness cracks correspond to in-plane yarn (warp yarn) breakage and resin crack failures, and the longitudinal cracks correspond to the yarn-resin debonding failure. On the other hand, for the Slice b which is parallel to weft direction as shown in **Fig. 5-14 (c)**, through-thickness crack exists at the center part, and limited delamination failures along weft and binder yarns exist, which is different from the Slice a. This is mainly due to the larger yarn density in weft direction, and thus larger load-bearing ability, less serious through-thickness failures, more limited delamination failures caused by shear force in an impact event. This corresponds to the larger failure area along warp direction in C-scan cross-shaped failure (**Fig. 5-12**).

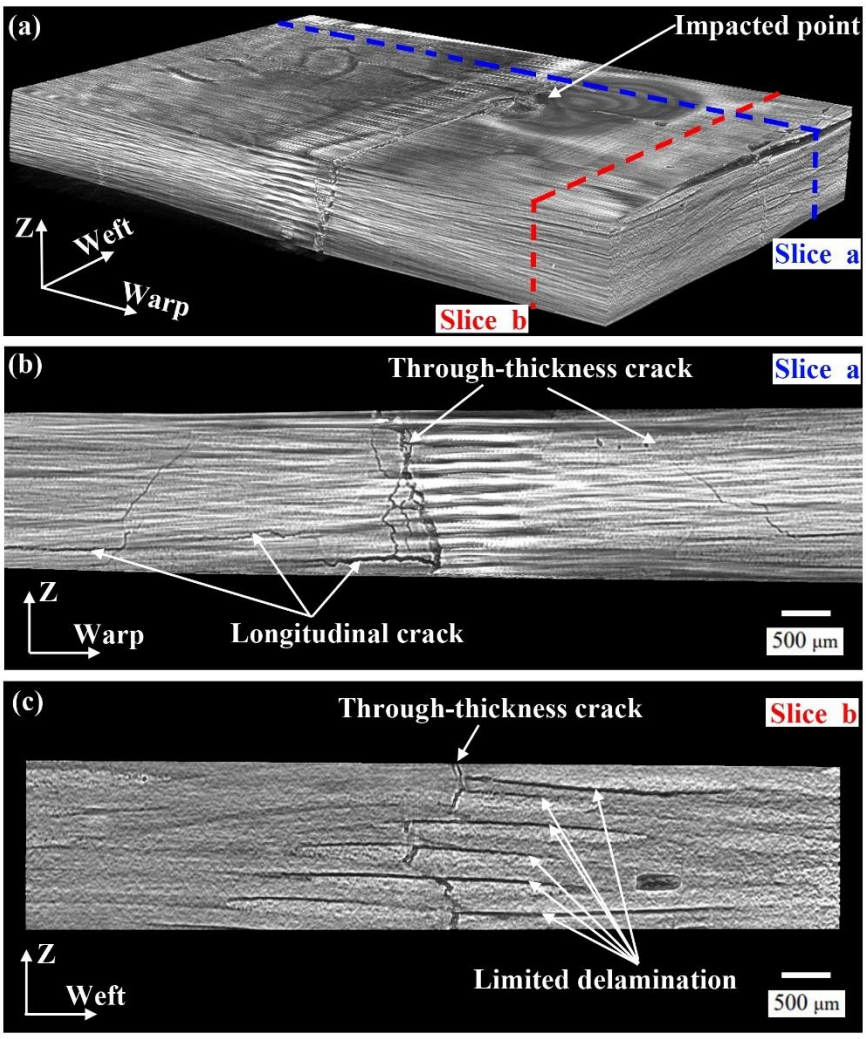

Fig. 5-14. X-ray μCT scanning images of 3D-a composite after 6-J impact. **(a)** 3D image, **(b)** slice projection image parallel to warp direction, and **(c)** slice projection image parallel to weft direction.

X-ray μCT scanning images of post-impacted 3D-c composite are shown in **Fig. 5-15**. For the Slice A which is parallel to the warp direction as shown in **Fig. 5-15 (b)**, there is no serious through-thickness crack at the center part, which is different from the 3D-a structure, there are numerus limited delamination failures at upper, middle, and lower layers along warp yarns, instead of serious warp-yarn breakage failure. This may be due to the structural difference, binder yarn goes in through-thickness direction, binding all the warp-yarn layers together in 3D-c, preventing the serious warp-yarn breakage failure; for the 3D-a, binder yarn binding adjacent two warp-yarn layers and lying more in in-plane direction, thus has less binding ability compared with 3D-c. For the Slice B which is parallel to weft direction as shown in **Fig. 5-15 (c)**, there is obvious limited

delamination failures along weft yarns and binder yarn, and this failure modes are also found in other slices parallel to Slice B. It should be noted that there is less or no binder-yarn breakage failure which is found in structure 3D-a, transverse crack which is weft-yarn breakage failure, stopped at the binder yarn and delamination or deboning failure along the binder yarn developed. This may be due to that the binder yarn in 3D-c goes in through-thickness direction, underwent less tensile load in an impact event, thus survived from the brakeage failure. The obvious failure mode difference between the 3D-a and 3D-c mainly come from the structural difference, the binder yarn lies more in through-thickness direction may survive more from through-thickness crack failure, leaves more impact-resistance ability for the developed 3D woven composites.

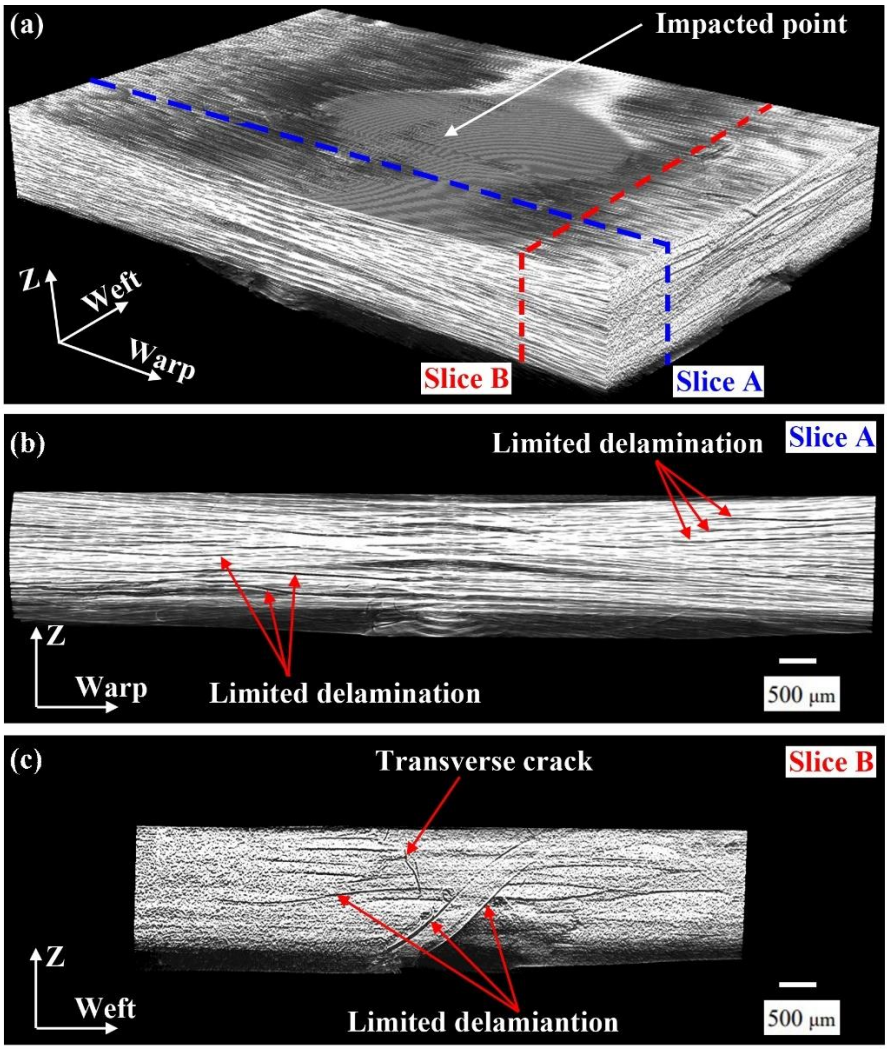

Fig. 5-15. X-ray μCT scanning images of 3D-c composite after 6-J impact. **(a)** 3D image, **(b)** slice projection image parallel to warp direction, and **(c)** slice projection image parallel to weft direction.

5.4 Conclusions

Four types of carbon fiber 3D woven textile-reinforced epoxy-resin composites with different woven structures were fabricated based on a traditional dobby sample weaving loom and VARTM techniques. Three-point bending tests and low-velocity drop-weight impact tests were conducted on the 3D woven composites to study the effect of woven structure on the composite out-of-plane quasi-static and dynamic flexural performance. Non-destructive ultrasonic C-scan and X-ray μCT were conducted on the impacted composites to characterize the internal failure mechanism. The main conclusions are as following:

(1) Based on the special weft-interlock woven structural design in which part of the weft insertions serving as binder yarns, as well as same warp-yarn density and same weft-insertion density set during weaving process, four woven structures have same textile-areal density for the woven preforms and same fiber volume fraction for the woven composites. The special structural design has great potential to develop more types of 3D woven structures and complex woven structures.

(2) Woven structure with various weft-to-binder yarn ratio and binder-yarn waviness degree, has an obvious influence on the quasi-static and dynamic flexural mechanical performance. Among the four developed 3D woven composites, 3D-a exhibits the best quasi-static flexural mechanical performance, followed with 2.5D, 3D-b, and 3D-c. Lower binder-yarn waviness in through-thickness direction and lower in-plane yarn waviness contribute more to quasi-static flexural performance for the developed 3D woven composites.

(3) In contrast, 3D-c exhibits the best dynamic flexural mechanical performance, followed with 3D-b, 3D-a, and 2.5D. Larger binder-yarn undulation in through-thickness direction as well as larger in-plane yarn waviness contribute more to impact performance.

(4) Moreover, woven structure has an obvious influence on the failure mode in impacted composites, the binder yarn lies more in through-thickness direction will survive more from through-thickness crack failures, exhibit more limited delamination or debonding failures, leaving better impact-resistance ability for the developed 3D woven composites. Proper structure design of the carbon fiber 3D woven composites is key

issue to achieve better flexural performance for specific engineering application. This work provides a woven structural design guidance for developing complex 3D weft-interlock woven composites.

References

[1] Graphene decorated carbon fiber reinforced polymer composites: An assessment of the influence of functional groups. Composites Part A: Applied Science and Manufacturing. 2019;122:36-44.

[2] Pittman Jr C, He G-R, Wu B, Gardner S. Chemical modification of carbon fiber surfaces by nitric acid oxidation followed by reaction with tetraethylenepentamine. Carbon. 1997;35:317-31.

[3] Rahmani H, Ashori A, Varnaseri N. Surface modification of carbon fiber for improving the interfacial adhesion between carbon fiber and polymer matrix. Polymers for Advanced Technologies. 2016;27:805-11.

[4] Dransfield K, Baillie C, Mai Y-W. Improving the delamination resistance of CFRP by stitching—a review. Composites Science and Technology. 1994;50:305-17.

[5] Cartié DD, Troulis M, Partridge IK. Delamination of Z-pinned carbon fibre reinforced laminates. Composites Science and Technology. 2006;66:855-61.

[6] Ferreira MTVHP. Crack bridging of surface structured z-reinforcements in CFRP laminates. 2016.

[7] Chen X, Taylor LW, Tsai L-J. An overview on fabrication of three-dimensional woven textile preforms for composites. Textile Research Journal. 2011;81:932-44.

[8] Potluri P, Hogg P, Arshad M, Jetavat D, Jamshidi P. Influence of fibre architecture on impact damage tolerance in 3D woven composites. Applied Composite Materials. 2012;19:799-812.

Chapter 6 Conclusions and future work

6.1 Conclusions

The aims and objectives of this dissertation mainly focus on developing 3D woven textile-reinforced composite materials and clarifying the relationship among the woven structure, composite out-of-plane mechanical performance and failure mode. Some 3D woven textile design parameters are drawn out for future 3D woven composite material manufacturing.

In this study, a new weaving technology with heddle position modification based on a self-built 3D weaving loom was designed and introduced to manufacture four typical 3D woven structures: LLOW, TTOW, TTAIW, and LLAIW. The new weaving technology has great potential for manufacturing various 3D woven structures effectively and efficiently. Six types of glass/aramid fiber hybrid 3D woven textiles were developed based on the new weaving technology successfully, and the textile-reinforced composites were fabricated with VARTM technology. Optical microscopy was used to observe internal geometry of the composites. Based on the proposed weaving system, the angle-interlock woven structures have the largest weft-yarn density (roughly 1.5 times larger than that of the orthogonal structures) and composite fiber volume fraction (roughly 1.3 times larger than that of the orthogonal structures). The through-thickness woven structures have a relative uniform yarn distribution than have the layer-to-layer woven structures. TTAIW is the optimal design based on this weaving system, and this structure could achieve larger weft-yarn density and has a uniform warp, weft, and binder yarn distribution at the same time. A further modification is needed to achieve higher weft-yarn density for orthogonal woven structures based on this weaving system.

The quasi-static flexural performance of the developed glass/aramid fiber hybrid 3D woven composites was studied under three-point bending tests. Different quasi-static mechanical behavior is shown along textile warp and weft directions for the designed 3D woven structures, weft-direction composite beam specimens have a higher flexural modulus but lower failure strain than have warp-direction composite beams. Moreover, the angle-interlock woven structures have a larger flexural strength and modulus than that of orthogonal structures: 50% and 40% larger, respectively. The quasi-static flexural modulus of such 3D woven composites is more sensitive to fiber volume fraction and flexural strength is more sensitive to woven structure. TTAIW structure along the

warp direction has the best flexural-failure resistance among all composites. Woven structure or binder-yarn path has an obvious influence on the composite failures after three-point bending. For weft-direction beams, there is no obvious propagating failure beyond beam center, but for warp-direction beams, obvious propagating weft-yarn debonding failure can be observed beyond the center part, which can be attributed to binder yarn running in the beam length direction for warp-direction beams, which transfers loads to adjacent interlaced weft yarns. The angle-interlock woven structures have slight weft-yarn debonding failure in the propagating-failure area compared with the orthogonal-woven structures, because the binder-yarn undulation angle is smaller, and they have less interlaced parts between the surface-weft yarn layers and binder yarns. It should be noted that binder yarns not only improve the out-of-plane interlayer strength of such 3D woven composites, but also influence the in-plane failure mode, due to that the binder yarns are both in through-thickness and warp directions. Proper structural or binder-yarn path design of 3D woven composite is key issue to achieve better quasi-static flexural performance.

The dynamic low-velocity drop-weight impact performance of the developed glass/aramid fiber hybrid 3D woven composites was studied under three impact energy levels: 10, 20 and 30 J. The 3D woven composites exhibit a quasi-penetration energy of 20 J except the TTAIW which exhibits a quasi-penetration energy of 30 J. TTAIW with the largest fiber volume fraction and a uniform binder yarn path, is the optimal structural design among the developed composites for specific engineering application that may be subjected to low-velocity impact. Fiber volume fraction has an obvious influence on the impact resistance of these 3D woven composites subjected to low-velocity impact. The angle-interlock group has a better impact resistance than has the orthogonal group from the perspectives of load-carrying ability, deflection characteristics, and energy characteristics. This is mainly due to angle-interlock group composites being capable of achieving a 31% higher fiber volume fraction in this weaving system compared with the orthogonal group composites. Achieving high fiber volume fraction is a top consideration for 3D woven composites to develop impact-resistance materials. Woven structure design is also a key parameter to improve impact-resistance ability for these 3D woven composites. In the angle-interlock group which has a nominal same fiber volume fraction, TTAIW composite with a uniform structure exhibits a superior impact-resistance performance. Woven structure has an obvious influence on failure mode of the

composites under low-velocity impact. The angle-interlock group has larger localized failure area than has the orthogonal group under all impact energy levels owing to the binder yarn path difference between the two groups. The failures in angle-interlock woven structures are more limited delamination failures and leaving of structural completeness. However, serious glass fiber fracture failure in warp and weft yarns is likely introduced for orthogonal woven structures. It is expected that perforation is likely induced for orthogonal woven structures subjected to higher impact energy due to its fiber fracture failure mode. Above all, angle-interlock and layer-to-layer woven structures are suitable for manufacturing with the modified heddle position system. TTAIW is the best structural design based on the new weaving system to develop impact-resistant composite materials.

Four types of carbon fiber 3D woven textile-reinforced epoxy-resin composites with different woven structures were fabricated based on a traditional weaving technology and VARTM technology. The quasi-static flexural performance of the CFRPs was studied under three-point bending test and the dynamic low-velocity drop-weight impact performance was studied under three impact energy levels: 3, 6 and 9 J. During weaving process, same warp-yarn density as well as same weft-insertion density were set for the four woven structures to acquire same textile preform areal density and same composite fiber volume fraction. Three-point bending and low-velocity drop-weight impact tests were conducted on the CFRPs to study the effect of woven structure on the out-of-plane flexural performance of these textile-reinforced composites.

Based on the special structural design of the 3D weft-interlock woven textiles which binder yarn lies in weft direction as well as the same warp-yarn density and weft-insertion density set during weaving process, the four types of woven structures have different weft-to-binder yarn ratio, and accordingly different weft- and binder-yarn densities. Among the four designed 3D woven composites, 3D-a exhibits the best quasi-static flexural mechanical performance, followed with 2.5D, 3D-b, and 3D-c. Binder yarn with small waviness has both interlayer binding/interlacing and in-plane load-carrying abilities. Compared with 2.5D structure in which weft yarn interlaces with warp yarn, 3D-a structure in which there is no interlacement between weft and warp yarns, could achieve a better quasi-static flexural mechanical performance. There is opposite mechanical behavior between quasi-static three-point bending tests and dynamic low-

velocity drop-weight impact tests for these designed CFRPs. 3D-c exhibits the best dynamic flexural mechanical performance, followed with 3D-b, 3D-a, and 2.5D. Larger in-plane yarn waviness degree as well as through-thickness binder-yarn path may contribute to better dynamic flexural mechanical performance. Moreover, woven structure has an obvious influence on the failure mode in impacted composites, the binder yarn lies more in through-thickness direction will survive more from through-thickness crack failures, exhibit more limited delamination or debonding failures, leaving better impact-resistance ability for the developed 3D woven composites.

With the new weaving technology based on the proposed modified heddle position system and special structure design based on the traditional weaving technology, different 3D woven structures have been designed and manufactured to develop advanced fiber-reinforced composite materials. The through-thickness angle-interlock woven composite developed based on the new weaving technology has superior out-of-plane mechanical performance, and, thus has great potential for specific engineering applications which may subjected to low-velocity impact. With successful development of these 3D woven composites and comprehensive studies of their quasi-static and dynamic flexural performance, some textile design parameters could be drawn out for future development of advanced 3D woven composites. Woven textile structure has an obvious influence on the composite out-of-plane mechanical performance. Proper structural design of 3D woven composite based on specific fiber selection and weaving technology is key issue to develop advanced composites with better flexural performance.

6.2 Future work

Based on the work done in the present research, several projects are possible to be continued:

(1) The new weaving technology could be further modified on beat-up system and yarn tension control system to acquire higher weft yarn density for orthogonal woven structures.

(2) A weaving software could be designed based on the modified heddle position system to develop 3D textiles more easily.

(3) More types of 3D/2.5D woven structures could be designed and manufactured based on the new weaving system.

(4) 3D woven textile structural design parameters could be further optimized to develop

textile composites with higher out-of-plane mechanical performance.

(5) Thicker woven composite materials with more warp/weft yarn layers could be manufactured to develop impact-resistance materials.

(6) Carbon fiber 3D woven textiles with higher warp-yarn density could be manufactured with a modification of warp yarn feeding system, and a higher fiber volume fraction could be achieved for CFRP materials.

List of publications

・**Yajun Liu**, Canyi Huang, Hong Xia, Qing-Qing Ni. Research on development of 3D woven textile-reinforced composites and their flexural behavior. Materials & Design. Vol. 212, No. 15, pp. 110267.

・**Yajun Liu**, Hong Xia, Qing-Qing Ni. Experimental investigation on low-velocity impact performance of 3D woven textile composites. Applied composite materials. (2022) :1-26.

・**Yajun Liu**, Qing-Qing Ni. Classification and development of 3D woven textile preforms (Poster Presentation). Proceeding of the 10th International Symposium on High-Tech Fiber Engineering for Young Researchers (August 24-30, 2018. Suzhou, China).

・**Yajun Liu**, Hong Xia, Chunhong Zhu, Akio Sakaguchi, Qing-Qing Ni. The research on flexural properties of 3D woven textile composites (Poster Presentation). Symposium of Advanced Composites (SAC) 2019 (October 18-22, 2019. Sapporo, Hokkaido, Japan).

・**Yajun Liu**, Hong Xia, Chunhong Zhu, Akio Sakaguchi, Qing-Qing Ni. The research on development of 3D textile composites and their bending performance (Oral presentation). Annual Autumn Meeting 2019, The Society of Fiber Science and Technology, Japan (November 9-10, 2019. Ueda, Nagano, Japan).

・**Yajun Liu**, Hong Xia, Qing-Qing Ni. The research on low-velocity impact performance of 3D woven textile composites (Poster presentation). China-Japan International Conference on Composites, China (August 26-27, 2021. Anhui, China (online)).

Acknowledgements

Firstly, I wish to express my sincere thanks to my supervisor, Prof. Qing-Qing Ni, for his guidance, valuable discussion throughout my PhD research.

I would also like to thank all the staff members from the Shinshu University who provided me with experimental and technical supports.

Special thanks to my academic colleagues and friends from the Ni LAB in Shinshu University during my PhD research.

Special thanks to the financial supports of Chinomori Scholarship (2018, 2019) from Shinshu University and Monbukagakusho Honors Scholarship for Privately Financed International Students (2020) from Japan Student Service Organization (JASSO). I also give my thanks to the scholarship received from Shinshu University supporting my academic visit to School of materials, the University of Manchester (2018).

Finally, I would like to express my great thanks to my family, thank you for your support and encouragement during my PhD research.